Analysis of specific design aspects of a thorium-uranium fuelled European Pressurised Reactor

MH du Toit

20517122

Thesis submitted in fulfilment of the requirements for the degree *Philosophiae Doctor* in Nuclear Engineering at the Potchefstroom Campus of the North-West University

Promoter: Dr VV Naicker

Co-Promoter: Dr SS Chirayath

May 2017

DECLARATION

I, Maria H. Du Toit, hereby declare that

1. I understand what plagiarism is and am aware of the University's policy in this regard.

2. I know that "plagiarism" means using another person's work and ideas without acknowledgement, and pretending that it is one's own. I know that plagiarism not only includes verbatim copying, but also the extensive (albeit paraphrased) use of another person's ideas without acknowledgement. I know that plagiarism covers this sort of use of material found in textbooks, journal articles, theses and on the internet.

3. This report on "Analysis of specific design aspects of a thorium-uranium fuelled European Pressurised Reactor" submitted in fulfilment of the requirements for the Philosophiae Doctor degree in Nuclear Engineering (PhD. Eng.) is my own original work.

4. Where other people's work has been used (either from a printed source, the Internet or any other source), this has been properly acknowledged and referenced in accordance with departmental requirements.

5. I have not used work previously produced by another student or any other person to hand in as my own.

6. I have not allowed, and will not allow, anyone to copy my work with the intention of passing it off as his or her own work.

_____ _____

STUDENT DATE

I hereby declare that I am the sole author of the thesis entitled: Analysis of specific design aspects of a thorium-uranium fuelled European Pressurised Reactor.

ABSTRACT

The global nuclear industry is an established industry, however, should governments decide to move forward with more nuclear power. Enough resources are required to succeed in this endeavour of generating the electric power for the years to come. The nuclear power technology has received increased attention in South Africa, especially after the publication of the IRP2010.

The IAEA reported that the available uranium resources are enough to provide nuclear energy for about 100 more years at the current rate of use (NEA & IAEA, 2012). This will however not be the case should nuclear power demand increase worldwide. This would necessitate the utilization of other resources to supply the growing global energy market. Uranium alone cannot carry this load and it also produces dangerous plutonium. Therefore, a need for an alternative nuclear fuel source exists. The current pressure on governments has forced researchers to investigate alternative fuel technologies that can burn more efficiently in order to increase fuel lifetime and therefore fuel-cycle length and minimise plutonium production.

The majority of thorium fuel research on PWRs is limited to reactor physics investigations and therefore require further R&D in core design and fuel-cycle optimisation in order to achieve practical and commercial implementation (IAEA, 2012). This thesis focuses on contributing research in terms of core design and fuel-cycle optimisation to help close the gap of reaching commercial readiness for thorium-uranium fuel.

The study focussed on developing a full-core reference 3D model of the EPR for neutron transport simulations using MCNP6. This is unique in the field of study, since most studies model only fuel assemblies using Monte Carlo methods Gen 2 PWRs. The reference model was compared with the Final Safety Analysis Report of the EPR. Coupling was introduced between MCNP6 and RELAP5 to take into account the feedback from the thermal hydraulic network of the core in support of the research activities of the reactor analysis group at the School of Mechanical and Nuclear Engineering. The coupling methodology was correctly implemented in NWURCS; however, it is recommended to repeat the process by reducing the relative errors in MCNP6. The results of the reference EPR model were evaluated with no major differences. This also gave confidence in the verification of NWURCS in generating the input decks. The EPR reference model can now be used as the basis for the thorium-uranium fuel development.

The systematic literature review was integral in understanding reactor physics when analysing thorium-based fuel in a standard PWR. The literature provided a solid foundation for the new fuel design, which formed a starting point for thorium-uranium fuel in the EPR. The design goals were that the fuel should be compatible with the compact EPR core design, while running 24-month fuel cycles and still adhering to the neutronics requirements and limits.

New thorium-uranium fuel for the EPR was developed and evaluated. The initial fissile content was changed to produce similar reactivity as compared with the uranium EPR. Different fuel compositions and combinations were tested. The newly designed thorium-uranium fuel was evaluated and the final fuel design had an equivalent atom % initial fissile content as the EPR. This was with the exception for fuel-pin sections where pure ThO_2 replaced the $(U\text{-}Gd)O_2$ sections in the original EPR design. In this way there was no need to increase the enrichment as predicted by (Herring, et al., 2001; Saglam, et al., 2003; Galperin, et al., 2001; Joo, et al., 2003) due to the effective fuel design of the EPR. This design followed the developed methodology by reducing the burnable poison (Gadolinium) requirements, optimising the initial fissile content and still achieving a 24-month fuel-cycle. Due to the fact that the initial fissile content was not increased, the reactivity coefficients and design limits for a fresh full-core Th-EPR are all within acceptable limits and there was no need to increase the soluble boron enrichment. The burnt EOL Th-EPR FAB1 properties were shown to be satisfactory. The newly designed thorium-uranium fuel for the EPR is therefore feasible and moderation control was applied to further enhance breeding.

The novel idea of utilising moderation control using existing control-rod positions in available fuel assemblies was tested on the Th-EPR FAB1. Results showed an increase in the breeding of fissile content when helium filled moderation rods were inserted (to change the neutron spectrum to be slightly more epithermal). The breeding of ^{233}U increased. Also an increase in ^{239}Pu caused the Xe and Sm concentrations to increase, which offset the addition of excess reactivity due to higher fissile content. However, the initial Th-EPR FAB1 design without the addition of moderation rods proved to be the best choice.

The project succeeded in designing thorium-uranium fuel for a new Gen 3+ PWR that reached 24-month fuel cycles without altering the geometry and disregarding any design limits. The thesis should contribute to research in terms of core design and fuel-cycle optimisation, which will support the fuel licencing and commercialisation of thorium-based PWR designs. The proposed fuel design can be investigated further as suggested in recommendations to continue the process of fuel commercialisation.

KEYWORDS: *thorium, thorium-uranium fuel, EPR, moderation, fuel cycle, 24-months*

ACKNOWLEDGEMENTS

I wish to express thanks to Eskom who has given me the opportunity to do this project while under their employment.

I am grateful for my supervisor Dr Naicker for all the time and effort spent to make this a success. Thank you to Dr Chirayath for helping me from the other side of the world.

Great appreciation for my close friends and family who have been closely involved and supporting me every step of the way.

I thank the Lord for providing me with this opportunity as well as the courage, patience and wisdom to complete this project.

TABLE OF CONTENTS

NOMENCLATURE

Abbreviation	Description
AO	Axial Offset
BOL	Beginning of Life
BP	Burnable Poison
BW	Boron Worth
BWR	Boiling Water Reactor
CBC	Critical Boron Concentration
CHF	Critical Heat Flux
CR	Control-Rod
CRW	Control Rod Worth
DC	Doppler Coefficient
DNBR	Departure from Nucleate Boiling Ratio
EFPDs	Effective Full Power Days
EOL	End of Life
EPR	European Pressurised Reactor
FCT	Fuel Centreline Temperature
FPs	Fission Products
FSAR	Final Safety Analysis Report
Gen	Generation
H/HM	Hydrogen to heavy metal ratio
HCF	Hot Channel Factor
HFP	Hot Full Power
HZP	Hot Zero Power
IAEA	International Atomic Energy Agency
ID	Inside Diameter
IFBA	Integral Fuel Burnable Absorber
IRP	Integrated Resource Plan
IRW	Integral Rod Worth
IXAF	Internally and externally cooled Annular Fuel
LEU	Low Enriched uranium
LOCA	Loss-of-Coolant Accident
LWR	Light Water Reactor
MA	Minor Actinide
MCNP	Monte Carlo N-Particle
MFR	Moderator to Fuel Ratio
MOX	Mixed Oxide of PuO_2 and UO_2
MTC	Moderator Temperature Coefficient
NWU HPC	North-West University High Performance Computing
NWURCS	North-West University Reactor Code Suite
OD	Outside Diameter
PCMI	Pellet Cladding Mechanical Interaction
PWR	Pressurised Water Reactor
RCCA	Rod Cluster Control Assembly
RELAP	Reactor Excursion and Leak Analysis Program
RI	Resonance Integral
RIA	Reactivity Initiated Accident

RIP	Rod Internal Pressure
RPV	Reactor Pressure Vessel
SA	South Africa
SDM	Shutdown Margin
SF	Spent Fuel
US NRC	United States Nuclear Regulatory Commission
WABA	Wet Annular Burnable Absorber

LIST OF SYMBOLS

Symbol	Description	Unit
k_{eff}	Effective system reactivity eigenvalue	-
β_{eff}	Effective delayed neutron fraction	-
Am	Americium	-
B	Boron	-
Gd	Gadolinium	-
I	Iodine	-
Np	Neptunium	-
Pa	Protactinium	-
Pm	Promethium	-
Pu	Plutonium	-
Sb	Antimony	-
Sm	Samarium	-
Th	Thorium	-
$T_{\frac{1}{2}}$	Half-life	years
U	Uranium	-
Xe	Xenon	-
η	Number of neutrons per fission	-
σ_c	Microscopic capture cross-section	barn
σ_f	Microscopic fission cross-section	barn

LIST OF FIGURES

LIST OF TABLES

1. INTRODUCTION

"There is no passion to be found playing small - in settling for a life that is less than the one you are capable of living."

~ Nelson Mandela ~

Overview

Chapter 1 presents the introduction to the thesis along with the problem statement and research objectives. Additionally, the structure and layout of the thesis are provided at the end of this chapter.

1.1 INTRODUCTION

Many countries around the world are facing the reality of increasing electricity demand and depleting natural resources. The recent focus on clean energy and security-of-supply has forced countries to diversify their electricity grid and to become less dependent on fossil fuels. Uranium supplies, like any natural resource utilized globally, are limited and hold the risk of price escalations.[1] For nuclear power to be sustainable, application of a larger selection of fuel sources is key. Thorium is one example of an alternative nuclear fuel source having many benefits, which include:

- Thorium irradiation produces fissile fuel material (^{233}U) and no plutonium,
- ^{233}U has excellent neutron physics characteristics,
- Thorium oxide is chemically more stable than uranium oxide,
- Thorium is about three to four times more naturally abundant than uranium,
- Thorium can be used with other fissile isotopes to achieve higher fuel utilisation or burnup,
- Long-lived radio-isotopes produced in thorium fuel cycle are less, compared to that of the conventional uranium fuel-cycle.

Chapter 3 presents a detailed discussion on the advantages and disadvantages of thorium fuel.

1. Recent findings shows that uranium supplies can become renewable with new seawater extraction methods, which makes uranium virtually inexhaustible (Conca, 2016). The need for fuel diversification using thorium will depend on the lead-time for uranium seawater extraction to become commercially viable.

Pressurised Water Reactors (PWRs) contribute more than 60% of the world's reactors. PWRs have proved to be a well-established technology (European Nuclear Society, 2015). South Africa has the only nuclear power station in the African continent, operating in Koeberg, which consists of two PWR units. Both units have been operating since 1985 with no serious incidents (ESKOM, 2011). The South African government has published an integrated resource plan (IRP2010), which states that South Africa will add 9600 MW nuclear power to their national grid by 2030 and that the PWR technology will be the design of choice for these reactors (SA, 2011).

Many previous studies have shown the benefits of using thorium-based fuel in PWRs and proposed many modifications and strategies of how to use thorium-based fuel in PWRs (Ashley, et al., 2014; Galperin, et al., 2001; Joo, et al., 2003; Nuttin, et al., 2006; Lindley & Parks, 2012; Todosow & Kazimi, 2004; Tsige-Tamirat, 2011; Tucker, et al., 2015; Wah Lau, et al., 2013). A master's study that evaluated thorium-based fuel options and the thorium-uranium fuel option has demonstrated great promise for its application. An economic comparison of the thorium-based fuel options versus uranium was also part of the study. An evolutionary strategy of introducing thorium-based fuel into existing and future reactor technologies was investigated. The thorium-based fuel implementation strategy contributes to the strategic plan of the South African government and can pay for front-end fuel facilities by saving on fuel-cycle costs and refuelling outage costs (Du Toit, 2013).

As further shown in the master's study, the proposed strategy can assist South Africa to become fuel independent, help Eskom (the South African utility) to provide continuous electric power and create more local job opportunities. Thorium-based fuel can supplement uranium to diversify the nuclear fuel sources and increase the current sustainability. South Africa can utilise local resources (thorium, currently under-utilized) to enhance fuel utilization (Du Toit, 2013). The masters concluded that thorium-based fuel designs are viable for use in PWRs but require further investigation. These required investigations include neutronic calculations, core design studies, fuel-cycle optimisation studies, fabrication investigations and irradiation analyses. The above-mentioned analyses will support fuel licencing in future and commercialisation of thorium-based PWR designs.

The current study introduces thorium-based fuel into a Generation 3+ PWR called the EPR (European Pressurised Reactor). The EPR is the choice for the reference PWR because it is a Generation 3+ PWR, which makes it a candidate for the South African fleet. The EPR also has added safety features and improved fuel efficiency. This thesis focuses on incorporating thorium–uranium mixed oxide (MOX) fuel for the purpose of enhancing fuel utilisation, fuel burnup and fuel-cycle length. The focus is to design fuel for 24-month fuel-cycles without altering the geometry of the fuel assemblies or the operational and safety characteristics of the reactor.

Parameters related to the neutron transport behaviour in the reactor core such as the fuel temperature dependent Doppler coefficient, moderator coefficient, delayed neutron fraction,

boron worth, control-rod worth, burnup, neutron spectrum, reactivity swing, etc. were analysed. The study of these parameters is required for safety fuel licencing.

1.2 PROBLEM STATEMENT

Nuclear power technology has received increased attention in South Africa, especially after the publication of the IRP2010. The nuclear industry should be prepared to take on the responsibility of generating the country's electric power for years to come, should government decide to move forward with nuclear power. However, enough resources are required to succeed in this endeavour.

The IAEA reported that the available uranium resources are enough to provide nuclear energy for about 100 more years at the current rate of use (NEA & IAEA, 2012). This will, however, not be the case should nuclear power demand increase worldwide, thereby necessitating utilization of other resources to supply the growing global energy market. Uranium alone cannot carry this load also dangerous isotopes of plutonium are produced. Therefore, a need for an alternative nuclear fuel source exists. The current pressure on governments has forced researchers to investigate alternative fuel technologies that can burn more efficiently in order to increase fuel lifetime and therefore fuel-cycle length and minimise plutonium production.

The majority of thorium fuel research on PWRs is limited to reactor physics investigations and therefore we require further R&D in core design and fuel-cycle optimisation in order to achieve practical and commercial implementation (IAEA, 2012). This thesis focuses on contributing research in terms of core design and fuel-cycle optimisation to help close the gap of reaching commercial readiness for thorium-uranium fuel.

1.3 RESEARCH AIMS AND OBJECTIVES

The main objectives of this study are to:

1. Develop a full-core reference model of the EPR for neutron transport simulations using MCNP6 to serve as the starting point for the investigation,
2. Compare the model against the Final Safety Analysis Report (FSAR) of the EPR,
3. Couple the MCNP6 calculations with RELAP5 for feedback from the thermal hydraulic core network in support of the research activities of the reactor analysis group at the School of Mechanical and Nuclear Engineering, North-West University,
4. Draw up a design methodology from literature as starting point for thorium-uranium fuel in the EPR,
5. Design homogeneously mixed thorium-uranium fuel that:
    a. is compatible with the compact EPR core design,

   b. runs on a 24-month cycle,
   c. has a minimized enrichment,
   d. meets neutronics and thermal-hydraulic requirements.
6. Evaluate the above mentioned design,
7. Apply the thorium-uranium fuel design to a full-core model,
8. Compare the thorium core to the reference EPR in terms of the neutronic, thermal-hydraulic and safety parameters and,
9. Enhance the thorium fuel burnup by moderation control.

1.4 STRUCTURE OF THE THESIS

The thesis consists of the following chapters:

Chapter 2 describes the theory of the neutronics and thermal-hydraulic properties with some important definitions provided as background for the chapters to follow. Chapter 3 provides the distinctive physical properties of thorium compared to uranium and previous work on the operational properties of homogeneously mixed thorium-uranium fuel inside the core. The literature on moderation control and the experience on thorium-based fuel in terms of the composition, geometry and configuration are given. Chapter 3 furthermore provides a description of the computational codes used for this project and details the fuel design limits.

Chapter 4 focuses on the reference model. This chapter describes the EPR in terms of geometry, safety, materials, burnup and thermal design. Chapter 4 also provides the assumptions and details of how this information is of use in order to develop the MCNP6 and RELAP5 models. The results of the reference model and comparison against the FSAR are shown in Chapter 4 thereby also serve to verify the reference model.

Chapter 5 provides the design methodology and results of thorium-uranium fuel introduction in the EPR. Comparison of the results of the thorium-EPR (Th-EPR) with reference uranium EPR and previous thorium-uranium studies is in Chapter 5. Chapter 6 uses the newly designed Th-EPR and applies moderation control to further enhance breeding and optimise the fuel-cycle. Chapter 7 concludes the research and suggests further research.

2. THEORY

"An adventure is only an inconvenience rightly considered. An inconvenience is only an adventure wrongly considered."

~ G. K. Chesterton ~

Overview

Chapter 2 presents the theory of the neutronic- and thermal-hydraulic properties as background for the chapters to follow. Section 2.3 discusses verification and validation.

2.1 NEUTRONIC PROPERTIES

2.1.1 BURNUP AND CORE-LOADING

Burnup is a measure of fuel depletion, which represents the integrated energy output of the fuel per unit mass of the heavy metal. The design of the fuel (specifically enough fissile content and mass) combined with an adequate number of fuel assemblies in the reactor core should ensure the desired fuel-cycle duration (for example 18 to 24 months per cycle) (Pal & Jagannathan, 2008). Typically, a fuel assembly is present in the core for three fuel-cycles, most likely in different positions in the core through the shuffling operations performed at the end of each fuel-cycle (Kok, 2009).

The effective neutron multiplication factor (also known as the system eigenvalue) $k_{eff,}$ normally decreases with time and as the fuel burnup increases. This happens due to many effects such as fissile fuel depletion and fission products (FPs) that accumulate in the core. In reality, k_{eff} is equal to unity during each fuel cycle. The presence of boron in the core with its neutron absorption capabilities is a means to keep $k_{eff} = 1$ through appropriate dilution. Newly-bred fissile material (like ^{239}Pu in uranium-fuelled reactors and ^{233}U in thorium-fuelled reactors) balances the decrease in k_{eff} during the cycle. The definition of core reactivity is as shown in Eq, 2.1, where the suffixes 1 and 2 represent two different states of the reactor core.

$$\rho = \frac{k_{eff_2} - k_{eff_1}}{k_{eff_2} \times k_{eff_1}} \qquad \text{Eq. 2-1}$$

Eq. 2-2 calculates the fuel burnup.

$$Burnup(\frac{\mathrm{MWd}}{\mathrm{tHM}}) = \frac{P(\mathrm{MW}) \times \mathrm{T}_c\,(\mathrm{days}) \times n}{M(\mathrm{tHM})} \qquad \text{Eq. 2-2}$$

Where: P is the total reactor thermal power, T_c is the cycle-length, n is the number of batches/cycles seen by fuel assemblies and, M is the total mass of the fuel.

2.1.2 REACTIVITY CONTROL

Reactivity feedback is the most fundamental process in a reactor and is vital for safe reactor operation. The reactivity coefficients determine how the core reacts to changes in operating conditions under normal- and accident conditions. These coefficients include the moderator temperature coefficient, and the fuel temperature-dependent Doppler coefficient. Other properties like the delayed neutron fraction; control-rod (CR) worth and shut-down margins are also vital for the control and safety of the reactor.

2.1.2.1 MODERATOR COEFFICIENT

The Moderator Temperature Coefficient of reactivity (MTC) is the fractional change in reactivity ρ due to the change in moderator temperature. This includes the impact of density change due to temperature change. If the soluble boron concentration in the moderator is too high, the MTC can become positive, which undermines a crucial safety limit of the reactor. The MTC is typically the least negative at Beginning of Life (BOL) (due to the high concentration of boron) and decreases with the removal of boron.

The MTC also decreases with burnup, due to the changes in isotopic composition and an increased variety of isotopes (Wah Lau, et al., 2014). This effect mostly depends on the neutron spectrum (Joo, et al., 2003) and burnup that plays a vital role in the behaviour of the axial offset (AO) (Wah Lau, et al., 2014).

Eq. 2-3 calculates the moderator temperature coefficient (Lindley & Parks, 2012).

$$\mathrm{MTC} = \alpha_{T,m} = \frac{1}{k^2} \cdot \frac{dk}{dT} \approx \frac{k_{eff}(T_0 + \Delta T) - k_{eff}(T_0)}{\Delta T \times k_{eff}(T_0 + \Delta T) \times k_{eff}(T_0)} \qquad \text{Eq. 2-3}$$

Where: ΔT is the change in temperature of the moderator.

2.1.2.2 DOPPLER COEFFICIENT

The Doppler reactivity coefficient (DC), also known as the fuel temperature coefficient of reactivity, is the fractional change in reactivity ρ due to the change in fuel temperature. The DC is a measure of the Doppler broadening of neutron absorbing cross-section of ^{238}U in the fuel (which has large resonance absorption peaks). The DC is vital in the safety of the reactor because when the fuel temperature increases the Doppler broadening of the neutron capture-resonances decreases the reactivity (Ghrayeb, 2008).

Eq. 2-4 calculates the Doppler temperature coefficient (Lamarsh & Baratta, 2001; Lindley & Parks, 2012).

$$\mathrm{DC} = \alpha_{T,f} = \frac{1}{k^2} \cdot \frac{dk}{dT} \approx \frac{k_{eff}(T_0 + \Delta T) - k_{eff}(T_0)}{\Delta T \times k_{eff}(T_0 + \Delta T) \times k_{eff}(T_0)} \qquad \text{Eq. 2-4}$$

2.1.3 DELAYED NEUTRON FRACTION

Neutron fission produces energy, fission products (FPs), photons and neutrons. Most of the neutrons produced from fission are emitted within ~10^{-14} seconds of the fission event and only a small fraction (less than 1%) consists of delayed neutrons that are produced later when the FPs decay (Shultis & Faw, 2002). β_{eff} is the measure of the fraction of delayed neutrons and plays a vital role in the time behaviour, reactor kinetics and essentially the control of nuclear reactors (Ghrayeb, 2008).

Delayed neutrons increase the reactor period, which is an indication of the temporal response of the reactor. When the reactor is critical on only prompt neutrons, the reactor is prompt critical (Lamarsh & Baratta, 2001). A small β_{eff} denotes a shorter reactor period, which can make the system very sensitive during reactivity changes and cause difficulties during reactivity-initiated accidents (RIAs).

2.1.4 CONTROL-ROD WORTH

The control-rod (CR) worth is the change in reactivity caused by control-rod motion and should be greater than 5000 pcm (Trellue, et al., 2011). The ‘pcm’ is a unit of measuring reactivity known as per cent milli-k. Reactivity (Eq. 2-1) multiplied by 10000 will result in ‘pcm’ units. The CR worth describes the effect of the control-rods on the reactivity of the core. Different values for k_{eff} at different CR positions are required to yield the control worth curve. The efficiency of a control-rod depends largely on the concentration of the neutron absorbing material such as boron in the control-rod and the neutron flux at the location of the rod. The control-rod worth is at a maximum where the flux is at a maximum (Anglart, 2005).

2.1.5 SHUT-DOWN MARGIN

The reactor shutdown margin (SDM) is determined by calculating the difference between the available reactivity in control-rod assemblies (most reactive rod stuck out of the core) and the reactivity required for control safety purposes (Odoi, et al., 2014). The shut-down margin can also be explained as the amount of reactivity required to shut down the core and keep it sub-critical after a reactor trip. It is important that control-rod insertions provide enough negative reactivity in the core to ensure complete shutdown at any time needed during the core lifetime.

The SDM takes into account the total power defect (which is the amount the core will increase in reactivity due to the trip from Hot Full Power (HFP) to Hot Zero Power (HZP), void effects, rod insertion allowances and control-rod worth uncertainty which generally adds up to 10% (Faghihi & Mirvakili, 2011; AREVA, 2013).

The US NRC (United States Nuclear Regulatory Commission) requirements are that the SDM should be greater than 1300 pcm for average coolant temperature above 450 K and greater than 1600 pcm for average coolant temperature below 450 K (NRC, U.S.; Fetterman, 2009).

2.2 THERMAL-HYDRAULICS

The thermal power distribution in the core is extremely important, as it provides the location of hot spots in the core, which can result in fuel melting. There are many factors to evaluate the power distribution in the radial and axial direction, such as hot channel factors and form factors like axial offset. The most important hot channel factors are the heat flux hot channel factor (F_Q) and maximum enthalpy rise hot channel factor ($F_{\Delta H}$).

2.2.1 AXIAL OFFSET

The axial offset (AO) is the ratio of the power difference between the top half and bottom half of the core, divided by the total power of the core. The AO is dependent on the CR movements, moderator, fuel temperature and spatial concentrations of absorbers such as xenon and boron and the axial fuel burnup.

The water density gradient between the top and the bottom of the core, due to an increase in water temperature causes a difference in neutron moderation. The bottom of the core will produce more power than the top of the core, resulting in a higher burnup at the bottom of the core, which means that the bottom fuel of the core will deplete faster compared to the top of the core. However, this reverses and finally reaches an equilibrium core.

The boron content in the moderator will influence the MTC indirectly affecting the AO. Another important factor to take into account is the formation of CRUD at the top of the core due to the increasing temperature and decreasing density. The CRUD is rich in boron and reduces the reactivity to the top of the core (Wah Lau, et al., 2014).

2.2.2 F_Q

The total power peaking factor or the total heat flux hot channel factor is F_Q. This factor is the ratio of the maximum local heat flux in a fuel rod to the average fuel rod heat flux (or power). When taking into account the manufacturing and measurement uncertainty factors, Eq. 2-5 calculates the total heat flux hot channel factor.

$$F_Q = F_Q^N \times F_E \times F_M \quad \text{Eq. 2-5}$$

Where: the nuclear heat flux hot channel factor is F_Q^N , the engineering HCF is F_E and F_M is the manufacture hot channel factor. An uncertainty factor and engineering tolerance factor of 1.05 and 1.03 respectively is generally acceptable (Lindley, et al., 2014).

2.3 VERIFICATION AND VALIDATION

Making use of computer modelling for purposes of predicting system and/or component behaviour is common place in the nuclear industry. Creating and developing computer algorithms to meet this end involves the transformation of the derived mathematical and statistical equations representing the system and its components into reusable computer code. Deriving the set of equations that predicts system response usually requires some limiting assumptions and may involve some form of empirical input data that is subject to experimental accuracy etc. Therefore, verification and validation of such modelling computer software are essential before its application to reactor design.

Verification in general terms is defined as the process of assuring that the developed model is correctly employed. With respect to verification of computer models, this process entails the verification in two discrete parts (Babuska & Oden, 2004). The first part is making sure that the input data to the model are correct and match the specifications. Examples of input data typically specified by the user are geometrical inputs, material specification, as well as initial - and boundary conditions. The onus for verifying the correctness of the input data lies with the user.

The second part is making sure that the modelling software solves the equations and physical models as intended by the governing equations. It is the code developer's responsibility to perform a sequence of benchmark calculations to verify and ascertain that the written computer algorithms are implemented exactly as prescribed by the governing equations and to affirm non-erroneous computer implementation.

Validation in terms of computer modelling is the process of checking the models' accuracy by comparing it to reality. The definition of validation is the process of proving that the underlying assumptions and correlations in use in the governing equations are acceptable in accurately predicting system behaviour. Naturally, this process usually implies comparison with actual test data. The model results should be similar to real-life experimental results (Sartor, et al., 2015).

Due to the latter requirement imposed by validation, it is understandable that new reactor designs can be extremely costly and difficult to validate, especially if no experimental or plant data exist that can be used for these purposes. This is especially true in the nuclear industry where building a small-scale test unit, mock-up model or full-scale reactor is time consuming, expensive and often impractical.

Computer codes can be quite useful in providing predictions of physical conditions, when validation is impossible. “Because the results of a particular criticality safety calculation are unlikely to be experimentally verifiable, it is important to have a formal validation of the computer methods” (Kok, 2009). Validation of computer methods includes validation of the code and the data used by the code.

ANSI/ANS-8.24-2007 describes the current active safety standard for validation of neutron transport methods for nuclear criticality safety calculations (Kok, 2009). Section 3.7 discusses the verification and validation of the computational codes used for this study.

2.3.1 FSAR

Using as example the United States of America, a new reactor design needs to apply for design certification at the NRC. When the U.S. Nuclear Regulatory Commission (NRC) issues the design certification, it means that the NRC approves a nuclear power plant design (valid for 15 years), apart from an application to construct or operate a plant. The design certification addresses the safety issues related to the proposed nuclear power plant design.

One of the application documents in the design certification process is the Final Safety Analysis Report (FSAR). The FSAR delivers information to support the NRC's approval and certification of the new reactor design, under the provisions of 10 CFR Part 50/52, "Licences, Certifications, and Approvals for Nuclear Power Plants." Chapter 14 of the FSAR addresses the verification programmes and Chapter 18 addresses the verification and validation (U.S. NRC, 2016). The FSAR of the EPR was accepted by the NRC and is available online at the NRC website.

As part of the FSAR, some activities of V&V include; a pilot study, which provides an opportunity to examine the competency of the test design, performance measures and data collection; an extensive initial plant test program and also a comparison to current similar reactor designs (AREVA, 2013).

One can trust that the information given in a FSAR has been through rigorous testing and scrutiny by the NRC and is therefore verified and validated to be used as the standard for comparison to the current study.

2.4 CONCLUSION

Chapter 2 presented the background to the neutronics properties such as burnup, reactivity control, delayed neutron fraction, control-rod worth and shut-down margin as well as some important thermal-hydraulic parameters for better understanding the chapters to follow. Verification and validation are discussed and the FSAR is introduced.

3. LITERATURE SURVEY

"The noblest pleasure is the joy of understanding."

~ Leonardo da Vinci ~

Overview

Sections 3.2 and 3.3 present the distinctive physical properties of thorium compared to those of uranium. Section 3.4 discusses the operational properties of thorium-uranium fuel inside the core. Section 3.5 presents changing the moderation in the core to enhance core properties and Section 3.6 reports the experience on thorium-based fuel in terms of the composition, geometry, and configuration. Section 3.7 briefly describes the computational codes used for this project while Section 3.8 discusses neutronic and thermal-hydraulic coupling. Section 3.9 defines the design limits for the fuel design.

3.1 INTRODUCTION

Thorium-based fuel behaves differently in the core compared to conventional uranium fuel. The material, fertile and fissile isotope properties form the background to understanding why thorium-based fuel behaves differently. Section 3.2 gives the advantages and disadvantages in each category related to thorium and compares it to uranium.

The systematic literature review presented here is integral in understanding reactor physics when analysing thorium-based fuel in a standard PWR. The literature provides a solid foundation on the new thorium fuel design. All of these insights will form the basis of the methodology to design the proposed thorium-uranium fuel for the EPR.

3.2 MATERIAL PROPERTIES

ThO_2 is the thorium fuel form used in PWRs. The section below discusses the material properties for ThO_2 and compares them to the reference materials such as UO_2 and mixed oxide (MOX).

3.2.1 DISADVANTAGES

ThO_2 has a ~10% lower density than UO_2 as can be seen in Table 3-1, which can be seen as a disadvantage, due to the resultant lower concentration of heavy nuclei (Wah Lau, et al., 2012). However, a reduced density can result in better fission product retention within the thorium fuel matrix (Kazimi, et al., 1999). The thermal conductivity for ThO_2 is lower than for UO_2 and mixing

ThO_2 with UO_2 may cause a drop in the thermal conductivity to values below that of pure UO_2 (Yang, et al., 2004), which might affect the maximum fuel temperature.

TABLE 3-1 MATERIAL PROPERTIES OF DIFFERENT OXIDE FUELS (GRENECHE, 2010)

	ThO_2	UO_2	Units
Melting point	3573	3033	K
Theoretical density	10	10.96	g/cm^3
Thermal conductivity at 600°C	0.044	0.0452	W/cm/K

3.2.2 ADVANTAGES

ThO_2 is more stable and robust than UO_2 from a metallurgical and chemical point of view (Caner & Dugan, 2000). ThO_2 is the highest oxide of thorium and does not vary considerably from this stoichiometric composition when subjected to air or water at temperatures up to 2000 K (Herring, et al., 2001).

Pure ThO_2 has a higher melting point compared to UO_2. A higher melting point (as shown in Table 3-1) could permit higher safety limits and high thermal efficiencies (IAEA, 2012), which could merit the increase of the specific power and burnup for reactors utilizing pure ThO_2 (Trellue, et al., 2011). However, in homogeneous mixtures of ThO_2 and UO_2, the melting point is lower than that of pure ThO_2.

(ThO_2/PuO_2), UO_2 and MOX have comparable physical characteristics and occur in the face centered cubic (FCC) crystalline form. This property is important for manufacturing and for the stability of hybrid-oxide fuels and certainly allows the manufacture of very high burnup fuels (Lung & Gremm, 1998).

3.3 ISOTOPE PROPERTIES

In thorium-uranium fuel-cycles, three fissile isotopes mainly maintain the reactor's criticality: ^{235}U (the enrichment of the fresh fuel), ^{233}U and ^{239}Pu (produced by transmutation of the fertile isotopes ^{232}Th, and ^{238}U respectively). ^{235}U depletes during the life of the reactor and should be replaced by ^{233}U and ^{239}Pu bred throughout the lifetime. The ^{235}U concentration should be enough to establish the initial criticality of the reactor (García, et al., 2013).

3.3.1 FERTILE ISOTOPE PROPERTIES, ^{232}TH

Thorium is naturally available as ^{232}Th. This section discusses and compares the fertile isotope properties to the reference fertile isotope, namely ^{238}U. The transmutation chains for ^{232}Th and ^{238}U are in Figure 3-1 and Figure 3-2 respectively.

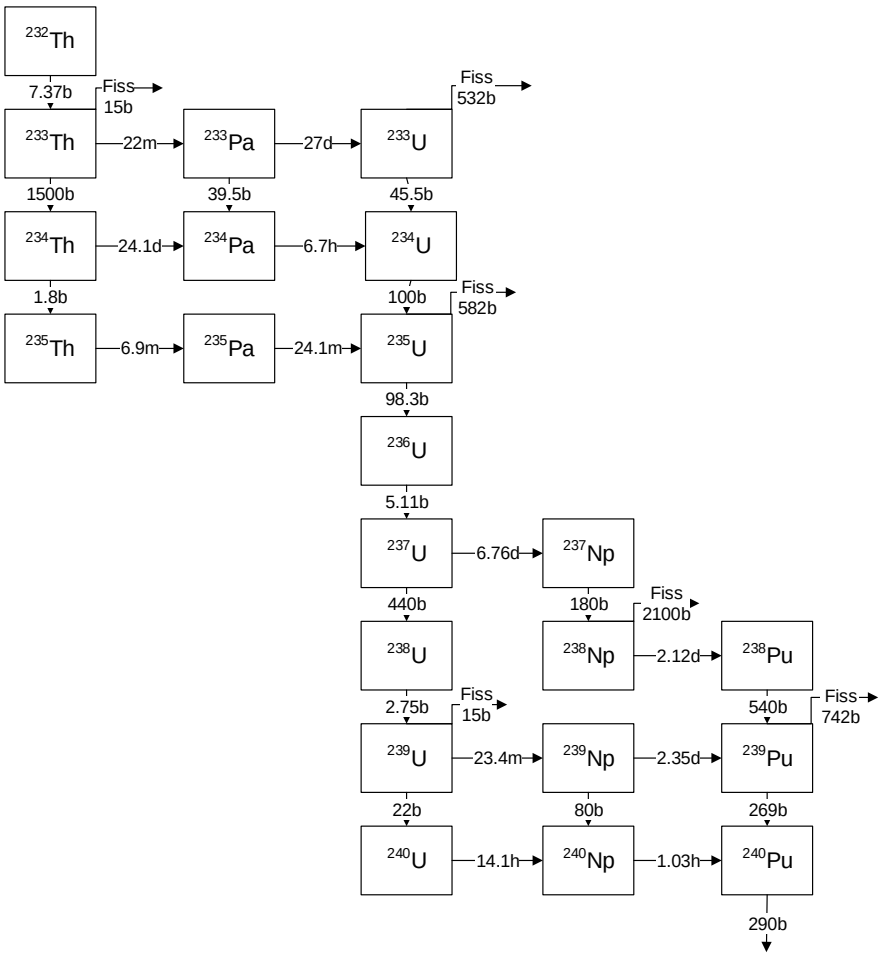

FIGURE 3-1 TRANSMUTATION-DECAY CHAIN FOR ^{233}TH (RUBBIA, 1999)

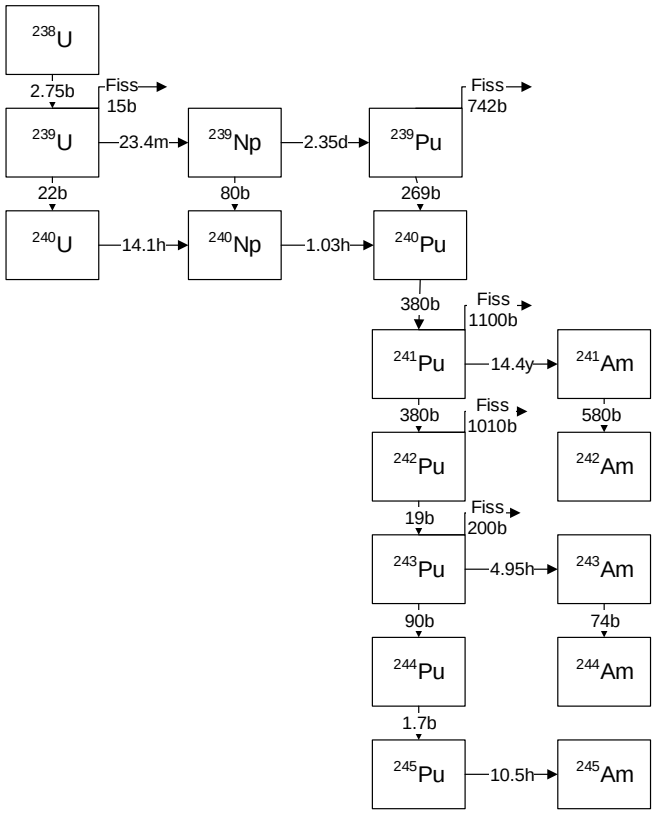

FIGURE 3-2 TRANSMUTATION CHAIN FOR ^{238}U (RUBBIA, 1999)

3.3.1.1 DISADVANTAGES

^{232}Th has a larger thermal neutron capture cross-section (to potentially breed ^{233}U) compared to ^{238}U (see Table 3-2), which would demand higher fissile enrichment requirements (Kim & Downar, 2001), in turn resulting in increased fuel cost. This has a significant impact on the conversion ratio (ratio of fissile material bred to fissile material consumed) (Puill, 2002). However, it can also be seen as an advantage, since ^{232}Th serves as a burnable absorber in the BOL. Due to the large thermal neutron capture cross-section of thorium, one can observe the neutron spectrum hardening (Wah Lau, et al., 2014).

The resonance integral (RI) for the neutron capture cross-section of ^{238}U is around three times larger than that of ^{232}Th (Kim & Downar, 2001) (see Table 3-2), which could lessen the negative Doppler reactivity feedback in overpower transients (Kazimi, et al., 1999).

Figure 3-3 illustrates the absorption cross-sections for ^{232}Th and ^{238}U. Note the higher capture cross-section for ^{232}Th in the thermal neutron energy region. Figure 3-3 also shows larger and more resonance integrals for ^{238}U (also see Table 3-2). Although both fertile isotopes show an increased probability of neutron capture (and potentially breeding) in the epithermal neutron energy region, breeding ^{233}U is more desirable than breeding ^{239}Pu in terms of nuclear material proliferation.

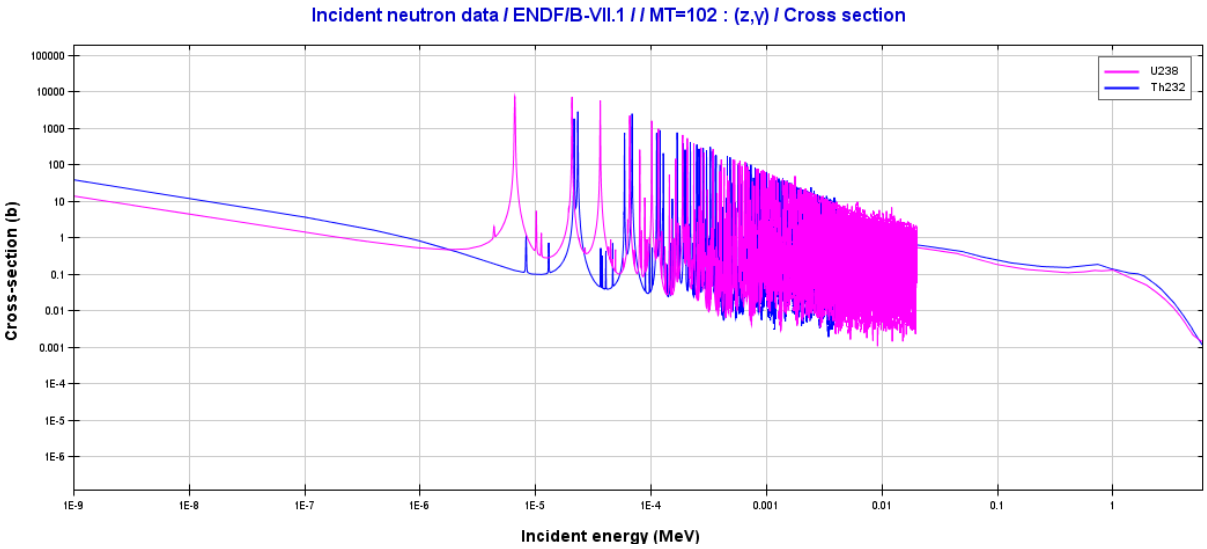

FIGURE 3-3 NEUTRON CAPTURE CROSS-SECTION OF FERTILE ISOTOPES

^{238}U has a lower fission threshold, as can be seen in Table 3-2 and the fission cross-section of ^{238}U in the fast-energy spectrum is between three and five times larger than ^{232}Th. However, the scope of this study focuses mainly on the PWR, which operates in the thermal to epithermal neutron spectrum. A lower fast fission cross-section will result in a more negative void coefficient for thorium-based fuel cores (Kim & Downar, 2001). Fast fission of ^{238}U contributes between seven and eight per cent of the total energy, compared to the two per cent of ^{232}Th (Puill, 2002).

TABLE 3-2 PROPERTIES OF THE FERTILE ISOTOPES OF THORIUM COMPARED WITH URANIUM

	^{232}Th	^{238}U	
Fission threshold	1.5[b]	0.8[b]	MeV
$\sigma_{c\ thermal}$	7.4[a,c]	2.7[a], 2.73[b], 2.683[d]	barn
RI at infinite dilution	85[a]	275[a], 272[b]	barn

[a] *(Greneche, 2010)*
[b] *(Puill, 2002)*
[c] *(Lamarsh & Baratta, 2001)*
[d] *(IAEA, 2013)*

3.3.1.2 ADVANTAGES

Thorium-based fuel presents a good breeding ratio at thermal neutron energies. High conversion rates from ^{232}Th to ^{233}U can be achieved in the thermal neutron spectrum due to the larger absorption cross-section of ^{232}Th, compared to ^{238}U (Kang-Mok & Myung-Hyung, 2005). The ratio of fertile absorption to parasitic absorption (neutron loss in the material) is higher for ^{232}Th than for ^{238}U (IAEA, 2012) making breeding for thorium fuels more effective. The thermal neutron capture cross-section of ^{232}Th is about three times larger than that of ^{238}U as shown in Table 3-2. Therefore, a comparable (but more efficient) breeding cycle similar to ^{238}U-^{239}Pu can be established with ^{232}Th-^{233}U (WNA, 2011).

Epithermal neutrons dominate the conversion of ^{232}Th to ^{233}U and could increase the conversion ratio in thorium-based fuel (Si, 2009). As stated in Garcia *et al.* breeding (^{238}U-^{239}Pu) in a uranium fuelled reactor is only possible with a fast neutron spectrum. For thorium-based fuels, breeding (^{232}Th-^{233}U) is possible within any type of neutron spectrum, thermal or fast (García, et al., 2013).

3.3.2 FISSILE ISOTOPE PROPERTIES, ^{233}U

3.3.2.1 DISADVANTAGES

^{233}U compared to ^{235}U has a lower delayed neutron fraction, β_{eff} (Trellue, et al., 2011). A lower delayed neutron fraction denotes a shorter reactor period, which can increase the likelihood of prompt criticality and make the system very sensitive during reactivity changes. Therefore, faster response of control systems during transients is required (Kazimi, et al., 1999).

One of the main weaknesses of thorium-based fuel is the high concentration and presence of ^{233}Pa in the transmutation chain of ^{233}Th displayed in Figure 3-1. ^{233}Pa has a long decay period (27 days) when compared with ^{239}Np (2.3 days) in the uranium cycle. The longer half-life of ^{233}Pa extends the time where the reactivity after shutdown will increase due to the build-up of ^{233}U (Herring, et al., 2001; WNA, 2011; Lung & Gremm, 1998). This would imply longer refuelling shutdown times.

^{233}Pa is also a strong absorber of neutrons, even stronger than ^{232}Th as seen in Figure 3-4. This, in turn, reduces the ^{233}U production (WNA, 2011; Lung & Gremm, 1998) and can lead to a significant reduction of the conversion factor during the lifetime of the reactor (Greneche, et al., 2007; Ghrayeb, 2008).

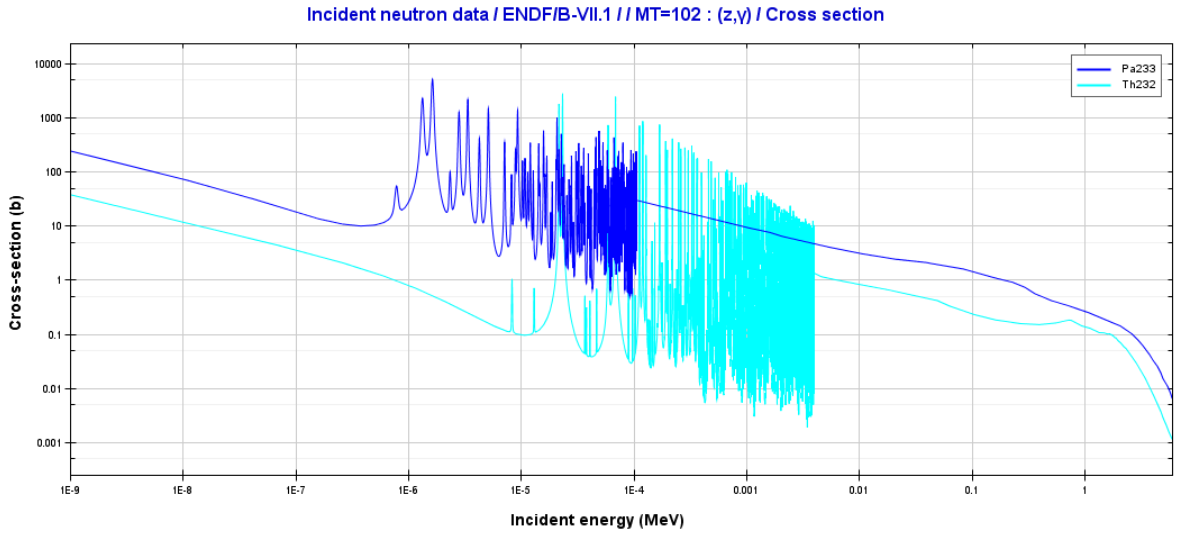

FIGURE 3-4 NEUTRON CAPTURE CROSS-SECTION OF ^{233}PA

A lower recoverable energy per fission of ^{233}U (see Table 3-3 below) requires more fissions per unit energy production, which in turn points to slightly more fuel (or higher enrichment) required to maintain the same power level as enriched uranium fuel (Trellue, et al., 2011). ^{233}U produces more fission gases, although with better retention capability of these gases in the fuel matrix (Kazimi, et al., 1999).

TABLE 3-3 COMPARISON OF NUCLEAR PROPERTIES FOR ALL THE FISSILE ISOTOPES

	^{233}U	**^{235}U**	**Units**
η_{th}	2.29[a], 2.27[b], 2.287[d]	2.07[a], 2.06[b], 2.068[d]	Neutrons/fission
η_{epi}	2.16[b]	1.67[b]	Neutrons/fission
Q	200.29[e]	202.61[e]	MeV/fission
Half-life	59.2 x 10^{3}[c]	703.8 x 10^{6}[c]	years
$\sigma_{c\ thermal}$	46[b], 47.7[d]	101[b], 98.6[d]	barn
$\sigma_{f\ thermal}$	525[b], 531.1[d]	577[b], 582.2[d]	barn
β_{eff}	270[a], 310[f]	650[a], 690[f]	pcm
^{135}I fission yield	0.0475[d]	0.0639[d]	atoms/fission
^{135}Xe fission yield	0.0107[d]	0.00237[d]	atoms/fission
^{149}Pm fission yield	0.00795[d]	0.01071[d]	atoms/fission
Combined yield	0.066[d]	0.077[d]	atoms/fission

[a] *(Greneche, 2010)*
[b] *(Puill, 2002)*
[c] *(Shultis & Faw, 2002)*
[d] *(Lamarsh & Baratta, 2001)*
[e] *(Trellue, et al., 2011)*
[f] *(Kazimi, et al., 1999)*

3.3.2.2 ADVANTAGES

^{233}U has the highest neutron yield among all the fissile isotopes at thermal neutron energies (Trellue, et al., 2011). This high value of η for ^{233}U results in much smaller swings of fissile content and reactivity than fuel-cycles using ^{235}U. Over the core lifetime, power peaking is less compared to uranium cores, which makes thorium-fuelled reactors more controllable (Greneche, et al., 2007).

^{233}U has a high neutron fission cross-section and low neutron capture cross-section, lower than ^{235}U as seen in Table 3-3. This low neutron capture cross-section of ^{233}U limits unwanted transmutation. The ratio of production to absorption by fission of ^{233}U is ~2.29, which is high in comparison to the other fissile isotopes and points to possibilities of a thermal breeding reactor (Puill, 2002).

At epithermal neutron energies, η for ^{233}U varies the least among fissile isotopes, which reduces the reactivity effects of changes in the neutron spectrum due to coolant transients. Neutron spectrum hardening affects ^{232}Th-^{233}U fuels less (when the neutron spectrum moves to more epithermal energies) (Kazimi, et al., 1999). Therefore, the nuclear parameters of ^{233}U, such as the cross-sections and η have a significant weaker dependence on power and temperature, than for ^{235}U, which eases reactor safety and operation when changing from cold to hot conditions (Greneche, et al., 2007).

^{232}U is seen as an undesirable by-product in thorium-based fuel-cycles, due to the daughter products emitting high-energy gamma rays (Hania & Klaassen, 2012), but the presence of ^{232}U is also the reason why thorium-based fuel has stronger proliferation resistance.

The production of important FPs such as Xe, Sm, etc. is considerably lower for ^{233}U, compared to that of ^{235}U and ^{239}Pu. This means that the average neutron absorption cross-sections of the FPs of ^{233}U decreases by about 25-30%, which results in reduced reactivity losses and increased core lifetime (Greneche, et al., 2007) (see Table 3-3 for the most important fission product yields).

3.4 IN CORE BEHAVIOUR

Sections 3.2 and 3.3 describe the specific properties for each isotope. Section 3.4 presents the combination of all these properties to help one understand the resulting effects by mixing thorium and uranium. One expects the properties of ^{235}U to dominate at the beginning of life but as ^{232}Th breeds ^{233}U, the properties of ^{233}U will become more pronounced.

Thorium fuel types demonstrate notably higher conversion rates compared with UO_2-fuel, which allows efficient fuel utilization in PWRs (IAEA, 2012). Thorium-uranium fuel cycles are technically viable in modern PWRs (Saglam, et al., 2003) and can replace UO_2 fuel without too much

mechanical rework (Joo, et al., 2003). This section also reports on some ideas for handling the difference in behaviour of thorium-based fuel.

3.4.1 BURNUP

Homogeneous (ThO_2/UO_2)-fuel has a slightly decreased burnup compared to typical UO_2 fuel with the same ^{235}U initial loading, especially when used with short cycle-length fuel reloading strategies (Joo, et al., 2003). (ThO_2/UO_2)-fuel requires a higher initial enrichment to achieve acceptable burnups (Weaver & Herring, 2002). A higher enrichment may require more burnable absorbers to offset the excess reactivity at the BOL, but the addition of thorium can decrease the reactivity at beginning of life and reactivity swing during life, due to the higher thermal neutron capture cross-section of ^{232}Th (Wah Lau, et al., 2012; Tucker, et al., 2015; Galperin, et al., 2001). The addition of thorium may decrease the amount of burnable poison needed, resulting in a more balanced power distribution between assemblies (Wah Lau, et al., 2012). Power peaking problems are easier to manage and lower reactivity swings ease operation for the thorium cycle (Kok, 2009).

Reactors using (ThO_2/UO_2)-fuel present more stable reactivity (k_{eff}) during long burnups than a UO_2 fuelled reactor, and this is due to thorium's conversion to ^{233}U (Herring, et al., 2001). In other words, the gradient of the reactivity vs. burnup graph is flatter for thorium fuel than with enriched uranium, which implies that less ^{235}U is required to reach the same discharge burnup. The infinite neutron multiplication factor has the potential to be higher at end of life (EOL), which could possibly increase the power at EOL (Wah Lau, *et al*., 2013). (ThO_2/UO_2) cores designed for long cycles and high burnup might require less enrichment, less separation, and less total heavy metal feedstock than a UO_2 core of the same cycle-length. High burnup (ThO_2/UO_2)-fuels will improve the weapons material proliferation-resistance in three aspects. Generation of separable weapons material will be less because the major fertile material is ^{232}Th and not ^{238}U. Extended refuelling periods will make diversion less probable and the isotopic content of the plutonium will be much less attractive for use in weapons (Herring, et al., 2001).

As ^{233}U builds into the fuel, recoverable energy per fission decreases, due to the smaller Q of ^{233}U compared to ^{235}U (see Table 3-3). A lower recoverable energy per fission (of ^{233}U) results in slightly more fuel to maintain the same power level as conventional UO_2-fuel (Trellue, et al., 2011). This may be more complicated due to other competing reactions and becomes prominent at later stages in the fuel-cycle when sufficient amounts of ^{233}U are present.

3.4.2 DELAYED NEUTRON FRACTION

The effective delayed neutron fraction of (ThO_2/UO_2) and UO_2 fuels is similar at BOL, due to the same main fissile isotope, ^{235}U. As the cycle progresses the fuel composition changes and β_{eff} is reduced due to the production of the fissile nuclide ^{233}U (^{233}U has a lower β_{eff} than ^{235}U, see Table 3-1). This is also the case with UO_2 fuels, due to the production of ^{239}Pu from ^{238}U (IAEA,

2012). A smaller β_{eff} may lead to difficulties during reactivity-initiated accidents (RIAs) (Fridman & Kleim, 2011) and these cores have a smaller margin to prompt criticality compared to conventional cores (Björk, et al., 2013). Nonetheless, the more negative Doppler Coefficient (DC) discussed in Section 3.4.3 may potentially compensate for this effect (Fridman & Kleim, 2011).

3.4.3 REACTIVITY COEFFICIENTS

The neutronic parameters in PWR cores with thorium–based fuels are within the range of current PWRs (Tsige-Tamirat, 2011). The Doppler and moderator temperature coefficients were noticeably more negative, but still within acceptable limits (Joo, et al., 2003; Dziadosz, et al., 2004). In general, the more negative MTC in (ThO_2/UO_2)-fuel will normally cause a comparatively lower AO compared with the standard core (Wah Lau, et al., 2014).

A major contribution to the more negative DC is the lower resultant resonance escape probability and the higher total capture reaction rates. Mixing two strong resonance absorbers such as ^{232}Th and ^{238}U adds more resonances peaks, reducing the resonance escape probability, which in turn enhances the Doppler effect (Wah Lau, et al., 2014).

The stronger negative feedback, like the Doppler and moderator temperature reactivity coefficients, results in the lower control-rod worth, which reduces the SDM (Wah Lau, et al., 2013) and makes thorium-based fuel more prone to cool down incidents or water temperature swings (Wah Lau, et al., 2012) than UO_2 cores (Dziadosz, et al., 2004). However, Lindley and Parks suggest that it might improve the performance during transients (Lindley & Parks, 2012).

3.4.4 CONTROL WORTH AND BURNABLE ABSORBERS

Reactivity worth is less due to the existence of high amounts of thermal absorbers (Björk, 2012; Dziadosz, et al., 2004). Thorium-based cores would require more dissolved boron at the Beginning of Life (BOL) when a higher initial enrichment is required. However, the maximum boron concentration is limited, due to the risk of the MTC becoming positive (Dziadosz, et al., 2004). This can possibly complicate the reactivity control and lower the SDM. The reduced reactivity worth is a familiar phenomenon for MOX-fuelled cores and does not lead to any operational limitations in modern LWRs (Björk, 2012). However, Saglam found that (ThO_2/UO_2) fuel-cycles have an inclination to have lower soluble boron concentration and burnable poison (BP) needs to be compared to conventional uranium fuel-cycles (Saglam, et al., 2003). The control-rod worth will depend strongly on the composition, enrichment and intended fuel cycle-length of the thorium-uranium fuel and can differ from study to study.

Gadolinium replaces some uranium, reducing the ^{235}U content while introducing an added resonance absorber into the (ThO_2/UO_2)-fuel (Saglam, *et al*., 2003). Adding Gd_2O_3 to fuel lowers the thermal conductivity, therefore the lowest possible Gd_2O_3 enrichment is better in order to elude high power in gadolinium-containing rods. Also (ThO_2/UO_2)-fuel is already a mixed oxide

and adding Gd_2O_3 would require a ternary mixture, which will hinder the fuel-fabrication process (Björk, et al., 2013).

Studies have suggested different burnable absorber designs for thorium-mixed fuel. Bjork proposed the Integral Fuel Burnable Absorber (IFBA) design, which adds a thin layer of zirconium boride to the surface of the fuel pellets (Björk, et al., 2013). Wet Annular Burnable Absorber (WABA) rods, where cladding and water surround a small burnable poison ring were also suggested (Fridman & Kleim, 2011). Saglam recommended discrete burnable poison rod assemblies (BPRAs) to help control reactivity and radial power peaking.

3.4.5 FEASIBILITY AND SAFETY

(ThO_2/UO_2) can replace UO_2 without large nuclear design limits changes (Joo, et al., 2003). The safety parameters in PWR cores with thorium–based fuels are within the range of current PWRs (Tsige-Tamirat, 2011). Wah Lau *et al*. proposed a uranium-thorium design (which requires less gadolinium) that resulted in the reduction of the pin peak power at BOL. Operation and safety are easier because the margin to reach DNB becomes larger (Wah Lau, et al., 2012).

Slight adjustments are required for current LWRs to increase core (ThO_2/PuO_2) loading above 33.3% of the total fuel assemblies to adhere to reactivity safety limits, however, this is also required for MOX fuel (Trellue, et al., 2011). Francois *et al*. proved that a 100% MOX fuel loading is possible in PWRs with added water rods or decreased fuel diameter, increasing the moderation, which increases the fissile consumption rate (Francois, et al., 2002). Thorium mixed-oxide fuel behaves similarly than MOX fuel (Hania & Klaassen, 2012) and recent reactor designs are capable of running 100% MOX (Björk, 2012).

3.4.6 FUEL PERFORMANCE AND THERMAL-HYDRAULICS

(ThO_2/UO_2)-fuel cycles have an inclination to have lower power-peaking factors (Saglam, et al., 2003). They have a notably higher thermal conductivity at low temperatures with a higher melting temperature. (ThO_2/UO_2)-fuel can operate in slightly cooler conditions and retain more FPs in the fuel during normal operation. This means that (ThO_2/UO_2)-fuel can achieve higher burnups, which will extend fuel-cycles, improve plant capacity factors and reduce the number of spent fuel (SF) bundles to handle (Herring, et al., 2001). Increased thermal conductivity results in a lower fuel pellet temperature, less swelling, less PCMI (Pellet Cladding Mechanical Interaction) and a larger margin for fuel melting (Björk, 2012).

(ThO_2/UO_2) combinations have slightly higher decay heat, lower thermal conductivity at very high temperatures and exhibit higher fission gas production. During accident conditions such as a large break loss-of-coolant accident (LOCA), (ThO_2/UO_2)-fuel will have less stored energy, but a somewhat higher internal heat production rate compared with UO_2-fuel. This will change the

settings for the maximum cladding temperature and the timing to fuel rod rupture (Herring, et al., 2001).

Wah Lau *et al*. proved that an equilibrium (ThO_2/UO_2) core can have a 33% reduced maximum AO due to the stronger MTC and an 8% lower minimum AO compared with a standard uranium core, due to a more homogenous radial power distribution. Incorporation of uranium-thorium-based fuel in a PWR can enhance thermal margins, due to improved pin peak power and an improved axial distribution. This could permit more adaptable core designs with lower neutron leakage, or be used for power uprates while adhering to safety margins (Wah Lau, et al., 2013).

3.4.7 WASTE

(ThO_2/UO_2) is subject to corrosive attack in air or oxygenated water, but considerably less than UO_2. This makes (ThO_2/UO_2) a better type of waste than UO_2 (Herring, et al., 2001). Introducing mixed (ThO_2/UO_2)-fuel in conventional PWRs reduces the plutonium production rate by 45% and save about 10% of natural uranium requirements (Galperin, et al., 2001). For thorium-based fuel, the decay heat increases after 2000 years due to the ^{233}U decay chain (Ashley, et al., 2014). When thorium replaces ^{238}U as the fertile element, the quantity of trans-uranic isotopes in the spent fuel (SF) reduces by two orders of magnitude (Hania & Klaassen, 2012).

3.5 MODERATION

Many studies have evaluated increasing or decreasing the moderation in the core to enhance different properties that are directly affected by the neutron spectrum (Björk, 2012; Fridman & Kleim, 2011; Mozafari & Faghihi, 2013; Permana, et al., 2008; Todosow & Kazimi, 2004; Trellue, et al., 2011; Waris, et al., 2009; Xu, 2003; Lindley & Parks, 2012; Lindley, et al., 2014). This is also known as spectrum shift moderation control by adjusting the MFR (moderator to fuel ratio), or Vm/Vf ratio, or H/HM (hydrogen to heavy metal) ratio.

A value of 1.95-2 for the MFR is typical for a standard PWR (Permana, et al., 2008; Todosow & Kazimi, 2004). The standard H/HM Ratio for PWRs is 3.4 and is by Eq. 3-1:

$$\frac{\mathrm{H}}{\mathrm{HM}} = 2 \times \frac{M_{fuel}}{M_{H_2O}} \times \frac{\rho_{H_2O}}{\rho_{fuel}} \times \frac{V_{H_2O}}{V_{fuel}} \qquad \text{Eq. 3-1}$$

Where: M is the atomic weight, ρ is the density and V is the volume (Weaver & Herring, 2002).

3.5.1 REDUCED MODERATION

A reduced moderated system can also be described by a low MFR, -Vm/Vf ratio, or -H/HM ratio. Lindley *et al.* achieved reduced moderation by a tighter pitch or thicker fuel pellets (Lindley, et al., 2014).

3.5.1.1 ADVANTAGES

When the system moderation is reduced, more epithermal neutrons are present (spectrum hardening), which favours the ^{232}Th-^{233}U conversion reaction. More neutrons will be absorbed in the resonances of ^{232}Th resulting to a more negative MTC (Wah Lau, et al., 2012; Todosow & Kazimi, 2004). Reduced moderation results in reduced production of certain Minor Actinides (MAs), enhanced discharge burnups and cycle-lengths while saving enrichment requirements (Lindley & Parks, 2012; Kim & Downar, 2001). Thorium-based fuel has the potential of enhanced safety characteristics in reduced moderated systems, compared to conventional uranium fuels, due to the lower RI (see Section 3.3.1) and higher fast fission threshold of ^{232}Th (Kim & Downar, 2001).

3.5.1.2 DISADVANTAGES

Unfortunately, the control-rod worth decreases in reduced moderated systems. Therefore, the use of soluble boron (SB) and B_4C enriched in ^{10}B is desirable (Björk, 2012). Reduced moderation can also make the void coefficient (VC) positive in some cases where thorium was mixed with plutonium, but enriched (^{10}B) soluble boron can alleviate the problem (Lindley & Parks, 2012) and improve the MTC (Lindley, et al., 2014). However, Kim and Downar did not find a problem with the void coefficient for thorium-uranium fuel and it was still negative in the intermediate spectrum. Reduced moderation increases the slowing down time, which results in a greater loss of neutrons by resonance absorption, which increases the neutron absorption and leakage (Mozafari & Faghihi, 2013).

3.5.2 INCREASED MODERATION

An increased moderated system can also be described by a high MFR, -Vm/Vf ratio, or -H/HM ratio. Increased moderation happens by insertion of water holes, using annular fuel pellets, reducing fuel diameter or increasing the fuel pitch.

3.5.2.1 ADVANTAGES

When the system is in an increased moderated state the fission reaction of ^{233}U is favoured (Weaver & Herring, 2002). Increased moderation will help with the reduced worth of control materials and decrease the neutron leakage (Mozafari & Faghihi, 2013). Increasing the moderation decreases the slowing down time of neutrons, which results in smaller loss of neutrons by resonance absorption, which means that the reactivity feedback is less negative compared to reduced moderation (Rachamin, et al., 2013). A high MFR is desirable to reduce the ^{238}U-^{239}Pu conversion reaction since there are some amounts of uranium present in thorium-uranium fuels (Todosow & Kazimi, 2004). Increasing the H/HM ratio degraded the discharge isotopic content (Weaver & Herring, 2002).

3.5.2.2 DISADVANTAGES

The downfall of increased moderation is that it results in a higher initial excess reactivity. Annular fuel pellets containing BP in the central zone are a suggestion to reduce the BOC reactivity in high burnup fuels (Xu, 2003). However, BOC reactivity reduces due to ^{232}Th acting as a burnable absorber. Increased moderation results in more neutron captures in the water, and reduces the thermal utilization factor (Mozafari & Faghihi, 2013; Weaver & Herring, 2002).

3.6 FUEL

Section 3.6 discusses different fuel options in terms of geometry, composition, and positions. Discussion on heterogeneous- and homogeneous fuel and annular fuel follows. The section concludes with the suggested fuel compositions from previous studies, to form the basis for the new design.

3.6.1 HETEROGENEOUS AND HOMOGENEOUS FUELS

There are different ways of introducing thorium-based fuel in reactors. One option is homogeneous fuels where (ThO_2/UO_2) fuel rods replace each of the UO_2 fuel rods. In this case, thorium and uranium mix in such a way that they are not identifiable from each other.

The other is the heterogeneous configuration where the uranium fuel and thorium fuel are physically separate. The fuel can be separated by means of separate thorium or uranium assemblies (seed and blanket), or separate thorium and uranium fuel pins inside one assembly or where both uranium and thorium are distinctly included within a single fuel rod.

Heterogeneous configurations can be more flexible, but the fuel management and reloading are more complicated (Todosow & Kazimi, 2004; Kang-Mok & Myung-Hyung, 2005). Heterogeneous (ThO_2/UO_2)-fuel does not necessarily increase burnup (Nuttin, et al., 2012) due to the thorium segments that are always sub-critical (Galperin, et al., 2001). However, MIT recommended the (ThO_2/UO_2) duplex fuel design with the thorium on the perimeter of the core and the uranium in the middle, which increases the discharge burnup compared with homogeneous (ThO_2/UO_2)-fuel (Joo, et al., 2003). The k_∞ can be improved by using heterogeneous (duplex) fuel, but additional investigation is necessary (Lindley & Parks, 2012).

A seed and blanket thorium-uranium design for the EPR exists. The decay heat for both the seed and blanket assemblies exceeded that of the reference EPR assembly although less SF discharge occurs in the life of the reactor (Ashley, et al., 2014). Kang-Mok and Myung-Hyun proposed a heterogeneous thorium-based assembly design that had similar neutronic performance, but a reasonably higher power peaking factor than that of conventional PWRs (Kang-Mok & Myung-Hyung, 2005).

Due to higher power peaking and more complex fuel management in heterogeneous fuel, the decision was for the design to be homogeneous as far as possible. Further studies can investigate modifying the EPR with heterogeneously mixed fuel.

3.6.2 FUEL COMPOSITION

In homogeneous thorium-uranium fuel, ThO_2 is mixed with UO_2. The UO_2 portion contains the fissile material where ThO_2 only contains fertile material. To adhere to the definition of the low-enriched uranium (LEU) non-proliferation limit, the local enrichment of uranium (^{235}U) in the UO_2 portion is limited to less than 20 wt.% (Weaver & Herring, 2002). By adding ThO_2 to the 20 wt.% UO_2, thorium will dilute the overall fissile content depending on the mixture.

The fractions of UO_2 and ThO_2 are adjusted in such a manner to obtain an initial overall fissile content between 6.5 wt.% -8 wt.% as shown in Table 3-4. It is noted that the required initial overall fissile content is higher than for normal UO_2-fuels. Table 3-4 shows compositions for homogeneous thorium-uranium fuel designed for 24-month fuel-cycles.

TABLE 3-4 FUEL COMPOSITIONS FOR PROPOSED (THO_2/UO_2)

	UO_2 fraction[a]	**ThO_2 fraction[a]**	**Enrichment[a]**	**Overall initial fissile content[b]**	**Burnup**
(Herring, et al., 2001)	32.5	67.5	20.0	6.5 wt.%	80.0 MWd/MT
(Saglam, et al., 2003)	37.3	62.7	19.5	7.3 wt.%	74.4 MWd/MT
(Galperin, et al., 2001)	35.0	65.0	20.0	7.0 wt.%	76.0 MWd/MT
(Joo, et al., 2003)	40.0	60.0	19.5	8.0 wt.%	80.0 MWd/MT

[a.] *wt.%*

[b.] *Initial fissile content= UO_2 Fraction x Enrichment*

Table 3-4 shows that to reach an overall initial fissile content of ~7 wt.% one needs to mix ~35 wt.% UO_2 with ~65 wt.% ThO_2. The overall initial fissile content (±7.2 wt.%) required to reach longer fuel-cycles is marginally (about 2.7 wt.%) higher than conventional uranium cycles, which require an initial fissile content (or enrichment) of ~4.5 wt.%. Considering all these references, the initial ^{235}U loading should be between 6.5- and 8 wt.% to reach 24-month fuel-cycles and burnups of 75-80 MWd/MT (Herring, et al., 2001; Saglam, et al., 2003; Galperin, et al., 2001; Joo, et al., 2003). Note that the suggested fuel compositions have only one fuel material definition in the axial direction and that these fuels were designed for Gen 2 PWRs.

3.6.3 ANNULAR FUEL

Although the studies below suggest increased benefits for annular fuel, replacing current uranium fuel with less dense thorium-uranium fuel will affect the total power and neutron spectrum. Changing the fuel to annular pins will alter the power and spectrum even further. Annular fuel will change the basic design of the reactor and one of the main goals of this study is to keep the original EPR dimensions, hence, the decision to study fuel properties systematically.

Investigation annular fuel pins will therefore be the follow-on step in the process after changing the composition and proving the feasibility. Annular thorium-uranium fuel pins in new generation PWRs with power up-rates are a suggestion for further studies.

Saidinezhad and Hamieh found that sintered annular fuel pellets have a lower fission gas release than solid PWR pellets (at the same power density). The cladding hydrogen concentration and oxide accumulation are similar to solid fuel. Annular fuel is also robust against flow instabilities and density wave oscillations (Saidinezhad & Hamieh, 2012).

Annular fuel pellets offer extra fuel rod plenum volume, which reduces the RIP (Rod Internal Pressure) and increases of the moderator-to-fuel ratio, which can increase the k_{eff} value (Mozafari & Faghihi, 2013). The annulus reduces the pellet average temperature and peak temperatures of the fuel, due to a shorter conduction path and heat removal from inner and or outer sides of fuel rod. This makes higher burnups more achievable and improves the safety limits (for instance increasing the DNBR margin) for different transient and accident scenarios (Xu, 2003; Mozafari & Faghihi, 2013).

An evaluation of the costs related to manufacturing annular fuel showed that there should be negligible manufacturing cost effects. Using annular fuel to uprate the power levels of PWRs can significantly increase the return on investment (ROI) (Lahoda, et al., 2007). One study assessed the thermal-hydraulics performance of annular pins of a typical Westinghouse four-loop PWR and showed that a power up-rate of 50% is achievable with only a slight increase in the coolant flow rate. The Korean OPR-1000 showed a 20% increase in power density with the same coolant flow rate (Mozafari & Faghihi, 2013).

However, the increase of the surface area results in larger pressure drops over the fuel rods and therefore on the Fuel Assembly (FA) (Mozafari & Faghihi, 2013).

3.7 ANALYSIS TOOLS

This study uses the MCNP6 code for neutron transport, criticality, and burnup calculations. RELAP5 is the thermal-hydraulic code used for estimating the temperatures of the fuel, cladding, and moderator. The following sections provide some related features of these two codes. The reader is referred to (LANL, 2013) and (RELAP, 2001) for further detail concerning MCNP6 and RELAP5 respectively.

3.7.1 MCNP6

To ensure that the results are accurate and close to reality, high-fidelity multi-physics codes are the ideal choice, unfortunately, the disadvantage is that these codes have high computational requirements. One such code is MCNP6 and a more detailed discussion follows.

MCNP5 is as a worldwide satisfactory and useful code (Mozafari & Faghihi, 2013). MCNP6 (Monte Carlo N-Particle) is the current generation of a chain of Monte Carlo transport codes that was developed at Los Alamos National Laboratory almost sixty years ago. MCNP6 is the result of a multi-year effort to unite the MCNP5 and MCNPX codes into a single product, including all features of both codes with some additional feature such as including physics model options for energies above the cross-section tabular range. MCNP6 is a three-dimensional code that has exact geometry modelling, and can run in parallel with OpenMP and/or MPI. MCNP6 uses the Monte Carlo probabilistic technique to attain solutions by modelling discrete particles and documenting certain quantities (tallies) of their average behaviour.

MCNP6 uses a so called continuous energy scale for the cross-section data. The code provides a diverse description of the source with adaptable tallies. MCNP6 has an S(α, β) feature that models the thermal scattering for example for hydrogen in light water (Odoi, et al., 2014). An additional code called MAKXSF (part of the distribution of MCNP6) can create cross-section libraries from existing libraries for instance; Doppler broadening of resolved cross-section data, interpolating thermal scattering kernels and interpolating unresolved resonance cross-section data between two temperatures (Bennett, 2015). MCNP has been used in many recent studies such as (Ghrayeb, 2008), (Faghihi, et al., 2011) and (García, et al., 2013).

MCNP6 is broadly utilised for reliable particle transport and fuel burnup calculations. The burnup calculations use the CINDER90 module, a transmutation code used comprehensively in nuclear investigations, which utilizes decay and energy integrated reaction rate probabilities along with fission yield information (Chiang, et al., 2014; Lorenzo, et al., 2013). MCNP6 completes individual criticality calculations for each time-step, thereafter CINDER90 changes the isotopic composition based on the neutron interaction rate in the criticality calculation. This process continues until an accurate long-term reactivity calculation is complete. MCNP6 is able to follow hundreds of fission product isotopes (FPs), depending on the level of the tier of fidelity defined by the user. Tier 1 uses the 12 most common FPs, 87 in Tier 2 and 220 for Tier 3 (Holschuh, et al., 2013). When the number of nuclides included is increased, the accuracy increases, unfortunately with a computational penalty. The library, ENDF/B VI.2, includes isotope decay and interaction probability data for 3400 isotopes, including ~30 fission yield sets and yield data for 1325 FPs (Lorenzo, et al., 2013).

MCNP6 utilizes an iterative procedure called the predictor–corrector method to take into account the time-based changes of isotope inventories and the neutron fluxes at the specified time-steps. The beginning of each time-step calculates the fluxes, and then the predictor step runs CINDER90 depletion to the middle of the time-step to obtain half time-step isotopic composition. With the new material composition, MCNP6 recalculates the half time-step one-group cross-sections and neutron fluxes. This assumes that half-time-step cross-sections and fluxes represent a realistic estimate over the full time-step. Then, half time-step values are utilised to

perform depletion calculation for full time-step (Bomboni, et al., 2010; Chiang, et al., 2014; Stankovskiy & Van den Eynde, 2012).

3.7.1.1 VALIDATION

Mosteller outlines the validation suites for MCNP criticality and radiation shielding (Mosteller, 2002) and all cases described in the suites are based on applicable experimental data for achieving meaningful comparisons. Sartor describes the latest validation and verification on MCNP6 (Sartor, et al., 2015) and tests include a variety of geometries and fuels. The MCNP6 library, ENDF/B-VII.1 is also tested, verified and validated in (Little, 2012) and (Kahler, et al., 2012).

3.7.2 RELAP5

RELAP5, developed primarily by Idaho National Laboratory for the US NRC to utilize in rulemaking, licencing and audit calculation, evaluation of operator guideline, and as a base for nuclear plant analysis (Aghaie, et al., 2012) is the code used for thermal hydraulic system calculations.

Reactor Excursion and Leak Analysis Program (RELAP5) is a generic transient analysis code for thermal-hydraulic systems. RELAP5 solves the transient, non-equilibrium, inhomogeneous, two-phase flow physics using the six-equation, two-fluid model including heat transfer processes (McDeavitt, et al., 2005). One-dimensional stream-tube and conduction models estimate the fluid- and energy flow paths. RELAP is useful for reactor transient or steady-state case analyses where average, hot and cold channels are modelled (Anders, et al., 2012).

The code is applicable to LWRs and includes accident analysis such as loss-of-coolant accidents, transients without SCRAM, loss of feed, loss-of-offsite power, and loss of flow transients (RELAP, 2001).

3.7.2.1 VALIDATION

Validation of RELAP5/MOD3 is outlined in (Shieh, et al., 1994) and (Chen, et al., 1993).

3.7.3 NWURCS

The North-West University Reactor Code Suite (NWURCS) is a suite of codes developed in FORTRAN by the Mechanical and Nuclear Engineering team of the North-West University, which produces the input files for codes such as MCNP6 and RELAP5 (Naicker, *et al.*, 2015). The user manual and description of NWURCS is detailed in Naicker *et al.*

The development of NWURCS was to allow easier and automated setup of intrinsically complicated MCNP input files. Two main contributors to this complexity stems from characterising the temperature and the isotopic dependence as a function of position. Since the

input files can contain as many as 300000 lines, manual input file specification becomes error-prone and unnecessarily time consuming.

“NWURCS allows the user to describe each section of the MCNP input file separately. In this way, it is easy for the user to navigate through each section to confirm if there are any errors made before even running the calculations” (Nyalunga, 2015).

3.7.3.1 VERIFICATION

NWURCS and the developed model need verification to ensure that they produce the correct geometry with all the needed information as defined in the literature. Studies (Nyalunga, 2015) and (Montwedi, 2014) have verified major parts of NWURCS. Methods of verification include a visual inspection by using VISED and line-by-line checks on the MCNP input files of the geometry, materials, tallies, and control-rod movements.

3.8 COUPLING

3.8.1 INTRODUCTION

The temperature inside a reactor has major effects on the neutron interactions with material. Hence, coupling neutronics and thermal-hydraulic effects is very important given the relationship between the nuclear fission heat generation and the temperature of the system. This relationship also depends on the coolant density fluctuations, Doppler broadening of neutron interaction cross-sections (specifically fuel material), moderation, fission and thermal neutron scattering (Chiang, et al., 2014). By coupling the neutronics and thermal-hydraulic codes, the neutron transport equation and dynamic flow equations remain coupled. The coupled calculation provides accurate simulations in a reasonable amount of computational time without compromising on the fidelity of the reactor core model (Vazquez, et al., 2012).

A coupled model consisting of both a neutronic and a thermal-hydraulic component will result in a more accurate model. Nuclear engineers are very interested in using best-estimate methods that can predict the essential safety margins and coupled calculations can provide such a reliable analysis of reactor behaviour. Safety analysis of current and new reactors depends largely on the accuracy and the spatial detail of the models, which suggest the use of coupled 3D neutronic and 3D thermal-hydraulic codes. Tools that achieve coupling between neutronic codes (both deterministic and stochastic) and thermal-hydraulic codes are the recent focus of research globally (Vazquez, et al., 2012).

The neutronics code requires information on the temperature distribution, the density distribution, and the material composition. The neutronic transport code produces a power profile and a thermal-hydraulics code and then calculates a new set of temperatures of the coolant and

materials. During this coupling process, the core geometry representation should remain accurate. A sufficient number of coupled iterations result in a converged solution.

In general, two types of coupling methods are in use, internal or external coupling. Internal coupling or also known as serial integration includes modification of the source codes, typically by employing a neutronics segment into the thermal hydraulics code.

External coupling, loose coupling or the parallel processing approach uses the two individually validated codes discretely and exchanges information between calculations. Data exchange between the codes is through a shared file, message passing and or a driver programme. External coupling has the advantage of independently updating and maintaining each code. External coupling is less difficult to implement while internal coupling requires applying for and acquiring the source codes. External coupling extracts the data and creates new input files (after each iteration) where internal coupling does not require reading and writing between iterations. External coupling may introduce a bias in the results due to rounding off errors in the codes (Bennett, 2015). We chose external coupling for this study due to the difficulty obtaining source codes, difficulty understanding the syntax of the source codes and the fact the new modified code requires additional validation (Vazquez, et al., 2012; Aghaie, et al., 2012).

3.8.2 OTHER WORK

Table 3-5 shows some coupled systems with different neutronic and thermal-hydraulic codes. Each code has its own advantages and disadvantages.

TABLE 3-5 DIFFERENT WORK DONE ON COUPLING

Reference	Neutronic transport	Thermal hydraulics	Coupling method	Start with	Relaxa-tion	Convergence parameter
(Aghaie, et al., 2012)	WIMSD4 CITATION	RELAP5	External	CITATION	-	
(Vazquez, et al., 2012)	MCNPX	COBRA-IV	External	MCNP	Yes	T
(Zare, et al., 2010)	WIMS CITATION	COBRA-EN	External	CITATION	-	T
(Ivanov, et al., 2013)	MCNP	SUBCHAN-FLOW	External	SUBCHANFLOW	T	T
(Ponomarev, et al., 2015)	MCNP	SAS-SFR	External	SAS-SFR	P	
(Espel, 2010)	MCNP5 NEM NJOY	COBRA-TF	Internal	-	T	P
(Bennett, 2015)	MCNP6	CTF	Internal	CTF	P	T

T=Temperature; P=Power

MCNP is capable of acquiring results without major approximations in the geometry and with point wise cross-section representation, compared to codes such as WIMS and CITATION. Deterministic codes solve the transport equation with various forms of approximations whereas MCNP solves the more accurate radiation transport equation (Zare, et al., 2010). The use of continuous energy compared to the multi-group approach is more accurate and makes MCNP a better choice; however, deterministic codes requires much less computational time. MCNP calculations always have statistical convergence restrictions on parameters of interest (Vazquez,

et al., 2012). Due to the stochastic nature of MCNP, one needs to simulate a large number of particles to acquire reliable tally estimates. Therefore, most of the computation time of coupled calculations with MCNP will be on the MCNP calculations compared to thermal-hydraulics code calculation time (Ivanov, et al., 2013).

3.8.3 CHALLENGES

Some issues that arise when coupling are:

- The execution of the thermal-hydraulic/neutronic feedback mechanisms (Ivanov, et al., 2013),
- The management of convergence during the iterations (ibid.),
- The treatment of the temperature effects on nuclear data (ibid.),
- The more heterogeneous the system, the weaker the stability of the system (Vazquez, et al., 2012),
- The fact that the power calculated by MCNP has an uncertainty, limits the precision of the coupled solution (ibid.),
- The under-estimation of the relative error in MCNP (Nuttin, et al., 2013),
- Choosing the convergence criteria in the two sub codes (Zare, et al., 2010) and
- Data exchange between codes can introduce some errors in calculations (Zare, et al., 2010; Ponomarev, et al., 2015).

3.8.4 COUPLING STRATEGIES

To overcome some of these challenges the following are the suggested coupling strategies.

Chose the correct (or as close as possible) initial values whether it is power or temperature distribution, because they are key to the coupling (Ivanov, et al., 2013).

One suggestion is to approximate the nuclear data by using the pseudo-material method. This method uses a weighted mixture of a specific nuclide at a lower temperature and higher temperature by mixing cross-sections at two different temperatures into one material. There is no need of new cross-section data-generation, but the precision depends on the size of the interpolation interval. Different interpolation methods exist namely: linear, logarithmic or square-root (Vazquez, et al., 2012). For example, square-root interpolation is done by calculating the fractions f_1 and f_2 with a non-linear Eq. 3-2, where $T_{S1} < T < T_{S2}$ and T_{s1} and T_{s2} is the lower and higher pre-existing cross-section libraries respectively (Ponomarev, et al., 2015).

$$f_1 = \frac{\sqrt{T} - \sqrt{T_{S2}}}{\sqrt{T}_{S1} - \sqrt{T_{S2}}} \text{ and } f_2 = 1 - f_1 \qquad \text{Eq. 3-2}$$

Another suggestion is to use the NJOY99 module, called BROADR, to generate Doppler broadened continuous energy cross-sections for succeeding use in the MCNP simulations. However, this would require large amounts of computational time memory (Ivanov, et al., 2013).

3.8.5 RELAXATION

Vazquez suggested the use of a relaxation method when the convergence is slow, or the system is not stable (Vazquez, et al., 2012). Either the power or the temperature can be relaxed. As an example Eq. 3-3 calculates the new temperature applicable in the next neutronic transport calculation. Eq. 3-4 calculates the relaxed power applicable in the thermal-hydraulics calculation.

$$T_{ijk}^{N'} = T_{ijk}^{N}\omega + T_{ijk}^{N-1}(1-\omega) \quad \text{Eq. 3-3}$$

$$P_{ijk}^{N'} = P_{ijk}^{N}\omega + P_{ijk}^{N-1}(1-\omega) \quad \text{Eq. 3-4}$$

Where: $0 < \omega < 1$, N is the number of the current iteration, i is the x coordinate, j the y coordinate and k the z coordinate of the node. Ivanov *et al* suggested a value of $\omega = 0.5$ in Eq. 3-3 that leads to optimal results for a PWR case (Ivanov, et al., 2013).

Bennet suggested a different relaxation method, where the new power/temperature is the weighted average of all the previous iterations. This form of the relaxation technique is just a weighted function of the current value of the power/temperature and the previous value of the power/temperature. In this way, the variance reduces (converges faster) with each coupled iteration (Bennett, 2015). Eq. 3-5 calculates the new temperature and Eq. 3-6 calculates the new power in each node.

$$T_{ijk}^{N'} = \frac{1}{N}\sum_{n=1}^{N} T_{ijk}^{n} \quad \text{Eq. 3-5}$$

$$P_{ijk}^{N'} = \frac{1}{N}\sum_{n=1}^{N} P_{ijk}^{n} \quad \text{Eq. 3-6}$$

Where: N is the number of the current iteration, i is the x coordinate, j the y coordinate and k the z coordinate of the node.

3.8.6 CONVERGENCE

To achieve convergence for the temperature distribution or power distribution of the fuel, gap, cladding and coolant, the difference between two consecutive iterations must be smaller than a presumed value, which is called the convergence criteria.

The reactivity (measure of the difference in neutron multiplication factor) also needs to converge within certain criteria and Ponomarev used a value smaller than 20 pcm (Ponomarev, et al., 2015). Ponomarev could reduce the relative change (between iterations) of the relaxed node

power in the last iteration to smaller than 0.02% and the fuel temperature to 0.3 K, with some cases at 3-6 K.

Vasquez *et al*. suggested a convergence criterion ε determined by the maximum relative error (statistical uncertainty) in the first MCNP calculation, multiplied by three. Vasquez achieved a relative difference of 0.5% in the temperature. If one chooses a very small ε without considering the statistical uncertainty (tally relative error), the system is not likely to converge (Vazquez, et al., 2012).

The fuel temperature shows the largest fluctuations during the coupling and therefore Ivanov *et al* chose it as the convergence parameter. Eq. 3-7 calculates the temperature convergence criterion by the relative variation of the node averaged fuel temperature (Ivanov, et al., 2013).

$$\Delta T_{ijk}^{N} = \left| \frac{T_{ijk}^{N} - T_{ijk}^{N-1}}{T_{ijk}^{N-1}} \right| < \varepsilon \qquad \text{Eq. 3-7}$$

Where: T is the temperature, i is the x coordinate, j the y coordinate and k the z coordinate.

Bennet used convergence criteria on the temperature of 1% (Bennett, 2015) and Ivanov used 0.2% (Ivanov, et al., 2013). Espel used a convergence criterion of 0.01% in the relative errors of the node power between two successive coupled iterations (Espel, 2010).

Note that the convergence criteria can range from 0.01% up to 1%, depending on the accuracy of the MCNP calculation. The current study convergence criteria will be determined by the maximum tally relative error as discussed above.

3.9 DESIGN LIMITS

When designing fuel one has to adhere to certain safety and operational criteria. If these properties do not fall within the criteria, the fuel licence is in question. PWR fuel must adhere to the following design limits and criteria:

- $F_Q \leq 2.60$ including uncertainties (Fetterman, 2009)
- MTC ≤ 0pcm/K (Delgado, et al., 1999)
- DC ≤ 0 pcm/K (Delgado, et al., 1999)
- DNBR margin ≥ 15% (Fetterman, 2009)
- SDM ≥ 1.6%Δρ (NRC, U.S., n.d.; Fetterman, 2009); SDM ≥ 1300 pcm (Lindley, et al., 2014)
- $F_{\Delta H} \leq 1.65$ (Delgado, et al., 1999)
- RIP ≤ 2600 psia (Delgado, et al., 1999)
- Core critical boron concentration (CBC) ≤ 1780 ppm (Delgado, et al., 1999)

- Fuel centre-line temperature an adequate margin has to be provided to ensure operation below the melting temperature (2600±2800°C) (Delgado, et al., 1999)
- Clad outside surface temperature ≤ 673.15 K (Delgado, et al., 1999).

3.10 CONCLUSION

The systematic literature review presented is integral in understanding reactor physics when analysing thorium-based fuel in a standard PWR. However, new generation PWRs like the EPR will have some differences and therefore a study such as the current one becomes important. The literature provides a solid foundation for the new fuel design selection. Some important factors for consideration in the study are:

- Homogeneously mixed thorium-uranium fuel provides better thermal-hydraulic performance and eases fuel reloading compared to heterogeneously mixed fuel (Todosow & Kazimi, 2004; Kang-Mok & Myung-Hyung, 2005).
- Thorium-uranium fuel may have a more stable reactivity than normal uranium fuel, (due to better conversion of ^{232}Th-^{233}U) which might imply that less uranium enrichment is required when longer burnup cycles are the goal (Herring, et al., 2001; Galperin, et al., 2001).
- Thorium-uranium fuels for PWRs require a higher enrichment (+2.7 wt.%) to reach extended fuel burnup (24 months), than normal 18-month uranium fuel-cycles (Herring, et al., 2001; Galperin, et al., 2001; Saglam, et al., 2003; Joo, et al., 2003).
- Gadolinium will decrease the thermal conductivity of the fuel and to fabricate (ThO_2/UO_2) fuel by adding Gd_2O_3 would provide some difficulties (Björk, et al., 2013), therefore the use of gadolinium needs to be limited or eliminated.
- ^{232}Th has a high thermal neutron capture cross-section and acts as an absorber in the beginning of life (Wah Lau, et al., 2012) and can, therefore, play the role of gadolinium.
- The control materials worth is reduced and B_4C control-rods are suggested instead of typical CR compositions (Dziadosz, et al., 2004).
- The control materials worth is reduced and enriched soluble boron or more soluble boron may be at BOL (Dziadosz, et al., 2004).
- The delayed neutron fraction will become less at the end of cycle as the ^{233}U isotope becomes dominant; therefore, the same strategies that MOX cores use need to be adapted in thorium-uranium cores (IAEA, 2012).
- Adjusting the moderation can enhance certain properties of the fuel and potentially enhance the fuel-cycle.

All of these insights will form the basis of the methodology followed to design new thorium-uranium fuel for the EPR.

4. REFERENCE MODEL

"If your dreams don't scare you, they aren't big enough."

~ Lowell Lundstrum ~

Overview

In order to develop the proposed thorium fuel, the reference model development of the EPR core and simulations using MCNP6 code is essential. Verification of the developed reference model against the values reported in the FSAR is the next task. This verified reference model fuel used in the core will form the reference core and will be used later to compare with the thorium-uranium core. Section 4.1 introduces the purpose of the reference model. Section 4.2 describes the EPR in terms of geometry, safety, materials, burnup and thermal design. Section 4.3 states the assumptions and explains how this information is useful to develop the MCNP6 and RELAP5 models. Section 4.4 presents the results of the reference model and compares it against the FSAR.

4.1 INTRODUCTION

To comprehend the characteristics of introducing (ThO_2/UO_2)-fuel into a PWR, a model of the conventional UO_2-fueled reactor core is used. The calculations started with the original uranium fuel to verify the model and compare it against the already validated FSAR (see section 2.3.1). It forms the benchmark for the characterization and comparison of the newly designed thorium-uranium based fuel in Chapter 5.

4.2 EPR

The reference reactor for this study is the EPR by AREVA, under construction in Finland, China, and France. The EPR is a Generation 3+ PWR with added safety and improved efficiency. The EPR forms the basis of the developed model in this study and detailed discussions follow.

4.2.1 GEOMETRY AND MATERIALS

The EPR reactor core consists of 241 fuel assemblies (FA) in a 17x17 core lattice. These assemblies consist of 289 fuel rods with a 420 cm active fuel length, which is longer than the standard 366 cm. Fuel pins are arranged in a 17x17 lattice with the central rod being a fuel pin instead of the conventional instrumentation pin. The instrumentation pin is located at an off-centre position as indicated in Table 4-2. Twenty-four positions in the 17x17 fuel assembly lattice

are equipped with M5 Monobloc guide thimbles, which are locations for the Rod Cluster Control Assemblies (RCCAs). The core has 89 RCCAS with seven bank types; four banks (A-D) are for controlling and the remaining three are shutdown banks. The remaining FAs that do not have control-rod banks (152 FAs) can house in-core instrumentation. The U.S. EPR also includes a heavy reflector around the core periphery to reduce vessel irradiation and neutron leakage, which enhances fuel savings by 2-3% (AREVA, 2011). Table 4-1 shows the fuel geometry parameters of the EPR used to develop the model, extracted from the FSAR (AREVA, 2013).

TABLE 4-1 EPR PIN AND FA GEOMETRY

	Value	Units
Fuel rods per assembly	265	-
Control-rods per assembly	24	-
Fuel rod OD	0.819	cm
Cladding OD	0.950	cm
Cladding ID	0.836	cm
Fuel rod pitch	1.260	cm
Assemblies per core	241	-
Assembly pitch	21.417	cm
Active fuel height	420.00	cm

A feature of the EPR is the fact that the fuel pins have different axial enrichments. The EPR has seven types of fuel assemblies: A1, A2, B1, B2, C1, C2 and C3 as shown in Figure 4-1 with average enrichments shown in Table 4-3 (AREVA, 2013).

Figure 4-1 shows the fresh core-loading pattern. The highlighted FAs are the locations for the 89 RCCAs. The reloading pattern, initial and final positions of assemblies, and the number of fresh assemblies depends on the future power requirements, as well as past burnup and power histories of the FA’s (AREVA, 2013).

	1	2	3	4	5	6	7	8	9	10	11	12	13	14	15	16	17
1						A1	A1	A1	A1	A1	A1	A1					
2				A1	A1	C1	C1	C2	C2	C2	C1	C1	A1	A1			
3			A1	C1	C2	C3	B2	B2	C3	B2	B2	C3	C2	C1	A1		
4		A1	C1	C3	B1	B1	B1	A2	B2	A2	B1	B1	B1	C3	C1	A1	
5		A1	C2	B1	C3	B2	C3	B2	C3	B2	C3	B2	C3	B1	C2	A1	
6	A1	C1	C3	B1	B2	A2	B2	A1	B2	A1	B2	A2	B2	B1	C3	C1	A1
7	A1	C1	B2	B1	C3	B2	A1	B2	A1	B2	A1	B2	C3	B1	B2	C1	A1
8	A1	C2	B2	A2	B2	A1	B2	B1	B1	B1	B2	A1	B2	A2	B2	C2	A1
9	A1	C2	C3	B2	C3	B2	A1	B1	C2	B1	A1	B2	C3	B2	C3	C2	A1
10	A1	C2	B2	A2	B2	A1	B2	B1	B1	B1	B2	A1	B2	A2	B2	C2	A1
11	A1	C1	B2	B1	C3	B2	A1	B2	A1	B2	A1	B2	C3	B1	B2	C1	A1
12	A1	C1	C3	B1	B2	A2	B2	A1	B2	A1	B2	A2	B2	B1	C3	C1	A1
13		A1	C2	B1	C3	B2	C3	B2	C3	B2	C3	B2	C3	B1	C2	A1	
14		A1	C1	C3	B1	B1	B1	A2	B2	A2	B1	B1	B1	C3	C1	A1	
15			A1	C1	C2	C3	B2	B2	C3	B2	B2	C3	C2	C1	A1		
16				A1	A1	C1	C1	C2	C2	C2	C1	C1	A1	A1			
17						A1	A1	A1	A1	A1	A1	A1					

FIGURE 4-1 INITIAL CORE-LOADING MAP

Fuel assembly B1 has an average enrichment of 2.62 wt.% and is chosen as reference assembly since its enrichment is the closest to the full-core, which is 2.66 wt.%. Details of Fuel Assembly B1 are in the following paragraphs.

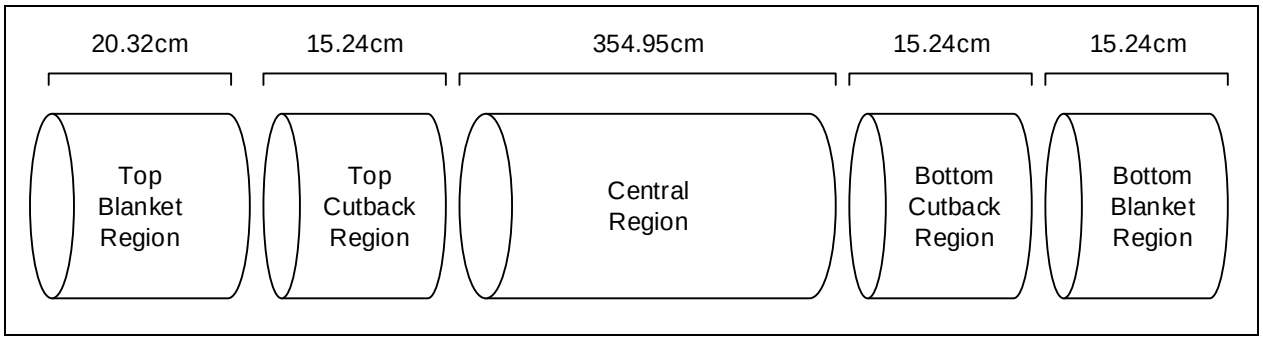

FIGURE 4-2 FUEL ROD AXIAL REGIONS (NOT TO SCALE)

As illustrated in Figure 4-2 there are five axial regions within each rod, viz. the top blanket region, top cutback region, central region, bottom cutback region and bottom blanket region. Note that the fuel pins are not axially symmetrical because of the length of the top blanket region being slightly longer in comparison with the bottom. The blanket regions have the lowest enrichment to minimize leakage to the top and bottom. The central region includes gadolinium to flatten the axial power and flux.

Assembly B1 has three different types of fuel pins, each with different axial enrichments. These three alternative pin types are distributed across the fuel assembly array. (see Table 4-2 for details of the axial enrichments and FA pin arrangement). The enrichments and fuel pin locations

in the FA provide maximum fuel utilisation and even intra-assembly power distribution while minimizing radial power peaking. Note that pin types 2 and 3 in the cutback regions feature a higher enrichment than the blanket and central regions and may result in higher power in these areas.

TABLE 4-2 FUEL ASSEMBLY B1 DETAILS (AREVA, 2013)

Axial Length (cm)	Zone	Composition			
		Pin type 1	Pin type 2	Pin type 3	
Number of pins		253	8	4	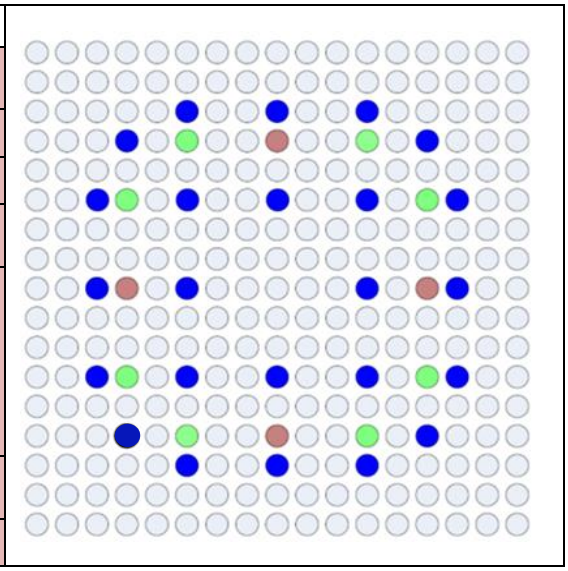
20.32	Blanket	2% ^{235}U	2% ^{235}U	2% ^{235}U	
15.24	Cut-back	2.7% ^{235}U	2.7% ^{235}U	2.7% ^{235}U	
354.95	Central	2.7% ^{235}U	1.89% ^{235}U 8% Gd_2O_3	2.56% ^{235}U 4% Gd_2O_3	
15.24	Cut-back	2.7% ^{235}U	2.7% ^{235}U	2.7% ^{235}U	
15.24	Blanket	2% ^{235}U	2% ^{235}U	2% ^{235}U	

**Composition in wt.%*

The other fuel assemblies (A1-C3) have similar layouts with the difference being different enrichments and the Gd concentration in the central regions. Table 4-3 shows average enrichments of the seven types of fuel assemblies: A1, A2, B1, B2, C1, C2 and C3 with (AREVA, 2013). See Appendix A for descriptions of the rest of the fuel assemblies in the EPR.

TABLE 4-3 INITIAL AVERAGE FA ENRICHMENT

FA type	^{235}U wt.%
A1	2.23
A2	2.23
B1	2.62
B2	2.61
C1	3.14
C2	3.13
C3	3.12
Core average	2.66

The EPR uses light water as coolant and moderator with natural boric acid (^{10}B at 19.9 wt.%) for control. The cladding used in the EPR is Zircalloy (M5-type) and the burnable absorber is gadolinium oxide, with a wt.% in the region 2-8% Gd_2O_3 homogeneously mixed with UO_2. Control-rods are AgInCd with weight compositions of Ag, In and Cd respectively 80 wt.%, 15 wt.% and 5 wt.%.

4.2.2 THERMAL DESIGN

The rated thermal power of the EPR is 4590MWt. Table 4-4 lists some of the important thermal properties:

TABLE 4-4 THERMAL PROPERTIES (AREVA, 2013)

	Value	Units
Core inlet temperature	568.38	K
Core outlet temperature	603.21	K
Outlet pressure	15 119	kPa
Pressure drop	382.869	kPa
Mass flow rate	2901.10	kg/s

4.2.3 BURNUP

The fuel-cycle length is 547.5EFPD or 18 months per fuel-cycle, which results in a maximum (Gd_2O_3-UO_2)- and UO_2 rod burnup of 18-22 GWD/MTU for one cycle and 55-62 GWD/MTU for a full cycle of three batches.

4.2.4 SAFETY

Although not investigated in this study, the safety of the EPR design was considered for information purposes. The EPR is a Generation 3+ reactor design with additional innovative safety features that reduce the core meltdown probability with improved containment ability for the fission products. Some of the features include:

- The safety injection system/residual heat removal system provides emergency core cooling for EPR. The system has four trains, one for each of the reactor coolant system loops. Each train charges from a low head safety injection pump, a medium-head safety injection pump, and an accumulator. These pumps extract water from the in-containment refuelling water storage tank for their emergency function.
- The EPR has many features to prevent the accumulation of combustible gas mixtures. For instance, the containment has adequate volumetric capacity for accommodating large volumes of combustible gas mixtures during design basis accidents and beyond design basis accidents in order to keep the concentration at safe levels. Other safety features include passive autocatalytic recombiners, rupture and convection foils, mixing dampers and a containment spray system.
- The reactor shield-building completely surrounds the reactor containment building and provides an additional containment barrier to airborne radio-active releases. The space in the annulus formed between the two buildings is filtered and regulated to sub-atmospheric pressure with the annulus ventilation system.

- A core catcher located below the RPV (made from a special concrete ceramic) prevents melted fuel from melting through the containment and cools the corium to prevent criticality.
- Provisions exist for temporary cooling of the melted core in a reactor pit and spreading the corium in the large dedicated area and flooding it with the in-containment refuelling water storage tank.
- Two additional diversified diesel generators handle station blackout for backing up the four main diesel generators (AREVA, 2013).

4.3 MODEL

4.3.1 MCNP6

4.3.1.1 ASSUMPTIONS AND CALCULATIONAL METHOD

Apart from details in Section 4.2, there is a need for several assumptions and calculations in order to model the EPR core using MCNP6. These assumptions and calculations can be categorised with respect to geometry, kcode parameters, temperature, power, burnup, delayed neutrons, reactivity coefficients and materials.

4.3.1.1.1 GEOMETRY

Although most of the information of the EPR is supplied by the FSAR, not everything is defined explicitly and some modelling assumptions were made, especially concerning geometry. The EPR is modelled in different sizes or sections, namely FA, 1/8 core and full-core. One of the 241 fuel assemblies is isolated to model a single fuel assembly, which includes the 17x17 array of fuel pins. A 1/8 core uses the core symmetry to model only a slice of the core but still includes the RPV and reflectors on the periphery. The full-core model accounts for all 241 fuel assemblies as well as the RPV and periphery structures.

4.3.1.1.1.1 ALL MODELS

For an FA, 1/8 core and full-core model calculation:

- A lattice at the bottom (30 cm) and top (30 cm) represents the heavy reflector (HR) in the model.
- At the top of the upper HR, another reflector with the thickness of 260 cm simulates the top support structures and RCCA's.
- The remaining top volume of the RPV is a water layer of 260 cm thickness.
- At the bottom of the lower HR, a water reflector layer of 220.26 cm simulates the remaining volume at the bottom of the RPV.

- The reflector dimensions take into account that the core is off-centre in the RPV (closer to the bottom) with a total RPV length of about 1270 cm.
- The model divides the active fuel region into 20 axial nodes for all models unless otherwise specified.
- Models did not include spacer grids.

Figure 4-3 illustrates the top and bottom reflectors included for all models.

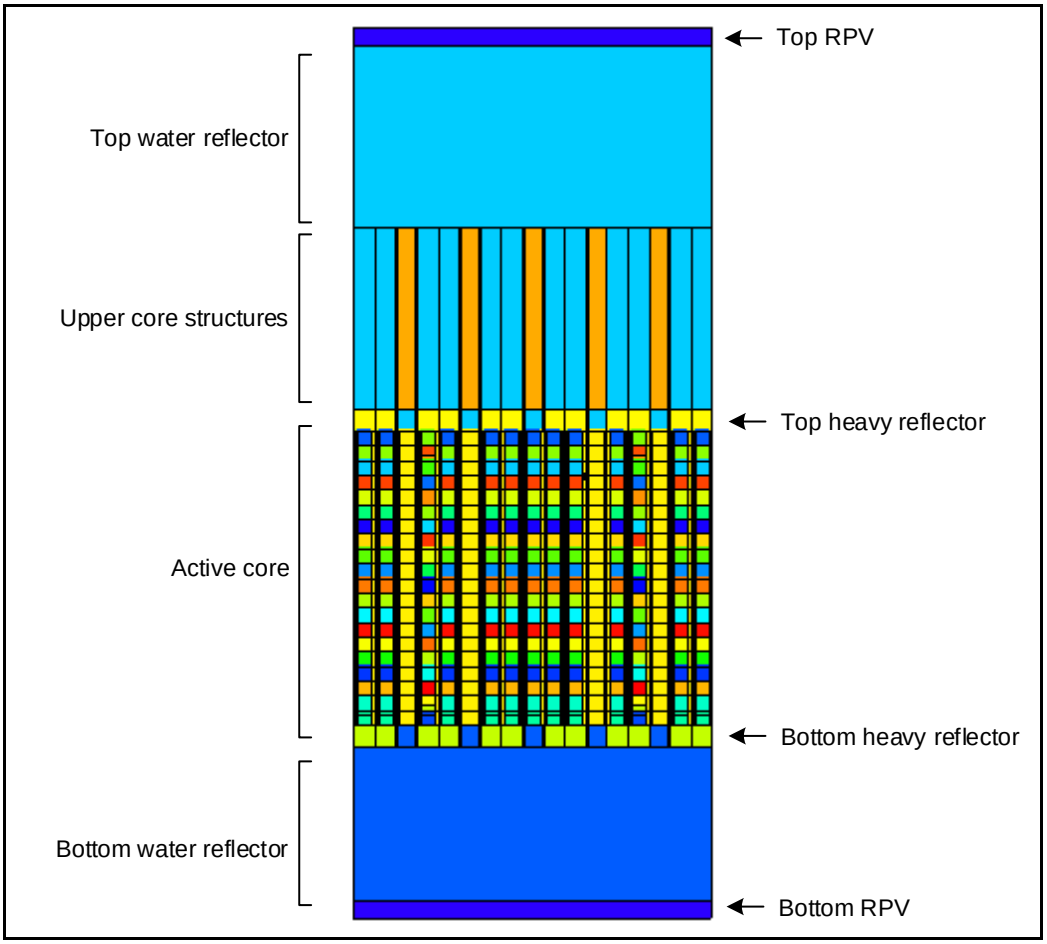

FIGURE 4-3 VISED FUEL ASSEMBLY MODEL

4.3.1.1.1.2 FUEL ASSEMBLY

For a fuel assembly calculation:

- Boundary conditions are reflected on all four sides.

4.3.1.1.1.3 1/8TH CORE

For a one 8th-core calculation:

- Boundary conditions for the 1/8th core use a 1/8 symmetry with radial reflecting conditions along the radial planes.

- The 1/8th core consists of the heavy reflector lattice blocks on the periphery of the core before the RPV.
- The radius of the core including the heavy reflector blocks is 203 cm.
- The core barrel of a thickness of 10 cm surrounds the heavy reflector on the side.
- A water reflector with a thickness of 28.5 cms surrounds the core barrel.
- The bottom and top shapes of the RPV in the model are a sphere with an inner radius of 241.5 cm.
- The RPV encapsulates the core with a thickness of 25.7 cm.

Figure 4-4 illustrates the 1/8 core dimensions in the XZ plane and XY plane.

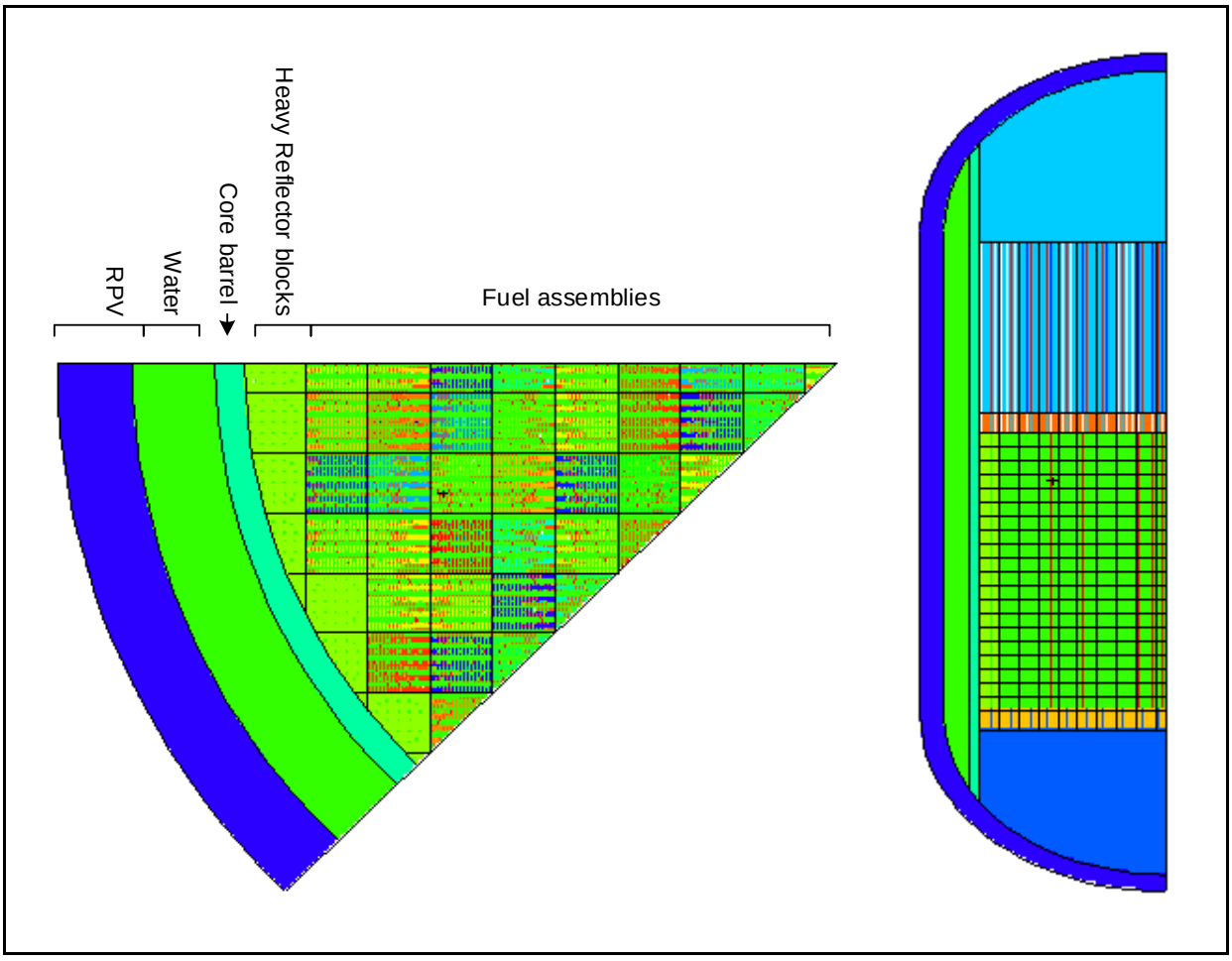

FIGURE 4-4 VISED 1/8TH MODEL FROM TOP AND SIDE

4.3.1.1.1.4 FULL-CORE:

For a full-core calculation:

- All 241 fuel assemblies are modelled.
- The model includes all the top, bottom and side structures to simulate leakage.
- The model has void boundary conditions on the external surfaces.

4.3.1.1.2 TEMPERATURE

One can define the temperature in MCNP6 in three different manners. Firstly, the nuclear data files contain cross-sections for neutron-induced reactions such as fission, absorption, and scattering. These cross-sections are a function of the incident neutron energy; in addition, they are also a function of the target temperature. Table 4-5 depicts the temperature dependent cross-sections.

TABLE 4-5 ENDF/B-VII.1 CONTINUOUS NEUTRON CROSS-SECTIONS

ENDF/B-VII.1	Temperature (K)
.80c	300
.81c	600
.82c	900
.83c	1200

In addition, when neutron energies are thermal, the environment of the target also becomes important and MCNP6 can treat the target using two distinct approaches.

Firstly, the TMP card modifies cross-sections by the free gas thermal treatment of low-energy neutrons when there is no thermal scattering (S(α,β)) data available. This application affects elastic scattering cross-sections and collision kinematics without affecting absorption cross-sections and thermal scattering kernels (LANL, 2013). TMP is in the cell card line in units of MeV.

Secondly the S (α, β) thermal neutron scattering treats materials as a molecular compound in the thermal regime (most effective below 2eV) (LANL, 2013). Using thermal scattering libraries will override the free-gas thermal treatment where available. Table 4-6 gives the available thermal scattering cross-section libraries at different temperatures.

TABLE 4-6 THERMAL NEUTRON SCATTERING CROSS-SECTIONS FOR LIGHT WATER

ENDF/B-VII.I	Temperature (K)
lwtr.20t	294
lwtr.21t	350
lwtr.22t	400
lwtr.23t	450
lwtr.24t	500
lwtr.25t	550
lwtr.26t	600
lwtr.27t	650
lwtr.28t	800

ENDF/B-VII.I is the standard cross-section library, which is used for burnup calculations, and another user defined cross-section library was created using MAKXSF (derived from ENDF/B-VII.I). This is useful for the more accurate coupling calculations, discussed in Section 4.3.3.

Table 4-7 shows the temperatures for initial assumptions in the HFP MCNP6 simulations.

TABLE 4-7 ASSUMED TEMPERATURES FOR DIFFERENT MATERIALS

Material	Temperature (K)
Water	586.9
Gap	630
Cladding	740
Fuel	1050

The fuel temperature was chosen from alternative references that noted average fuel temperature at 1100 K and 1065.8 K respectively (Greifenkamp, et al., 2008; Nuttin, et al., 2006). The choice of gap and cladding temperatures is also similar to Greifenkamp *et al*. The water temperature used is an averaged temperature from the FSAR.

4.3.1.1.3 KCODE PARAMETERS

4.3.1.1.3.1 FUEL ASSEMBLY

Source points for neutron starting points in the simulation of the fuel assembly are 80000 with 230 inactive cycles and 450 total cycles. These cycle numbers are from repetitive scoping simulations and from previous experience to achieve source convergence, tally convergence and k_{eff} convergence with statistical errors less than 14pcm and relative tally errors of less than 1%.

4.3.1.1.3.2 1/8TH CORE

Source points for the one-8th core are 100000 with 200 inactive cycles and 400 total cycles.

4.3.1.1.3.3 FULL-CORE:

Source points are 280000 with 50 inactive cycles and 300 total cycles. The model adds 150 more cycles when the source does not converge.

4.3.1.1.4 POWER

Calculation of the flux and the power averaged in a cell utilised the MCNP6 tally cards F4 and F7.

The F4 tally in MCNP6 gives neutron flux per one fission neutron generation and the conventional units for the flux tallies are particles per unit time per unit area (n/s.cm^2). The tally value produced by MCNP6 needs to be multiplied by a constant to convert to conventional units. Eq. 4-1 calculates the multiplication constant.

$$C_1\left[\frac{neutrons}{s}\right] = \frac{P\left[W\right] \times \bar{\nu}\left[\frac{neutrons}{fission}\right]}{1.6022E^{-13}\left[\frac{J}{MeV}\right] \times Q\left[\frac{MeV}{fission}\right] \times k_{eff}} \qquad \text{Eq. 4-1}$$

Where: P is the core power, $\bar{\nu}$ is the average number of fission neutrons per fission, the average recoverable energy and k_{eff} the eigenvalue of the system (Ghrayeb, 2008). The power is an input by the user and MCNP6 calculates the system-averaged, $\bar{\nu}$, Q and k_{eff} values (Bakkari, et al., 2009).

Equally, a unit conversion is required for the energy deposition tally F7. MCNP6 produces an output value with the unit MeV/g per starting fission neutron. The tally needs a multiplication by a constant shown in Eq. 4-2. Note that the conversion from Joules to MeV is not present in the equation because the tally calculated result is in MeV.

$$C_2\left[\frac{neutrons}{s}\cdot\frac{W}{MeV}\right]=\frac{P\left[W\right]\times\bar{\nu}\left[\frac{neutrons}{fission}\right]}{Q\left[\frac{MeV}{fission}\right]\times k_{eff}} \qquad \text{Eq. 4-2}$$

The resulting units of the F7 tally are $\frac{W}{g}$ or $\frac{MW}{T}$, which is the specific power.

The power given is an average of all the pins in each fuel assembly and axial node. Many studies use axial nodes to take into account the axial difference in flux, fuel material, moderator density, and temperature. The choice of the number of axial nodes can range from eight (Kotlyar, et al., 2011; Agung, et al., 2013) to 24 (Xu, 2003; Delgado, et al., 1999; Todosow & Kazimi, 2004). In the majority of cases, they are discretised into twenty axial nodes, except in cases with time constraints such as burnup calculations.

4.3.1.1.5 BURNUP

MCNP6 relies on the assumption that the time-step-averaged neutron flux varies negligibly during a single time-step. The assumption of large burnup steps, such as 400 days can be too long and smaller steps will be more accurate in estimating the neutron cross-sections data according to changes in neutron spectra due to burnup. It is common practice to increase the time-steps as the burnup increases (Dalle, 2009). Tsige-Tamirat suggested burnup steps in increments of 30 EFPDs (Tsige-Tamirat, 2011). Nuttin used optimized time-steps that consist of 10-day steps until 50 days (the three first steps are 1, 4 and 5 days), 20-day steps until 150 days and 50-day steps thereafter (Nuttin, et al., 2012). Trellue used 0.5, 1 and 5.5 days for the first three time-steps with the rest being 90.14 days (Trellue, et al., 2011). Table 4-8 presents the time-steps used.

TABLE 4-8 MCNP6 TIME-STEP DURATION IN EFPD

#	Time-step	Total time
0		-
1	0.5	0.5
2	1	1.5
3	5	6.0
4	10	16.0
5	10	26.0
6	10	36.0
7	40	76.0
8	40	116.0
9	40	156.0
10	40	196.0
11	40	236.0
12	40	276.0
13	40	316.0
14	40	356.0
15	40	396.0
16	40	436.0
17	40	476.0
18	40	516.0
19	40	556.0

Fuel assembly B1 has an average enrichment of 2.62 wt.% and is chosen as reference assembly since its enrichment is the closest (slightly less) to the full-core, which is 2.66 wt.%. Further studies should include other fuel assemblies, which are not considered here due to time constraints.

An equilibrium core is characterized by a constant refuelling rate and a constant discharge burnup (Lindley, et al., 2014). The lowest enrichment assemblies of the fresh core design should have a reactivity corresponding to the highest (or two times) burned fuel. The medium-enriched assemblies should have a reactivity corresponding to once-burned fuel. The highest enrichment assemblies are the fresh fuel that is not burned (Pal & Jagannathan, 2008). In the specific EPR case, assemblies of type B are equivalent to medium enriched assemblies and correspond to once-burned fuel. This also confirms the choice of assembly B1 as an average representation of full-core.

Assuming a three-batch core management scheme results in about 52 fresh fuel assemblies in each cycle.

The number of axial nodes for the FA burnup calculation reduces to six to take into account axial flux and power difference but still limit the computational time. Ivanov *et al* used 10 nodes for a

PWR model (Ivanov, et al., 2013). The power applied to the fuel assembly is 19.046MW, derived from the total core power divided by the total number of fuel assemblies.

Two burnup options were modelled; the first where the boron is kept constant at 1350 ppm, which is the CBC; the second option is where all three fuel cycles are modelled without any boron in the water. This second option forms a reference case and starting point in order to design and compare to the thorium-uranium fuel.

4.3.1.1.6 DELAYED NEUTRONS

The TOTNU feature in MCNP6 calculates the delayed neutrons contribution by switching on and off the effect of delayed neutrons on criticality calculations (Feghhi *et al*., 2013). Eq. 4-3 uses the multiplication factors for both simulations and calculates β_{eff} (Tucker, et al., 2015).

$$\beta_{eff} = 1 - \frac{k_{eff}^{p}}{k_{eff}^{tot}} = \frac{k_{eff}^{d}}{k_{eff}^{tot}} \qquad \text{Eq. 4-3}$$

Where: k_{eff}^{tot} is the default criticality value, k_{eff}^{p} is the criticality eigenvalue of only the prompt neutrons and k_{eff}^{d} is the criticality eigenvalue of only the delayed neutrons.

4.3.1.1.7 REACTIVITY COEFFICIENTS

Section 2.1.2 discussed the reactivity coefficients and Eq. 2-3 to Eq. 2-4 calculated the MTC and DC respectively. All the water in the core is in the calculation model of MTC. A temperature difference of 20 K is assumed in both MTC and DC calculations (Lindley & Parks, 2012).

4.3.1.1.8 CRW AND SDM

The definition of CRW is in Section 2.1.4. The model consists of a full-core with fresh fuel and critical boron concentration (CBC), which corresponds to BOL at HFP. Two scenarios were modelled, the first with all the RCCAs fully inserted and the second with all the RCCAs completely withdrawn. The difference in the reactivity would be the total CRW.

4.3.1.1.9 MATERIALS

The UO_2 fuel density stated in Table 3-1 has 95% theoretical density for modelling which results in a density of 10.41 g/cm^3. The same principle is true for Gd_2O_3, which results in 7.04 g/cm^3 (Espe, 1968).

M5 cladding is a (Zr–Nb–O) alloy, composed of 1 wt.% (10000 ppm) Niobium, 1250 ppm oxygen impurity and the remainder Zirconium (Olander & Motta, 2011). Based on the individual densities of these elements an alloy density of 6.505 g/cm^3 is calculated and used.

The reactor pressure vessel (RPV) is made of low-alloy steel, with the internal surface covered by cladding for corrosion resistance (not included in the model). According to the FSAR, the RPV

material for upper/lower core shells should adhere to ASME SA-508 Grade 3 Class 1. The properties specified elsewhere (Key to Metals AG, 2014) are in the MCNP6 input model and the density is 8.03 g/cm^3.

The material composition of the heavy reflector (HR) is 95 vol.% metal (stainless steel) and five vol.% water. According to the FSAR, the heavy reflector metal should adhere to AMS SA-336 Grade F304. Since the FSAR did not have the composition of stainless steel, the properties specified elsewhere (STEELGS, 2014) is in the MCNP6 input and the density of stainless steel is 8.03 g/cm^3 (see Table 4-9 for both compositions of the RPV and stainless steel component of the HR).

The material composition of the Barrel is not in the FSAR and therefore assumed to have the same stainless steel composition of the HR.

TABLE 4-9 STAINLESS STEEL COMPOSITION OF HR AND RPV IN WT.%

Elements	HR	RPV
C	0.015	0.125
Si	0.5	0.2
Mn	1	1.35
P	0.0225	0.0125
S	0.015	0.0125
Cr	19	0.125
Ni	10.5	0.7
Mo	-	0.525
Cu	-	0.1
Fe	68.95	96.85

4.3.2 RELAP5

RELAP is a useful tool for transient and steady state cases where average, hot and cold channels are modelled (Anders, et al., 2012). For the purposes of this study, RELAP5 models a more accurate representation of the core by modelling 1/8 of the core fuel assemblies instead of three. The objective is to model each fuel assembly of the core individually.

Thermal-hydraulic models can be even more accurate by modelling individual flows around groups of pins inside a fuel assembly (or groups of fuel assemblies) with sub-channel codes such as COBRA-IV (Vazquez, et al., 2012). The goal of this study is to achieve a more accurate representation of reality to better implement thorium fuels, but not investigate sub-channel temperature distributions and therefore a systems code is appropriate.

Eq. 4-4 calculates the hydrodynamic diameter used for the volumes to model each fuel assembly.

$$\text{Hydraulic diameter} = \frac{4 \times \text{volume flow area}}{\text{wetted perimeter}} \qquad \text{Eq. 4-4}$$

The flow area, axial length and axial discretization are identical to the geometry specified for the MCNP input generation. The transfer of power profiles (see section 4.3.1.1.4) is from MCNP6 to RELAP5 heat structures. RELAP5 then calculates the fluid flow characteristics and the heat transfer across the fuel pins. The heat structure consists of three concentric cylinders, the first being the fuel, the second the helium gap and finally the cladding. RELAP5 uses the built-in UO_2 and Zr thermal conductivities and heat capacities and a gap thermal conductivity of 0.278 W/mK (MIT, 2010). Axial temperature profiles of the coolant, gap, cladding, and fuel are available in the output at the end of the RELAP5 calculation. Pressure drops due to spacer grids are absent due to the exclusion of spacer grids in the model.

Modelling all 241-fuel assemblies in RELAP5 posed some challenges:

1. In practice, the flow in each fuel assembly is not equal, since hotter fuel assemblies require higher flow rates compared with colder fuel assemblies. The flow distribution at the bottom plenum is proprietorial and geometry information on the inlet manifold is not readily available in open literature. Therefore, a multiple junction, with the same number of junctions as the number of channels, connects the bottom plenum with the core and another multiple junction connects the core with the upper plenum. In order to set these mass flow distributions, a single volume connects the multiple junction to each core channel. Adjusting the flow areas of these single volumes, achieves the assumed flow distribution.
2. RELAP is unable to model all 241-fuel assemblies due to insufficient memory, therefore, the one octant ($1/8^{th}$) core symmetrical model is utilised. This results in 38 fuel assemblies, for which the model consists of individual RELAP channels.
3. In reality, the coolant flow is not isolated in each fuel assembly and some cross-flow occurs. This was modelled by multiple junctions connecting assemblies in the x and y directions in each axial node. The flow area in each junction is specified and modelled. Not all axial nodes could model the cross-flow, due to memory constraints and on average 10 of the 20 axial nodes included cross-flow. The friction loss in cross =-flow junctions is zero in the model.

The inlet temperature is 568.38 K as specified in Table 4-4 with the inlet pressure calculated outside of RELAP as 15896 kPa considering outlet pressure and pressure drop. The outlet pressure is assumed equal to the system pressure due to its proximity to the pressurizer. Adjusting the water mass flow rate then achieves the same outlet temperature as specified in the FSAR and Table 4-4.

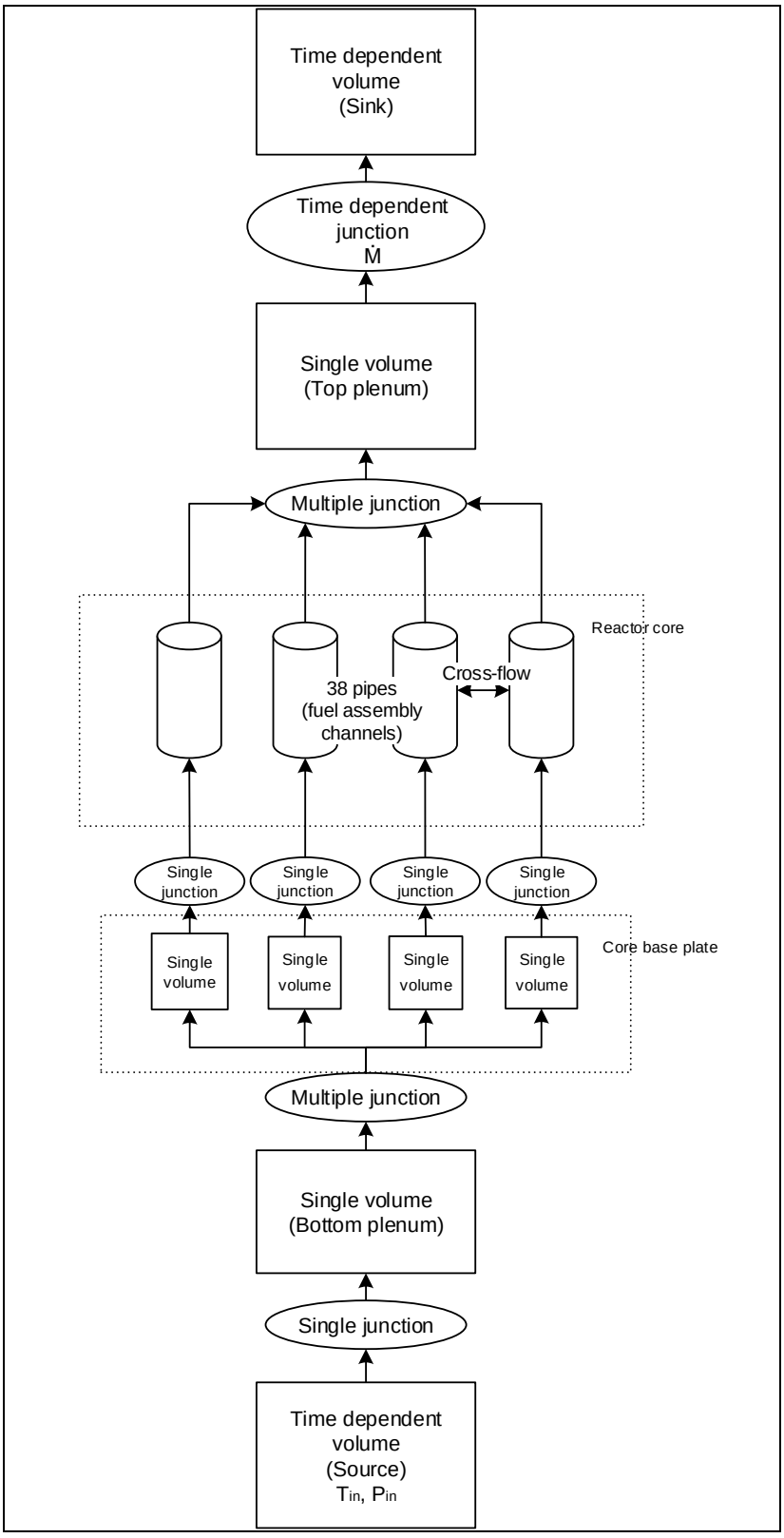

FIGURE 4-5 SCHEMATIC OF RELAP EPR MODEL

4.3.3 COUPLING

The description of the coupling methodology is in the following Section 4.3.3.1.

4.3.3.1 COUPLING METHODOLOGY

As explained in Section 3.7, both the neutronics code and the thermal hydraulic code are individually validated and execute calculations starting from input data and assumptions previously discussed. The steady-state coupled calculation procedure has the following sequence:

1. NWURCS creates the MCNP input for the EPR with core averaged uniform starting temperatures for the coolant, fuel, cladding and helium as shown in Table 4-7 with the number of predefined axial nodes.
2. Full-core calculations with MCNP6 and tally f7 calculate the average power in each of the 241×k fuel assembly axial nodes to create a core power distribution.
3. Thermal-hydraulic simulations usually employ only a few channels (for instance hot, cold and average) to represent different core assemblies with similar power, thermal-hydraulics, and geometry (Aghaie, et al., 2012). RELAP5 is unable to model all 241-fuel assemblies, and NWURCS symmetrises it to one octant ($1/8^{th}$) with one-eighth of the total power. RELAP5 models all 38 fuel assemblies individually as channels. Each fuel assembly model is a “pipe” hydrodynamic component divided into the same amount of predefined axial nodes as used in the neutronic calculation.
4. RELAP5 receives nodal power values from MCNP6 and the user defines the coolant inlet temperature, pressure, and exit mass flow rate. RELAP5 calculates the temperature in the fuel, coolant, cladding and gap for each node.
5. NWURCS exports temperatures from the RELAP5 output and creates the MCNP6 input by applying these temperatures according to the method outlined in Section 4.3.1.1.2. NWURCS uses the lower available cross-section library in Table 4-5. For instance, if the temperature is 850K, the .81c library is used. The temperature of the coolant is an input to NWURCS, which calculates the coolant density at the specified constant reactor pressure, and converts it to the associated atomic density for the neutronic calculation.
6. MCNP6, in turn, calculates the power in the assemblies and NWURCS feeds the values to RELAP5. This procedure is repeated until conformance with the convergence criteria is achieved. Section 4.3.3.4 discusses the convergence criteria.

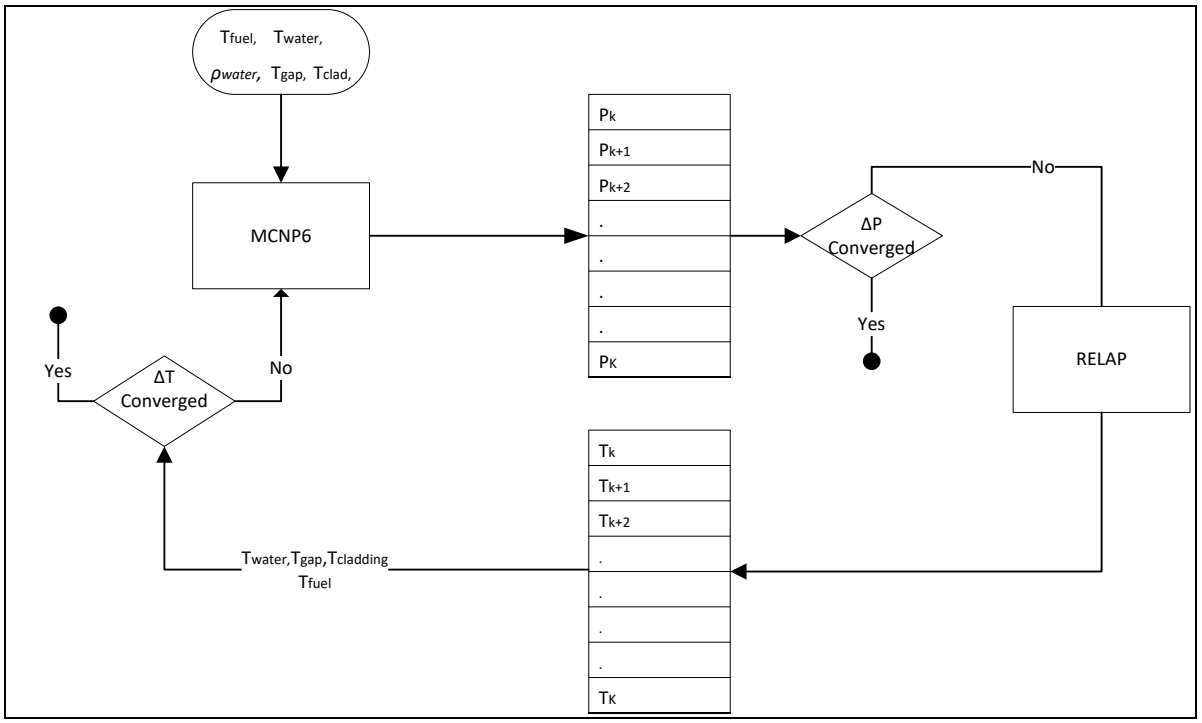

FIGURE 4-6 COUPLING METHODOLOGY BETWEEN MCNP6 AND RELAP5

4.3.3.2 CHALLENGES

Reaching convergence is sometimes troublesome with frequent oscillations in both the temperature and power (refer to Section 3.8.3). Apart from the potential reasons discussed in Section 3.8.3 some other identified factors that can complicate the coupling are:

1. Variations of the physical properties of the materials with temperature,
2. The strong negative moderator temperature coefficient and Doppler temperature coefficients result in increased feedback, which causes oscillations between consecutive power profiles,
3. The cross-sections listed in the data files have 300 K intervals, for instance at 300 K and then 600 K as shown in Table 4-5. These 300 K intervals might be too hefty when applying the lower cross-section library thereby leads to an inaccurate representation.

Due to these factors, the coupling methodology needs amendment and optimisation by implementing the proposed strategies in Section 3.8.4 with appropriate relaxation as discussed in Section 3.8.5.

4.3.3.3 COUPLING STRATEGIES

When using the coupling methodology in Section 4.3.3.1, there was no convergence due to the reasons discussed above.

Different strategies adopted to reduce these oscillation effects are as follows.

1. Inaccurate estimation of nodal power in a coarse mesh could cause oscillations; therefore, the number of axial nodes is 20 (k=1…20).
2. Start with a flat axial power distribution; in order to reduce the effects of a tilted axial power profile, which usually gives rise to increased oscillations.
3. Pseudo-materials are utilised since the cross-section evaluation is at discrete temperatures with 300 K gaps.
4. Makxsf, a module provided in the MCNP6, creates new temperature libraries at predefined temperatures based on previous calculations. The new additional cross-section libraries are generated from the existing set at 550 K,575 K, 625 K, 750 K, 800K, 850 K, 950 K, 1000 K, 1050 K, 1100 K, 1150 K, 1200 K, 1250 K,1300 K and 1350K. The difference between cross-section libraries is now 50 K. Maksf also created new thermal scattering libraries for water at 550 K, 575 K, and 625 K.
5. Due to the negative Doppler broadening in the fuel, tilting in the axial power profile was visible in consecutive iterations. For instance, the first iteration will have a high temperature at the top of the core and due the larger resonance width of ^{238}U, the flux (and power) will decrease, which causes a drop in the temperature. Using the relaxation scheme in Eq. 3-6 on the power will reduce this effect.
6. Relaxing only the power could be insufficient, therefore the coupling strategy also applies the simple temperature relaxation scheme, presented in Eq. 3-3, in conjunction with the power relaxation.

4.3.3.4 CONVERGENCE CRITERIA

As discussed in Section 3.8.6, limitations to the convergence criteria result due to statistical errors in MCNP. Due to the time intensive nature of a MCNP calculation and the fact that multiple iterations are required for coupling, the KCODE parameters were chosen to optimize for time whist maintaining adequate convergence. Multiplying the maximum power tally error for the current full-core calculation by three (Section 3.8.6) is one suggestion for the minimum convergence limit.

The convergence studies found in the literature are based on comparing a given iteration temperature or power profile with either the previous iteration (Ivanov, et al., 2013) or some average of previous iterations (Bennett, 2015). The parameters' values for the next iteration is then a sum of these two fields, together with some suitable relaxation factor, as given in equations Eq. 3-5 and Eq. 3-6. Convergence was achieved when the difference between the present iteration and the previous iteration or average of all previous iterations was less than a given value ε.

This works quite well with deterministic calculations and if physical properties behave well (as outlined in Section 4.3.3.2). However, when the physical properties present challenges to

coupling in their behaviour, or when stochastic codes are used, then such a convergence scheme becomes difficult to achieve.

Instead of using a convergence criterion ε this work employs convergence measures, which are called figures of merit in this case. These figures of merit measure the efficiency of the convergence. Section 3.8.6 showed that previous studies used either power or temperature to measure the convergence. For this study, both the power and the temperature convergence measures are used. Due to the presence of two different relaxation techniques as presented in Eq. 3-3, Eq. 3-4, and Eq. 3-5, Eq. 3-6, the choice is to investigate both methods in terms of power and temperature for convergence. The first method only compares the previous iteration to the current iteration and the second compares the average of the previous iterations to the current iteration. By taking into account all four of these convergence parameters, a firmer convergence criterion is set. Eq. 4-5 to Eq. 4-8 calculates the figures of merit to measure the convergence.

$$FOM_1^N = \Delta T_{ijk}^N = \max\left|\frac{T_{ijk}^N - T_{ijk}^{N-1}}{T_{ijk}^{N-1}}\right| \qquad \text{Eq. 4-5}$$

$$FOM_2^N = \overline{\Delta T_{ijk}^N} = \max\left|\frac{T_{ijk}^N - \frac{1}{N-1}\sum_{n=1}^{N-1} T_{ijk}^n}{\frac{1}{N-1}\sum_{n=1}^{N-1} T_{ijk}^n}\right| \qquad \text{Eq. 4-6}$$

$$FOM_3^N = \Delta P_{ijk}^N = \max\left|\frac{P_{ijk}^N - P_{ijk}^{N-1}}{P_{ijk}^{N-1}}\right| \qquad \text{Eq. 4-7}$$

$$FOM_4^N = \overline{\Delta P_{ijk}^N} = \max\left|\frac{P_{ijk}^N - \frac{1}{N-1}\sum_{n=1}^{N-1} P_{ijk}^n}{\frac{1}{N-1}\sum_{n=1}^{N-1} P_{ijk}^n}\right| \qquad \text{Eq. 4-8}$$

Where: N is the number of the current iteration, i is the x coordinate, j the y coordinate and k the z coordinate of the node. The figures of merit are calculated by identifying the maximum relative difference for all N and ijk.

All four of these figures-of-merit form part of the overall convergence. Normalising the values of the relative differences in all four cases (so that each convergence parameter can carry equal weight) makes the summation possible. Eq. 4-9 is the set of normalisation equations.

$$\sum_{n=1}^{N} \Delta T_{ijk}^N = 1,\ \sum_{n=1}^{N} \overline{\Delta T_{ijk}^N} = 1,\ \sum_{n=1}^{N} \Delta P_{ijk}^N = 1,\ \sum_{n=1}^{N} \overline{\Delta P_{ijk}^N} = 1 \qquad \text{Eq. 4-9}$$

Finally, the respective normalized convergence criteria are added together to form the final figure-of-merit shown in Eq. 4-10.

$$FOM^N = \min\left[\frac{FOM_1^N + FOM_2^N + FOM_3^N + FOM_4^N}{4}\right] \qquad \text{Eq. 4-10}$$

Iteration N is the coupled solution, where the final combined figure of merit FOM^N is a minimum.

4.4 RESULTS

The Final Safety Analysis Report is the benchmark for comparison in order to obtain confidence in the current model. Section 4.4.1 explains the reasoning behind the assumption that the FSAR is a verified and validated (V&V) document.

As part of the process to set up the reference model, several new features of NWURCS were added and tested and form part of the results. Discussion on the added features in NWURCS are in Section 4.4.2.

The results obtained using the newly-built MCNP6 core model of the EPR and a comparison with the FSAR values are in this section. ITER01 are the results at HFP (see assumed temperatures in Table 4-7) and includes the neutronic results as well as thermal-hydraulic results. The neutronic results (from MCNP6) are exported to RELAP5 for thermal hydraulics coupling (one iteration between neutronic and thermal-hydraulic codes).

ITERX will be the coupled solution after accounting for the feedback from the thermal-hydraulics for an educated guess of field temperature values used for ITER01. The exercise of coupling is included in this study to develop and test the functionality of coupling in NWURCS.

4.4.1 FSAR

As discussed in Section 2.3.1 the US EPR by AREVA has been under review for obtaining design certification at the NRC as a new reactor design. When the U.S. Nuclear Regulatory Commission (NRC) issues the design certification, it means that the NRC approves a nuclear power plant design (valid for 15 years), apart from an application to construct or operate a plant. The design certification addresses the safety issues related to the proposed nuclear power plant design. One of the application documents in the design certification process is the Final Safety Analysis Report (FSAR). The FSAR for the EPR was accepted by the NRC and is available online at the NRC website.

The FSAR delivers information to support the NRC's approval and certification of the standard U.S. EPR design, under the provisions of 10 CFR Part 52, "Licences, Certifications, and

Approvals for Nuclear Power Plants". Chapters 14 and 18 of the FSAR address the verification programs and verification and validation respectively (U.S. NRC, 2016).

Some activities of V&V include a pilot study, which provides an opportunity to examine the competence of the test design, performance measures, and data collection; an extensive initial plant test program and a comparison to current U.S. 4-Loop French N4, German and KONVOI PWRs (AREVA, 2013). The information in the FSAR uses analysis codes developed/acquired by the plant designer (i.e. Areva). In terms of validation of the analysis codes for the U.S. EPR, the neutronic, thermal-hydraulic and thermo-mechanical disciplines are governed by several methodology topicals each of which uses one or more major codes to perform the design calculations. All these methodology topicals have been reviewed and approved for use by the NRC (AREVA NP Inc., 2006).

One can trust that the information given in the FSAR has been through rigorous testing and scrutiny by the NRC and is therefore verified and validated to be used as the standard benchmark for comparison to the current study.

4.4.2 NWURCS

As part of the process to set up the reference model, several new features added to NWURCS and are tested. Some of the features include:

- Defining and normalising tally 4 and 7 as well as mesh-tallies to units of n/s.cm^2 and Watt,
- Implementation of tally 4 in terms of neutron energy spectrum by using energy bins,
- Implementation of source definition (sdef) for repeated structures,
- The addition of the burnup card to the MCNP6 input file,
- Correction of the control-rod movement input generation, because an earlier version of NWURCS had a computer bug, which introduced voids into the control-rod volumes (Nyalunga, 2015),
- The introduction of separate control banks movements as well as the addition of different types of control-rods,
- Pseudo-materials and MAKXSF integration with the MCNP6 input file,
- Boric acid concentration in the water for MCNP6 input,
- Integration of reactivity coefficient calculations in the MCNP6 input file,
- The inclusion of RPV in full-core models,
- Modelling cross-flow in RELAP5,
- Flow distribution modelling at the bottom of the core in RELAP5,
- RELAP output data extraction,
- Automation of coupling between MCNP6 and RELAP5 using the HPC via a Linux platform,

In addition to laying the foundation for the work to follow on thorium fuel, these results further assist in verification of NWURCS. Monte Carlo codes such as MCNP6 and Keno form part of high fidelity codes because of their accurate modelling of the geometry and the use of continuous energy neutron cross-sections. Such codes are useful, for example, in benchmark exercises. However, full-core MCNP6 models are still under development and NWURCS in this sense will add to this development.

4.4.3 ITER01

4.4.3.1 NEUTRONIC TRANSPORT

The neutronic results for a full-core EPR with fresh fuel at CBC and HFP follow. Table 4-7 presents the assumed temperatures at HFP for the fuel, gap, and cladding. ITER01 is the reference name of these results. The NWU HPC carried out most of the calculations by using 12 processors. The results are in the sections of criticality, flux, power, reactivity coefficients, and control-rod worth. The comparison with the FSAR follows.

4.4.3.1.1 CRITICALITY

4.4.3.1.1.1 BORON WORTH

The boron worth (BW) for both the FSAR and ITER01 cases is negative and they are in close agreement, with ITER01 being slightly more negative (see Table 4-10). The critical boron concentration (CBC) required resulting in a k_{eff}=1.00000 is calculated at 1349.5 ppm which is 33.5 ppm less than the specification in the FSAR and is in good agreement. One of the reasons for a lower CBC might be due to a slightly stronger boron worth in ITER01.

4.4.3.1.2 FLUX

4.4.3.1.2.1 AXIAL FLUX DISTRIBUTION

Figure 4-7 shows the flux distribution in the EPR core in a 19x19 core and the effects of the axial enrichment on the flux. The flux decreases from bottom to top as expected, due to the decrease in moderator density. The middle axial section has a “smooth” radial flux distribution due to the distribution of lower enriched assemblies between higher enriched assemblies. The axial distribution of the middle section is also “smooth”, due to the presence of gadolinium in the centre of the rods. The top middle section shows a radial asymmetry on the periphery of the core. This radial asymmetry is due to the statistical nature of MCNP6 and by running more source points and active cycles, may provide a more symmetrical result. On the right-hand side of Figure 4-7 is the model repeated with ~3 times more source points (1000000) to reduce the statistical errors. Note the improvement in the radial symmetry in the top middle and bottom middle sections upon increasing the number of source points.

300 000 Source points	1000 000 Source points	
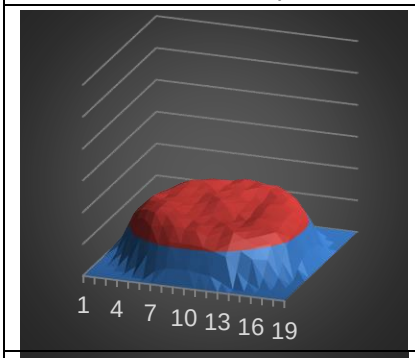	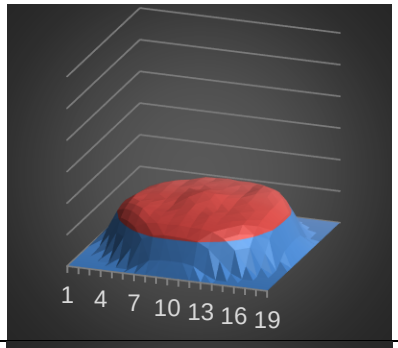	Top [420 cm-399 cm]
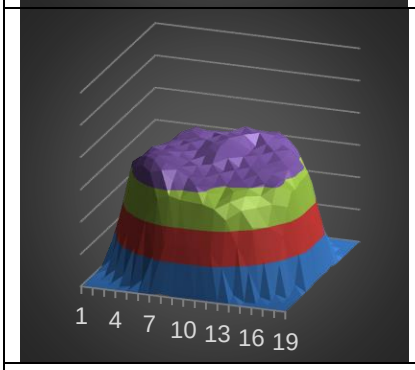	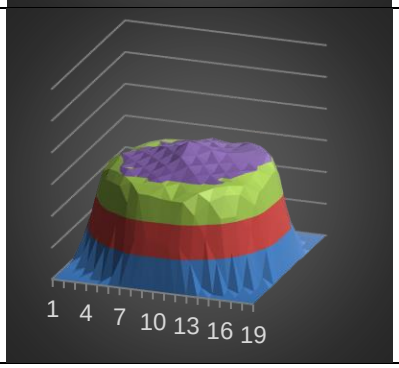	Top middle [378 cm-399 cm]
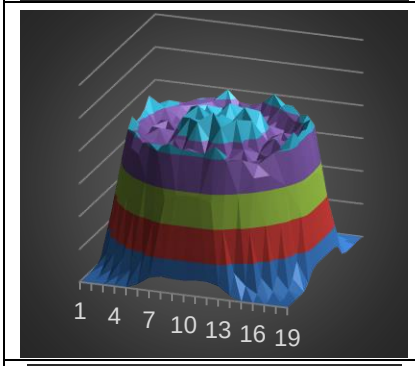	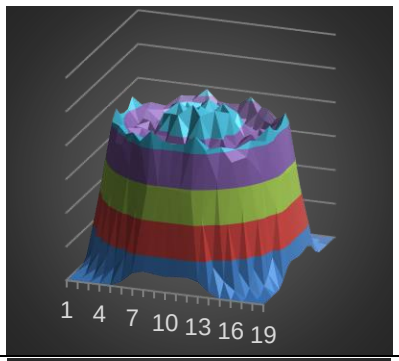	 n/s.cm^2 Middle [189 cm-231 cm]
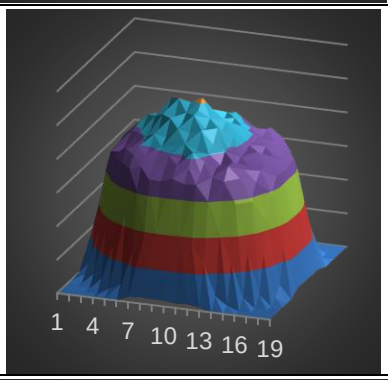	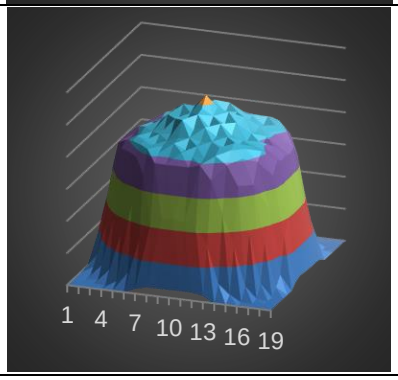	Bottom middle [21 cm-42 cm]
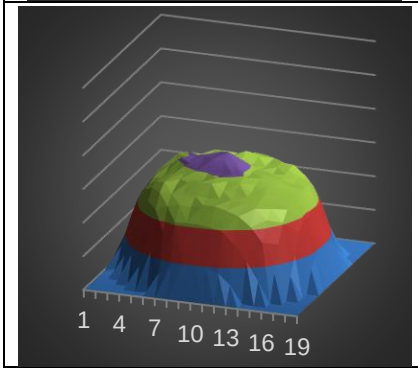	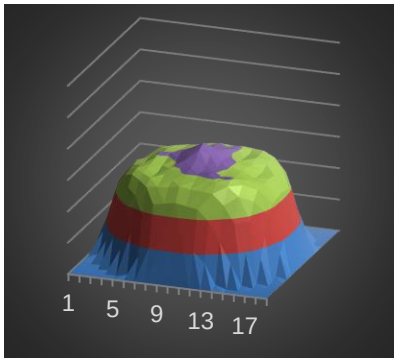	Bottom [0 cm-21 cm]

FIGURE 4-7 AVERAGE FLUX AT DIFFERENT AXIAL SECTIONS OF THE CORE (N/S.CM^2)

4.4.3.1.2.2 NEUTRON FLUX SPECTRUM

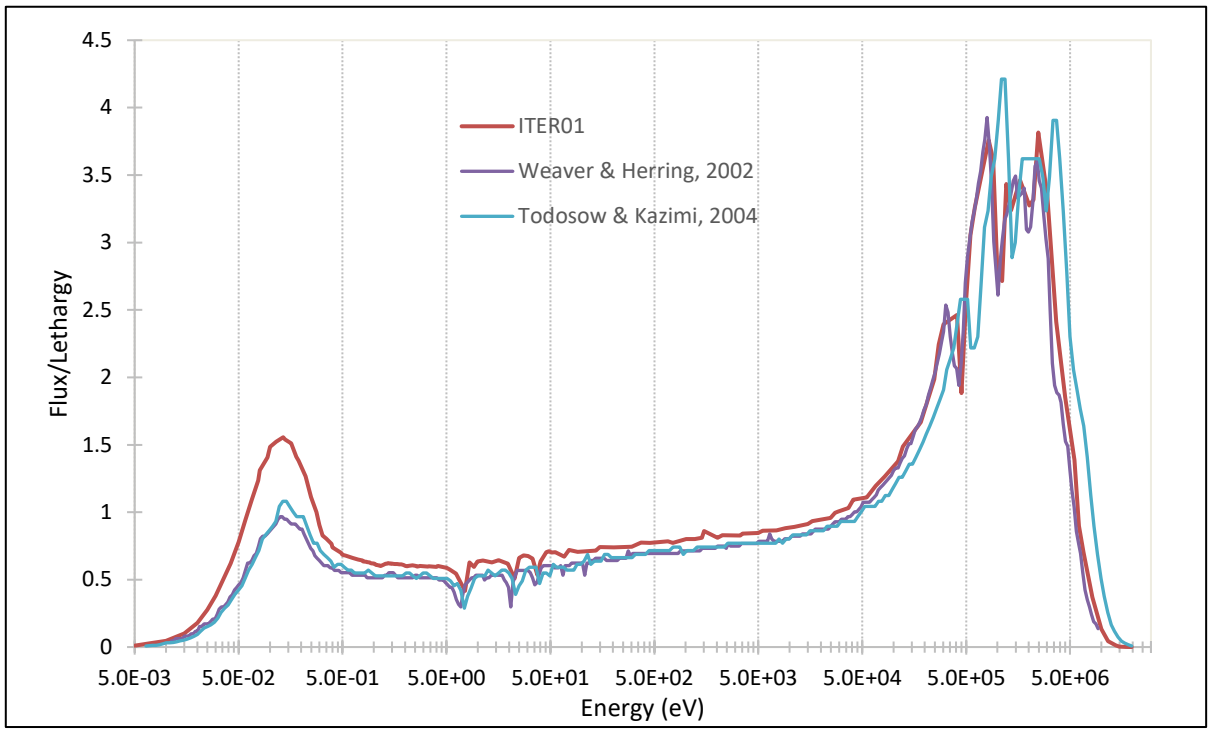

FIGURE 4-8 NEUTRON ENERGY SPECTRUM IN FUEL FOR ITER01

The FSAR does not specify the neutron flux spectrum explicitly. The comparison of the neutron spectrum tallied in the fuel of ITER01 with standard PWRs reported in Weaver and Herring and Todosow and Kazimi is in Figure 4-8. Both of these references modelled a standard PWR with 4.5% ^{235}U enrichment. Results were normalised for comparison. Figure 4-8 shows that the neutron energy spectrum for the EPR agrees closely with the standard UO_2 PWR spectrum reported by the other references. ITER01 has a higher thermal neutron spectrum peak and lower fast spectrum peak. The slight differences can be explained by a lower (~2.6 wt.% ^{235}U) enrichment, which results in more neutrons in the thermal region and less fast neutrons due to fission (Todosow & Kazimi, 2004; Weaver & Herring, 2002). One should also note that the axial definition of the EPR fuel pins is different from standard PWR fuel pins.

4.4.3.1.3 POWER PROFILE

The flux shape relates to the power shape and Figure 4-9 shows the difference in the axial power shapes of the beginning of life (BOL) with fresh fuel. The FSAR graph is a typical axial power shape and not necessarily the average of the full-core, where the ITER01 graph is the average for the full-core. Note that the FSAR graph is smoother and that ITER01 has higher peaks at the top cutback region, due to the higher enrichments in that region for some fuel pins. However, these two graphs are in close agreement.

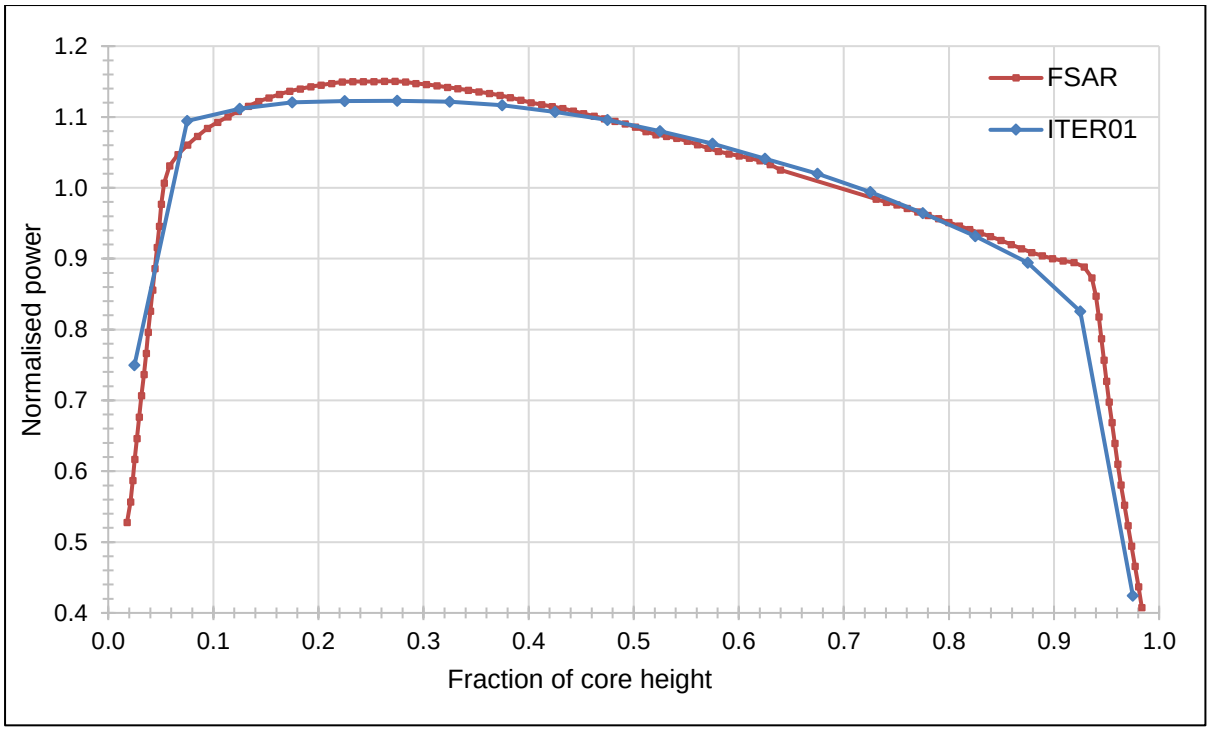

FIGURE 4-9 AXIAL POWER SHAPE AT BOL FOR ITER01

4.4.3.1.4 REACTIVITY COEFFICIENTS

Table 4-10 compares the FSAR results to the reference model called ITER01. The reference case has a slightly less negative Doppler Coefficient, but taking into account the ranges, it is still within acceptable limits. The moderator temperature coefficient is negative and falls within the range provided by the FSAR as well as the range of acceptable limits.

The equations presented in Section 2.1.2 calculate the reactivity coefficients and Eq. 4-11 to Eq. 4-16 calculate the standard deviation of reactivity coefficients. Using the definitions of reactivity coefficients given in Eq. 2-3 to Eq. 2-4, the uncertainty in the reactivity coefficients becomes:

$$\sigma_{RC} = \sigma_{(\frac{\Delta\rho}{\Delta T})} \qquad \text{Eq. 4-11}$$

When assuming that the variance in ΔT is zero and that in ΔT is a constant, Eq. 4-11 can be written as:

$$\sigma_{RC} = \sigma_{(\frac{\Delta\rho}{\Delta T})} = \frac{\sigma_{\Delta\rho}}{\Delta T} = \frac{\sigma_{(\rho_2-\rho_1)}}{\Delta T} \qquad \text{Eq. 4-12}$$

Following the rule of addition/subtraction of measured quantities (Harvard University, 2007) Eq. 4-12 transforms as:

$$\sigma_{RC} = \frac{\sigma_{(\rho_2-\rho_1)}}{\Delta T} = \frac{\sqrt{\sigma^2_{\rho_1} + \sigma^2_{\rho_2}}}{\Delta T} \qquad \text{Eq. 4-13}$$

Where: σ_{ρ_1} and σ_{ρ_2} are the standard deviations of ρ_1 and ρ_2 respectively in the MCNP6 calculations of k_1. and k_2. Defining ρ_1 and ρ_2 as (Anglart, 2005):

$$\rho_1 = \frac{k_1 - 1}{k_1} = 1 - \frac{1}{k_1} and\, \rho_2 = \frac{k_2 - 1}{k_2} = 1 - \frac{1}{k_2} \quad \text{Eq. 4-14}$$

Then from the rule of multiplication/division of measured quantities (Harvard University, 2007) the uncertainties in ρ_1 and ρ_2 are:

$$\sigma_{\rho_1} = \frac{\sigma_{k_1}}{k_1} and\, \sigma_{\rho_2} = \frac{\sigma_{k_1}}{k_1} \quad \text{Eq. 4-15}$$

Substituting Eq. 4-15 back into Eq. 4-13 finally provides Eq. 4-16.

$$\sigma_{RC} = \frac{\sigma_{(\rho_2 - \rho_1)}}{\Delta T} = \frac{\sqrt{\left(\frac{\sigma_{k_1}}{k_1}\right)^2 + \left(\frac{\sigma_{k_2}}{k_2}\right)^2}}{\Delta T} \quad \text{Eq. 4-16}$$

4.4.3.1.5 DELAYED NEUTRON FRACTION

The delayed neutron fraction β_{eff} calculated for the reference case is (6.7%) smaller than the FSAR and can be considered to be in good agreement. Note that Lamarsh reported a delayed neutron fraction for ^{235}U at thermal energies of 0.0065, which is closer to ITER01 results than the FSAR (Lamarsh & Baratta, 2001). As discussed in Section 2.1.3, the delayed neutron fraction is important during transients and a smaller value is not desirable. However, β_{eff} relates directly to the main fissile isotope, ^{235}U, which is the same for the FSAR and ITER01 cases. Therefore, the difference might originate due to different neutron data libraries used for the two cases (Todosow & Kazimi, 2004).

TABLE 4-10 FULL-CORE ITER01 COMPARISON OF NEUTRON PARAMETERS

	Limits	FSAR	ITER01[d]	Units
DC	(-4.90;-2.90[a])	(-3.24;-2.34)	-2.00±0.57	pcm/K
MTC	(-70.0;0.00[a])	(-60.12;5.22)	-17.45±0.57	pcm/K
$\boldsymbol{\beta_{eff}}$	(0.0043;0.0072[c])	0.0074	0.0069±0.0001	-
BW	(-10.86;-5.71[a])	(-9.5;-7.9)	-9.01±1.13	pcm/ppm
CBC	(0;1780[b])	1383.0	1349.5	ppm

a. *(IAEA, 2003)*

b. (Delgado, et al., 1999)

c. (Björk, et al., 2013)

d. BOL, HFP, k_{eff}=1.00000 RCCAs out, no xenon, CBC

4.4.3.1.6 CRW

The total CRW from all banks was determined (as discussed in Section 4.3.1.1.8) to be 10322±10 pcm compared to 10942 pcm from the FSAR. The reference case CRW is 5.7% smaller than the FSAR, which is in close agreement.

Figure 4-10 compares the integral rod worth (IRW) curve for bank B of the modelled EPR to the IRW curve reported in the FSAR. It should be noted that the values reported in the FSAR did not indicate the specific bank/banks used. Therefore, the integral rod worth was normalised for both cases to compare. Results for ITER01 in Figure 4-10 show higher worth's at the top of the core whereas the FSAR shows that most of the rod worth is in the final 20% of insertion. Note the similarity in the general exponential trend in both cases.

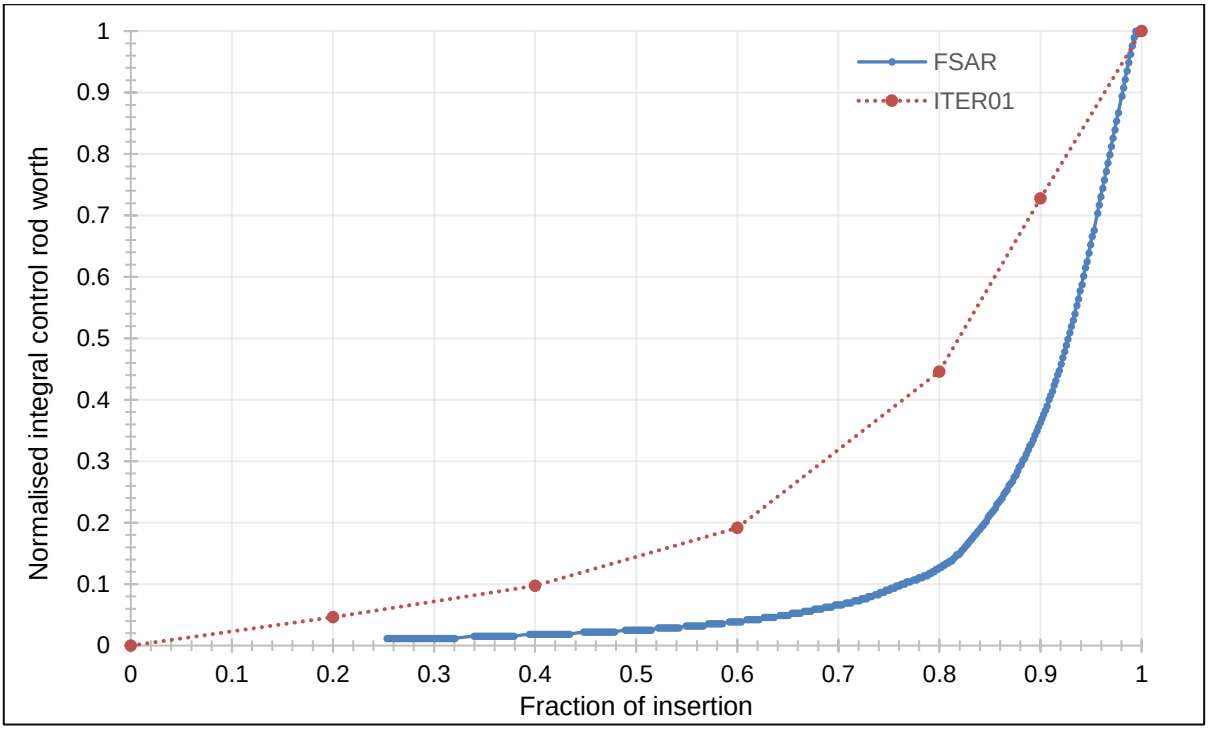

FIGURE 4-10 INTEGRAL CONTROL-ROD WORTH FOR ITER01

4.4.3.2 THERMAL-HYDRAULICS

The manner in which the RELAP input was constructed was to specify inlet temperature and pressure as well as the outlet mass flow rate shown in Figure 4-5. However, the data that were used from the FSAR for the RELAP calculation were the inlet pressure, the inlet temperature and the outlet temperature. From Eq. 4-17, note that both these sets of boundary conditions are equivalent, provided the mass flow rate is constant. ITER01 models the mass flow rate as an input value of the RELAP model and is adjusted to obtain the required outlet temperature.

$$\dot{Q} = \dot{m} \times C_p \times \Delta T \qquad \text{Eq. 4-17}$$

Where: ΔT and $\dot{Q}$ are in the FSAR.

TABLE 4-11 THERMAL PROPERTIES (AREVA, 2013)

	Value	Units
Core inlet temperature	568.38	K
Core outlet temperature	603.21	K
Outlet pressure	15 119	kPa
Pressure drop	382.869	kPa
Mass flow rate*	2901.10	kg/s

**Adjusted later to obtain required core outlet temperate*

Table 4-12 shows the comparison of the thermal-hydraulic results for the FSAR and ITER01 (one iteration between MCNP6 and RELAP5).

Results show that the thermal volume flow for ITER01 is higher than for the FSAR even though the mass flow rate is slightly less. One of the possible reasons could be that the ITER01 model does not take into account bypass flow and another reason might be that the density of water used for the ITER01 model is smaller than that of the FSAR. Table 4-12 also shows that the pressure drop model (by adjusting the forward losses in the pipes) is accurate.

TABLE 4-12 THERMAL-HYDRAULIC PROPERTIES COMPARISON

	FSAR	ITER01	% Difference *	Units
Outlet temperature	603.206	602.921	0.0%	K
Thermal volume flow rate	3.78	4.29	-13.7%	m^3/s
Mass flow rate	2901.10	2800	3.5%	kg/s
Average heat flux	5.830E+05	5.827E+05	0.1%	W/m^2
Maximum heat flux	1.45E+06	9.49E+05	34.7%	W/m^2
Fq	2.60	1.63	37.4%	-
Pressure drop	3.829E+05	3.782E+05	1.2%	kPa
Outlet pressure	1.551E+07	1.552E+07	0.0%	kPa

$* \%\ Difference = \frac{FSAR - REF}{FSAR}$

The average heat flux is in good agreement and the maximum heat flux is lower for the ITER01 compared to the FSAR, this result in a lower Fq (see Section 2.2.2). Fq can be smaller due to a uniformly assumed temperature distribution and a coupled calculation may produce different results. The specific state of the data from FSAR is not clear; therefore, the specific comparison between the FSAR and ITER01 will not yield identical results.

Table 4-13 shows the RELAP5 calculated temperatures for ITER01.

TABLE 4-13 AVERAGE CALCULATED TEMPERATURES FOR DIFFERENT MATERIALS

Material temperature	MCNP temperature field	RELAP5
Average fuel centreline temperature	-	1251.63
Average fuel temperature	1050	1031.11
Average gap temperature	740	730.10
Average cladding temperature	630	616.11
Average coolant temperature	586.9	588.32

The FSAR did not report these temperatures for comparison with the current model, but a representative temperature field is required for accurate representation of the core. Initial values were made from literature as shown in Table 4-7 together with the experience of scoping coupling calculations. Table 4-13 shows that the average temperatures were close to the assumed starting temperatures, which proves that the initial temperature assumptions are in close agreement.

4.4.3.3 CONCLUSION

This section presented the neutronic results for a full-core EPR with fresh fuel and CBC at HFP for ITER0. The results in terms of boron worth, axial flux distribution, neutron flux spectrum, power profile, reactivity coefficients and control-rod worth showed similar results compared to the FSAR and are within acceptable limits. The only difference was the delayed neutron fraction and a possible reason might be the different neutron data libraries used for the two cases.

The thermal-hydraulic results for ITER01 are in good agreement with the FSAR. There is scope for improvement through improved coupling.

These results give confidence in the following two ways: (a) expansion of the model to include Th in the core and (b) verification of NWURCS in generating the input decks.

4.4.4 COUPLING

The minimum value for the convergence criteria calculated in Section 4.3.3.4 resulted in a coupled solution at N=26. Nuttin *et al*. achieved a converged coupled solution with 12 iterations even though different coupling methodologies were used (Nuttin, et al., 2013). The results at iteration 26 show that the temperature figures of merit are FOM_1^{26}=0.2%, FOM_2^{26}=0.4%, which are a differences of 2.1 K and 5.0 K respectively.

For iteration 26 the power figures of merit are FOM_3^{26}= 21.9% and FOM_4^{26}=15.3%. The relative differences in the power parameters are larger compared to those for the temperature mainly due to the limiting statistical uncertainty of the power tallies in MCNP6. These results are the maximum differences while the average values are 4.7% and 4.1% respectively, which is significantly smaller. Multiplying the maximum tally uncertainty by three as suggested by

Vasquez, prohibit reaching relative errors smaller that 7.4% and therefore the power figures of merit are satisfactory.

The relative difference between k_{eff} of iteration 26 and 25 is 9.00 pcm and the relative difference between iteration 26 and the average of all the previous iterations is 23.87 pcm, which is slightly larger than the specification of 20 pcm (Ponomarev, et al., 2015). These figures are, however, small enough to ensure coupling in the eigenvalue.

The results show that when considering only the temperature to measure the convergence, the relative differences are quite small and close to the suggested differences of between 0.1% and 1% from previous studies (Section 3.8.6). Nuttin *et al*. assessed the underestimation of the standard deviations of MCNP tallies suggesting that is most likely four factors larger (Nuttin, et al., 2013). Considering this, the power convergence is still large and increasing the KCODE parameters can reduce the maximum tally error to 0.5% instead of 2.5%. However, this would entail in an increase in computing resources and time therefore future studies can aim to optimise the KCODE parameters.

One should note that the combination of using two methods in relaxing the temperature and power is a new method for relaxation. In addition, the approach of using four figures of merit in measuring the convergence is an extremely firm and robust method and therefore adequate for the current study. Further studies should repeat these methods by enhancing the relative errors in MCNP.

The next section evaluates the coupled Iteration 26 to verify against the FSAR.

4.4.5 ITERX

4.4.5.1 NEUTRONIC TRANSPORT

The neutronic results for a full-core EPR with fresh fuel and CBC at HFP follow. The model uses temperatures predicted by several iterations between MCNP6 and RELAP5 (referenced as ITERX from here onwards). The NWU HPC calculated the majority of cases by using 12 processors. The results are in the sections of criticality, flux, power, reactivity coefficients, and control-rod worth. The comparison with the FSAR follows.

4.4.5.1.1 CRITICALITY

4.4.5.1.1.1 BORON WORTH

The boron worth for both the FSAR and ITER0X cases are negative and are in close agreement, with ITERX being more negative than the FSAR and ITER01 but still within the limits (see Table 4-14). The critical boron concentration (CBC) required resulting in a k_{eff}=1.00000 is calculated

at 1340 ppm which is 43 ppm less than the specification in the FSAR and is in good agreement. A possibility for a lower CBC might be due to slightly increased boron worth in ITERX.

4.4.5.1.2 FLUX

4.4.5.1.2.1 AXIAL FLUX DISTRIBUTION

Figure 4-11 shows the flux distribution in the EPR core in a 19x19 core lattice and the effects of the axial enrichment on the flux. ITERX is on the left-hand side whilst ITER01 is shown on the right-hand side in the figure. From previous experience, more source points are used (1000000) to reduce the statistical errors. The flux for ITERX decreases from bottom to top as expected, due to the decrease in moderator density. The decrease is more for ITERX than for ITER01. The top section of ITERX has a smaller flux while the bottom section features a larger flux compared to ITER01. The middle axial section has a “smooth” radial flux distribution due to the distribution of lower enriched assemblies between higher enriched assemblies. The axial distribution of the middle section is also “smooth”, due to the presence of gadolinium in the centre of the rods.

ITERX 1000 000 Source points	ITER01 1000 000 Source points	
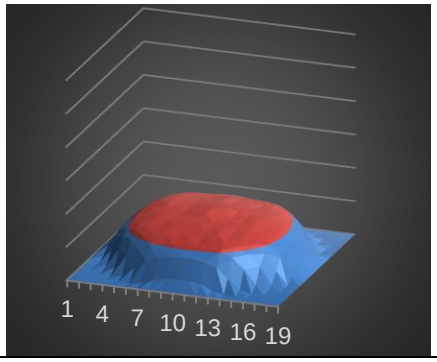	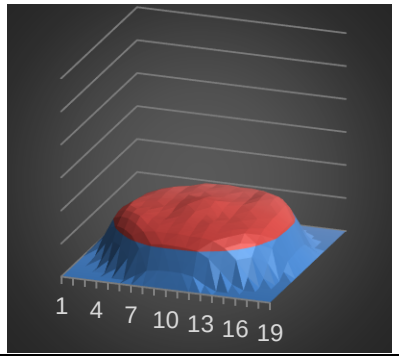	Top [420 cm-399 cm]
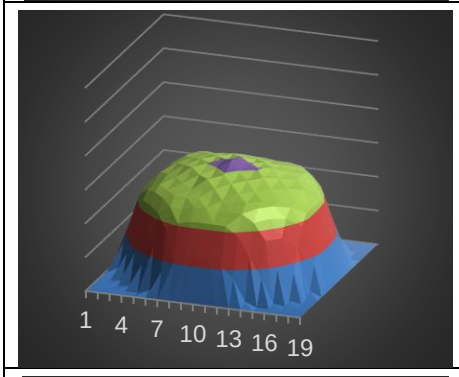	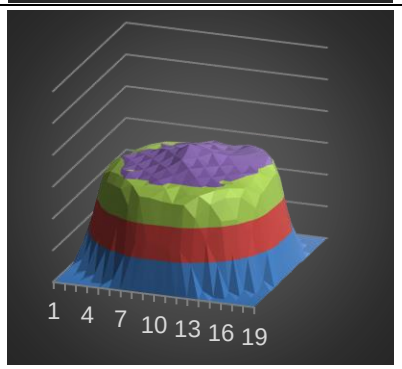	Top middle [378 cm-399 cm]
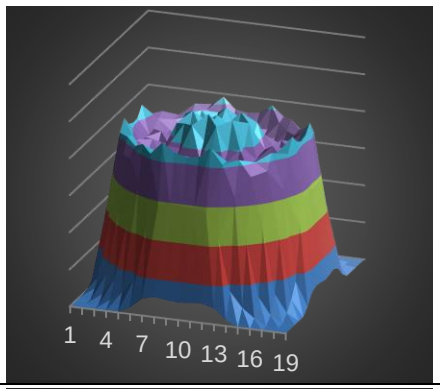	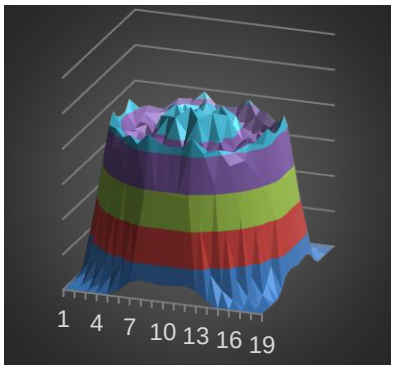	 n/s.cm^2 Middle [189 cm-231 cm]
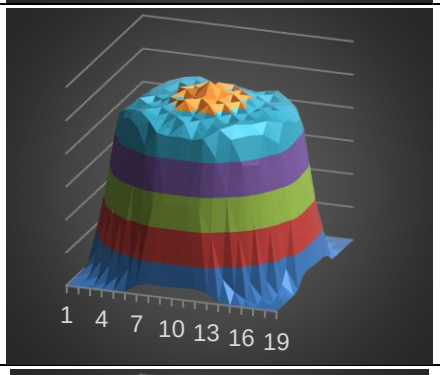	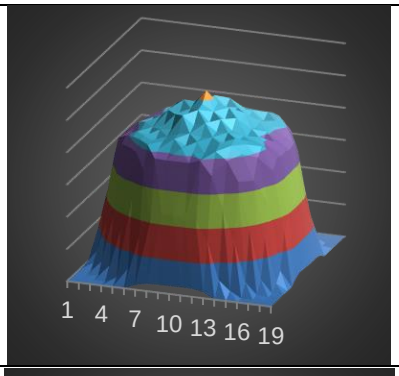	Bottom middle [21 cm-42 cm]
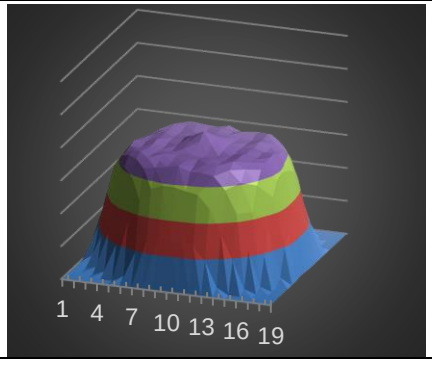	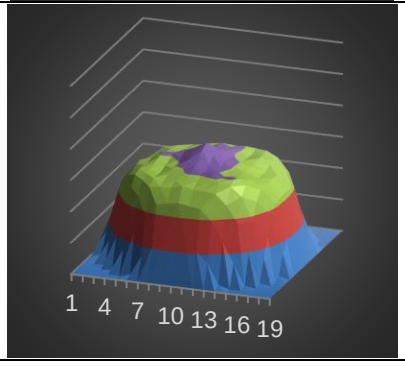	Bottom [0 cm-21 cm]

FIGURE 4-11 AVERAGE FLUX AT DIFFERENT AXIAL SECTIONS OF THE CORE (N/S.CM^2)

4.4.5.1.2.2 NEUTRON FLUX SPECTRUM

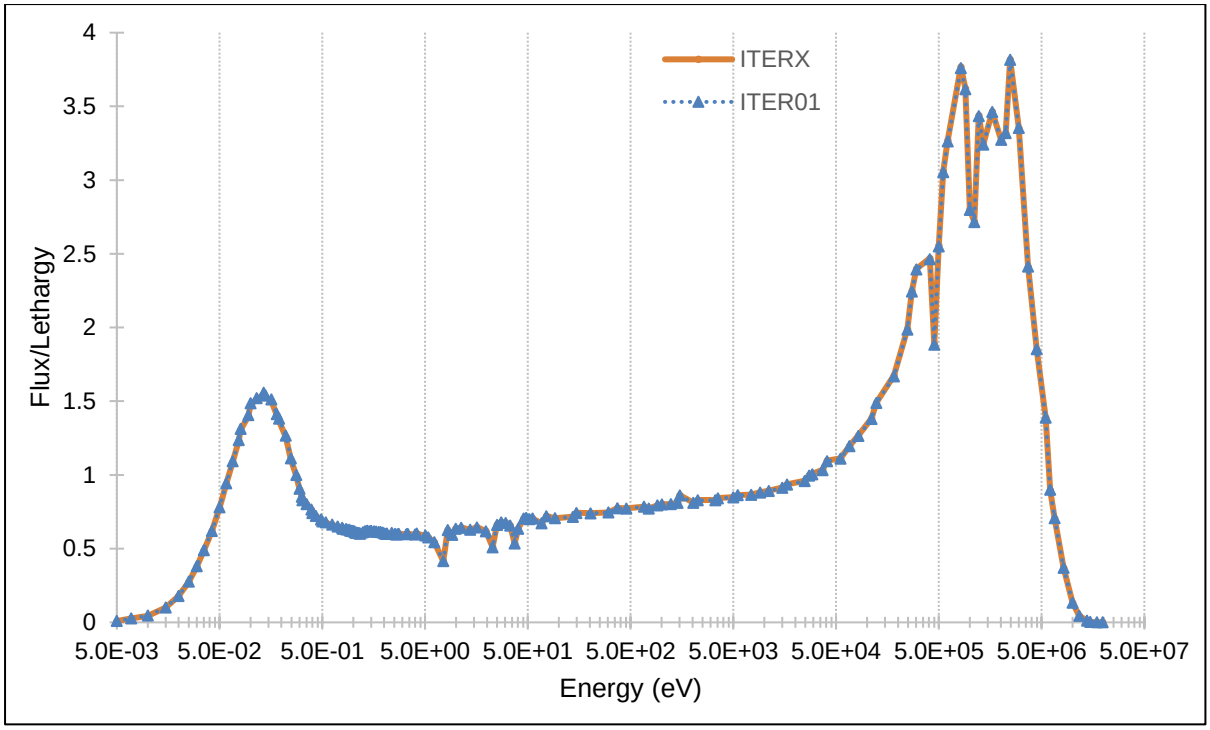

FIGURE 4-12 NEUTRON ENERGY SPECTRUM IN FUEL FOR ITERX

The FSAR does not specify the neutron flux spectrum explicitly and results compare the neutron spectrum tallied in the fuel of ITERX to ITER01 from the previous section. Figure 4-12 shows that the thermal neutron energy spectrum for ITERX remains the same as for ITER01 after coupling has been completed. This is because the H/HM did not change.

4.4.5.1.3 POWER PROFILE

Figure 4-13 shows the difference in the axial power shapes of the BOL fresh fuel for the FSAR, ITER01 and ITERX. ITERX shows a larger AO (axial offset is the power gradient between bottom and top of the core). Coupling temperature and power profiles in multiple iterations could cause this steeper gradient. As stated before, the FSAR graph is a typical axial power shape and not necessary the average of the full-core.

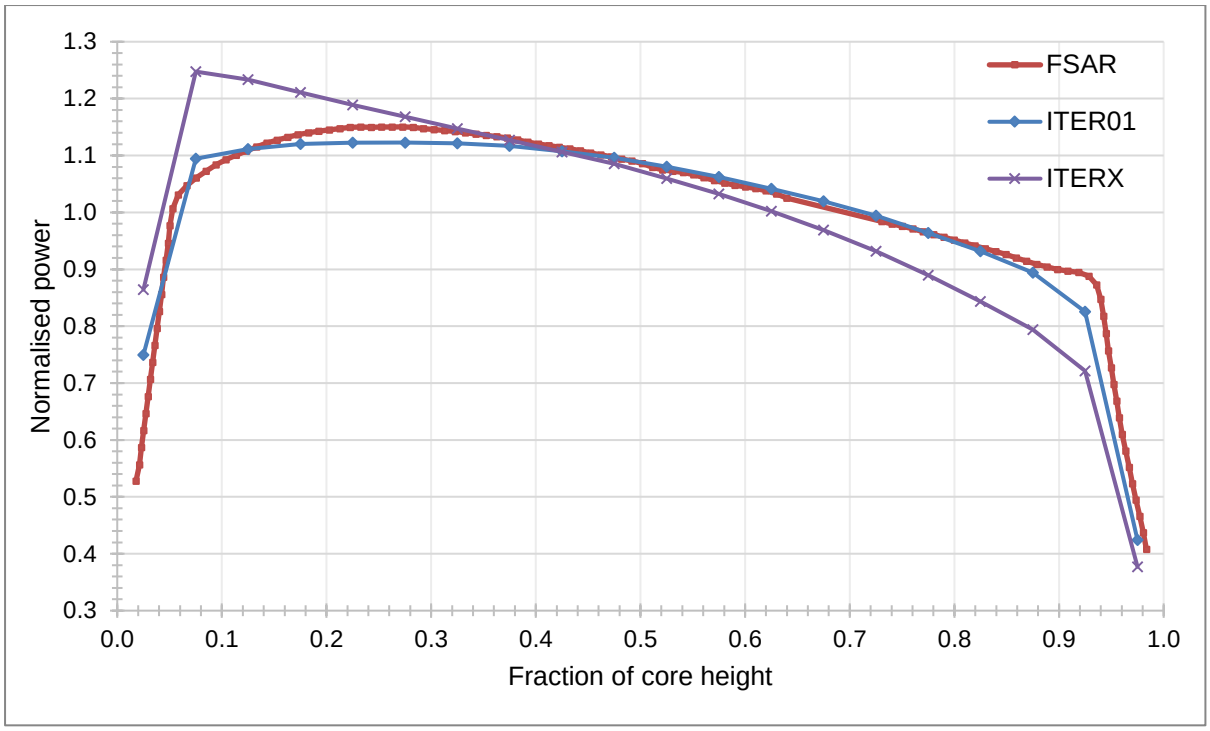

FIGURE 4-13 AXIAL POWER SHAPE AT BOL FOR ITERX

4.4.5.1.4 REACTIVITY COEFFICIENTS

Table 4-14 compares the FSAR results to ITERX and ITER01. ITERX has a less negative Doppler Coefficient, compared to the FSAR and ITER01. A value of -1 pcm/K falls outside the limits and standard deviations. Nonetheless, the DTC remains negative. The steeper AO of ITERX may be a reason for the increase in the DC since the Doppler effect (dependence on temperature) does not behave in a linear manner (Uto, 1999). This means that a 20 K difference on the top of the core may not have the same effect as a 20 K difference at the bottom of the core where temperature is higher.

The MTC for ITERX is in close agreement with the MTC results of ITER01.The moderator temperature coefficient for ITERX is negative and falls within the range provided by the FSAR as well as the range of acceptable limits.

4.4.5.1.5 DELAYED NEUTRON FRACTION

The delayed neutron fraction, β_{eff} for ITERX is (6.7%) smaller than the FSAR and the same as ITER01. Note that Lamarsh reported a delayed neutron fraction for ^{235}U at thermal energies of 0.0065, which is closer to current results compared to results in the FSAR (Lamarsh & Baratta, 2001). The difference between ITERX and the FSAR might originate due to different neutron data libraries used for the two cases as mentioned previously (Todosow & Kazimi, 2004).

TABLE 4-14 FULL-CORE ITERX COMPARISON OF NEUTRON PARAMETERS

	Limits	FSAR	ITER01[d]	ITERX[d]	Units
DC	(-4.90;-2.90[a])	(-3.24;-2.34)	-2.00±0.57	-1.00±0.57	pcm/K
MTC	(-70.0;0.00[a])	(-60.12;5.22)	-17.45±0.57	-16.67±0.53	pcm/K
β_{eff}	(0.0043;0.0072[c])	0.0074	0.0069±0.0001	0.0069±0.0001	-
BW	(-10.86;-5.71[a])	(-9.5;-7.9)	-9.01±1.13	-10.49±1.13	pcm/ppm
CBC	(0;1780[b])	1383.0	1349.5	1340	ppm

a. *(IAEA, 2003)*

b. (Delgado, et al., 1999)

c. (Björk, et al., 2013)

d. BOL, HFP, k_{eff}=1.00000 RCCAs out, no xenon, CBC

4.4.5.1.6 CRW

The total CRW for ITERX from all banks was determined (as discussed in Section 4.3.1.1.8) to be 10263±10 pcm compared to 10322 pcm from ITERX and 10942 from the FSAR. The reference case CRW is 6.2% smaller than the FSAR, which is in close agreement.

Figure 4-14 compares the integral rod worth (IRW) curve for bank B of the modelled EPR (ITERX) to the result in Section 4.4.3.1.6 (ITER01) as well as the IRW curve reported in the FSAR. The integral rod worth was normalised for both cases to compare. Results for ITERX in Table 4-15 show the same trend as ITER01; however, the graph is not as smooth compared with ITER01. Possible reasons are the statistical uncertainties in MCNP6 calculations and a different power profile.

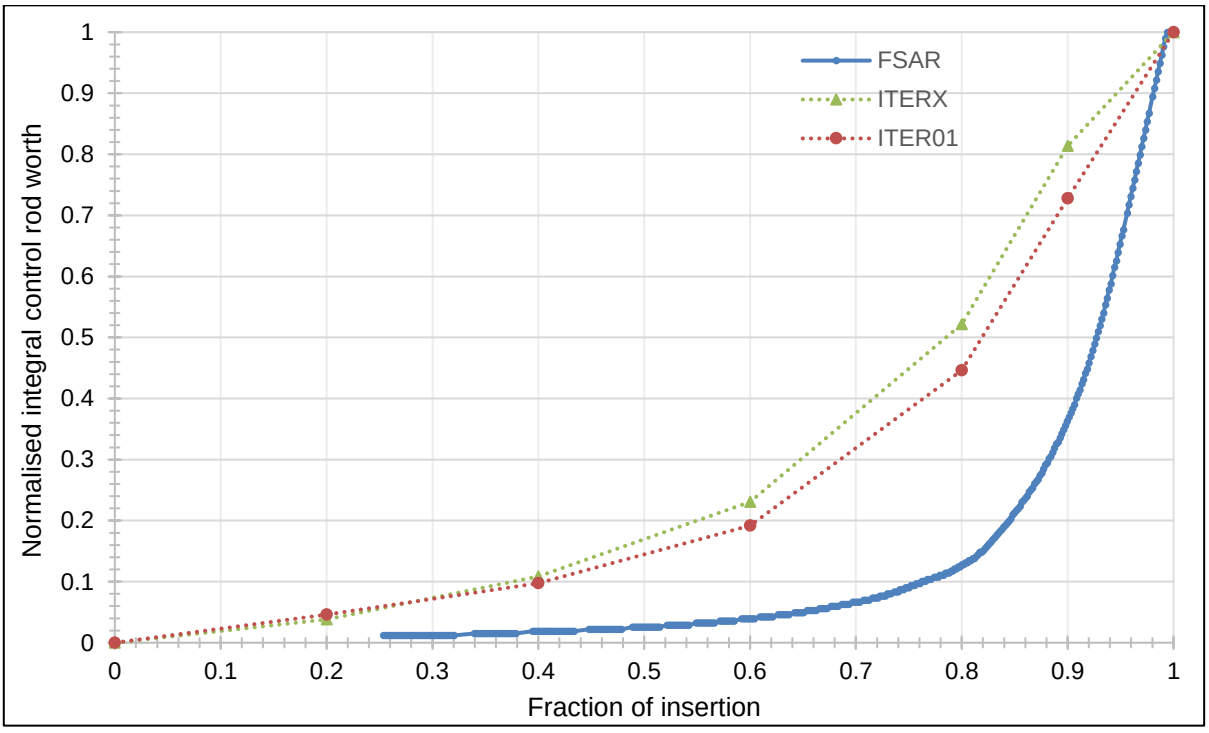

FIGURE 4-14 INTEGRAL CONTROL-ROD WORTH FOR ITERX

4.4.5.2 THERMAL-HYDRAULICS

Results show that the thermal volume flow for ITERX is the same as ITER01, which is larger than that for the FSAR even though the mass flow rate is slightly less. Table 4-15 also shows that the pressure drop model (by adjusting the forward losses in the pipes) is accurate.

TABLE 4-15 THERMAL-HYDRAULIC PROPERTIES COMPARISON

	FSAR	ITER01	ITERX	Units
Outlet temperature	603.206	602.921	602.921	K
Thermal volume flow rate	3.78	4.29	4.29	m^3/s
Mass flow rate	2901.10	2800	2799.99	kg/s
Average heat flux	5.830E+05	5.830E+05	5.814E+05	W/m^2
Maximum heat flux	1.45E+06	9.49E+05	9.77E+05	W/m^2
Fq	2.60	1.63	1.68	-
Pressure drop	3.829E+05	3.782E+05	3.821E+05	kPa
Outlet pressure	1.551E+07	1.552E+07	1.552E+07	kPa

$* \% Difference = \frac{FSAR - REF}{FSAR}$

The average heat flux for ITERX is slightly lower than for the ITER01 and FSAR cases. This difference might originate from small errors in the normalisation and relaxation calculations as well as rounding off differences within NWURCS. Fq is higher for ITERX than for ITER01 as was expected due to the coupling. Fq is smaller than for FSAR because the FSAR may have calculated another case, for instance the worst-case scenario. The specific state of the data from FSAR is not clear; therefore, the specific comparison between the FSAR and ITER01 will not yield identical results.

Table 4-16 shows the RELAP5 calculated temperatures for ITERX.

TABLE 4-16 AVERAGE CALCULATED TEMPERATURES FOR DIFFERENT MATERIALS

Material temperature	MCNP temperature field	ITER01	ITERX
Average fuel centreline temperature	-	1251.63	1251.76
Average fuel temperature	1050	1031.11	1031.16
Average gap temperature	740	730.10	730.40
Average cladding temperature	630	616.11	616.73
Average coolant temperature	586.9	588.32	589.00

The FSAR did not report these temperatures for comparison to the current model, but a representative temperature field is required for accurate representation of the core. Table 4-16 shows that the average temperatures from ITER01 to ITERX did not change by much. The largest difference was in the coolant at 0.7 K, which is acceptable and shows that the initial assumed temperatures are in order. The average cladding temperature increased by 0.6 K, the average gap temperature changed by 0.3 K and the average fuel temperature changed by as little as .0.05 K.

4.4.5.3 CONCLUSION

Section 4.4.5.1 presented the neutronic transport results for a full-core EPR after coupling with fresh fuel and CBC at HFP. The results compared ITERX to ITER01 and the FSAR to evaluate the model. The power profile showed a steeper AO. All the results were in good agreement with ITER01 and the FSAR; however, the DC showed a larger (less negative) value than expected and possible reasons were proposed.

The thermal-hydraulic results for ITERX are in good agreement with the FSAR and the value for Fq was more realistic.

These results give confidence in the following two ways: (a) expansion of the model to include Th in the core and (b) verification of NWURCS in generating the input decks.

The results for ITERX are satisfactory and the coupling methodology implemented in NWURCS produced reasonably good results. However, it is recommended to repeat the process by enhancing the relative errors in MCNP.

4.4.6 BURNUP

Fuel assembly B1 has an average enrichment of 2.62 wt.% and is chosen as the reference fuel assembly since its' enrichment is the closest to the full-core, which is 2.66 wt.%. Note that the first option for burnup is at the calculated CBC of 1350 ppm and HFP, and therefore one can expect a multiplication factor close to or less than one. The boron for the model stays at 1350 ppm whereas in practice it is adjusted during the cycle. Maintaining the CBC constant at 1350 ppm will result in k_∞ dropping below one. This is an approximation since the boron worth will change during the cycle, which will influence the MTC.

The second calculation modelled fuel assembly B1 for all three cycles without any boron in the water and forms a reference case and starting point in order to design the thorium-uranium fuel. Section 4.3.1.1.5 discussed the calculation and modelling of the burnup for assembly B1. Figure 4-15 shows the infinite multiplication factor for FAB1 for one cycle at 1350 ppm and for all three cycles at 0 ppm boron.

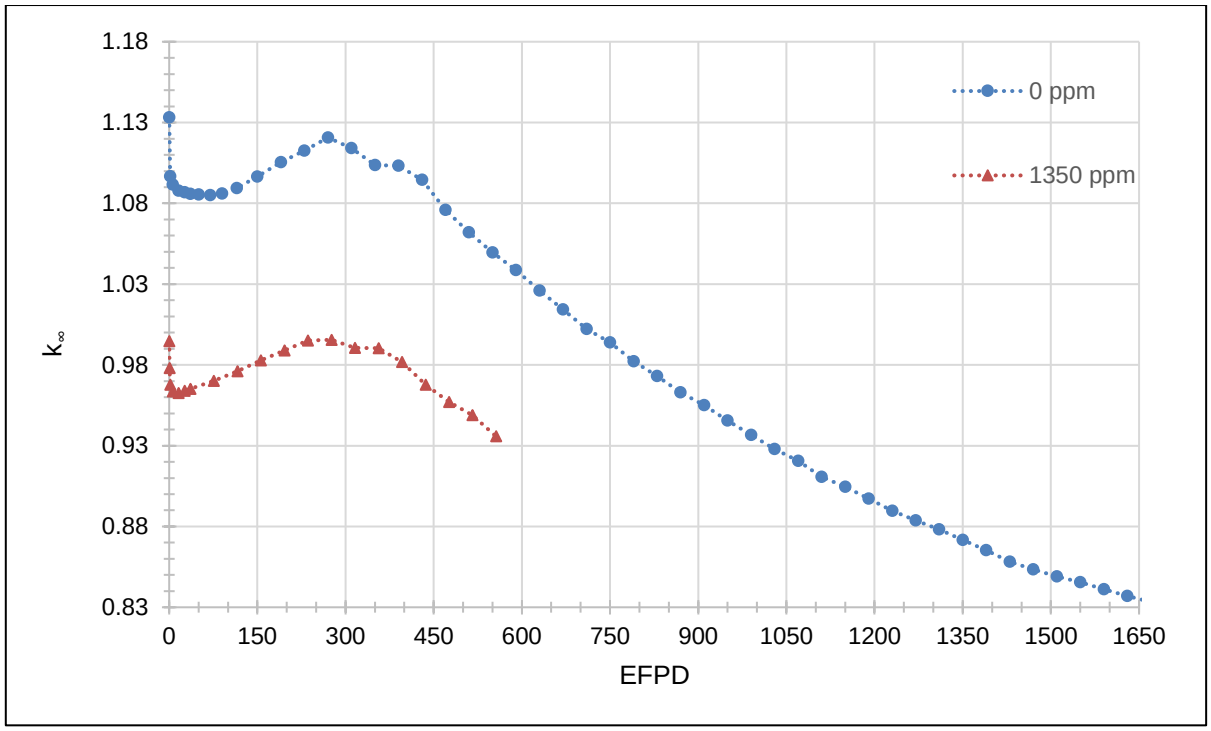

FIGURE 4-15 REACTIVITY OF FAB1 AT DIFFERENT BORON CONCENTRATIONS

The end of life infinite multiplication factor at 1642.5 EFPD is 0.83590±.0.00015 (calculated by interpolation of the final two data points). This value of k_∞ will form the reference point for the thorium-uranium end of cycle value. The total reactivity swing is 29738 pcm. Note that both the burnup options (blue at 0 ppm boron and red at 1350 ppm boron) show the same trend from 0 to 556 EFPD and almost a constant offset can be noticed due to boron.

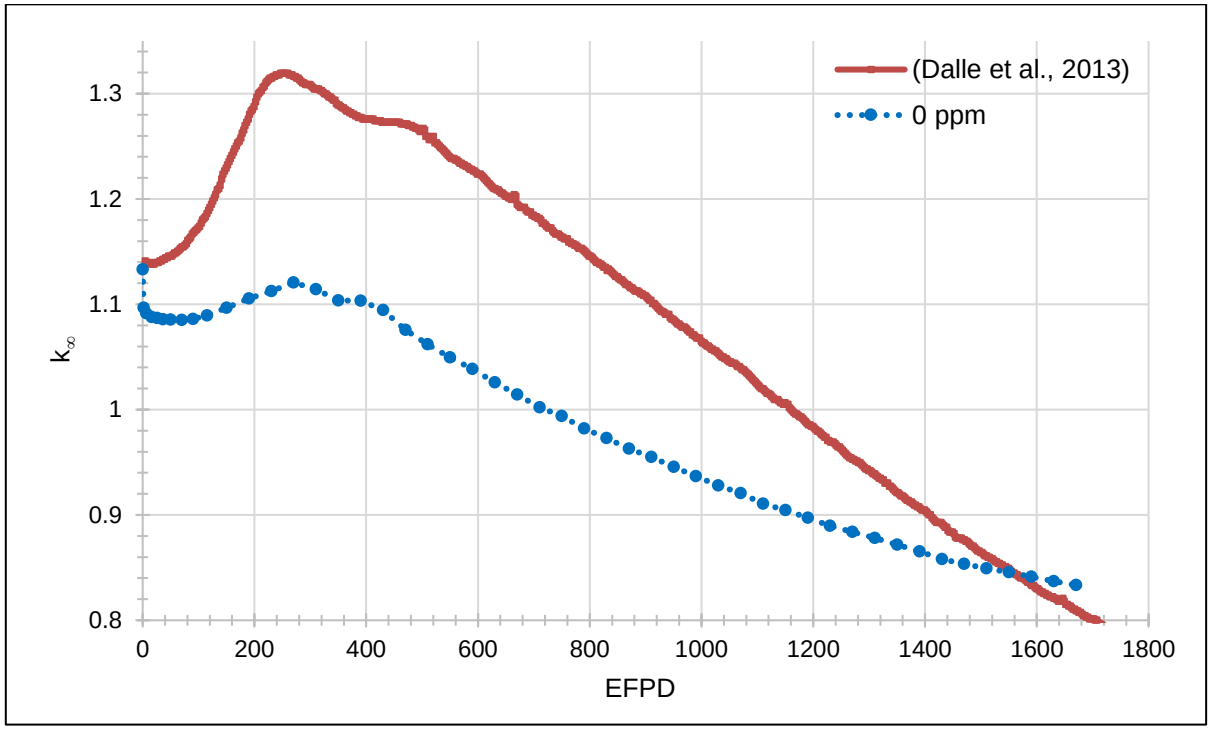

FIGURE 4-16 REACTIVITY OF FAB1 COMPARED TO (DALLE, ET AL., 2013)

The FSAR does not produce results for burnup in order to compare to the current model. However, the burnup of FAB1 is compared to results in Dalle *et al.*. Figure 4-16 compares the burnup curve for FAB1 at 0 ppm boron to a similar model with 4% Gd_2O_3 content and 3.5% enrichment. Dalle *et al.* modelled a 3x3 subassembly of 9 pins, where 7 pins are UO_2, one is the instrumentation pin and one is the gadolinium-containing pin. The enrichment is 1% higher and the Gd_2O_3 content is also larger compared to FAB1. Therefore, one expects a higher eigenvalue and a more pronounced effect of Gadolinium on the eigenvalue. Nonetheless, notice for both curves the turning point at ~270 days when the gadolinium burns out. A second turning point can also be noticed at ~430 days when the eigenvalue starts to decrease again. The general trend for both graphs are the same and this gives confidence that the burnup model for FAB1 is being modelled correctly.

Figure 4-17 focuses on the first cycle to evaluate the initial change in k_∞ at 1350 ppm. The cycle starts with a k_∞ of 0.99477±.0.00020 and ends at 547.5 EFPD (which is the specified cycle-length of the FSAR) where k_∞ is 0.93855 (calculated with linear interpolation). This eigenvalue will form the reference point for the design of the thorium-uranium fuel. The reactivity swing of one cycle is 5651.82 pcm. The initial drop of reactivity during the first five days is due to the accumulation of poisonous fission products such as xenon and samarium as shown in Figure 4-18.

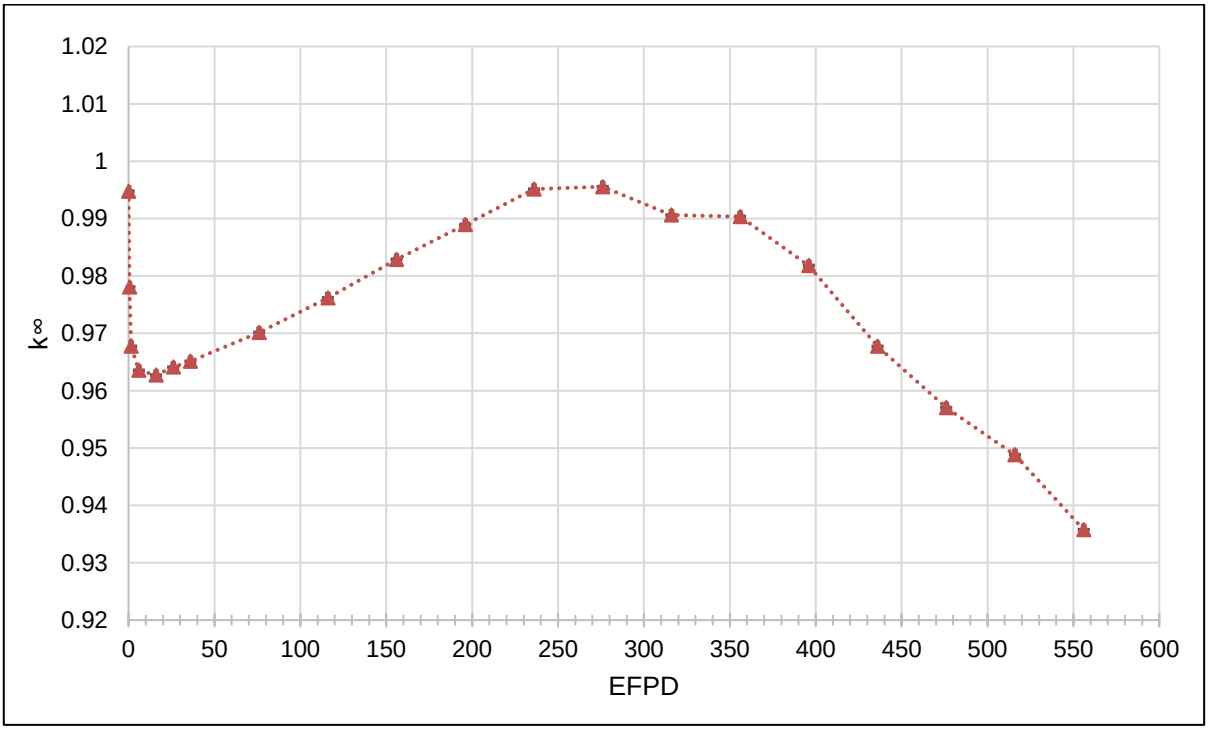

FIGURE 4-17 REACTIVITY OF FAB1 FOR THE FIRST CYCLE AT 1350 PPM

These isotopes like Xe and Sm increase in the first few days and then approach equilibrium values. Stacey also reported this behaviour, where the ^{135}Xe concentration stabilises at 1.5 days and ^{149}Sm stabilises at 25 days (Stacey, 2007).

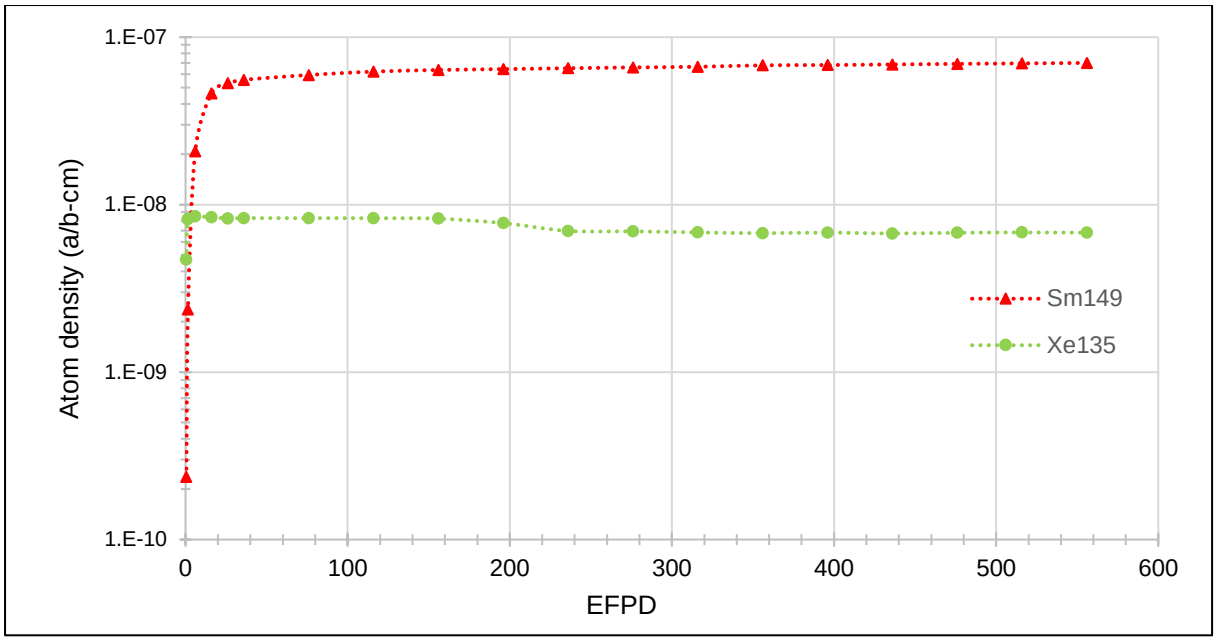

FIGURE 4-18 XENON AND SAMARIUM BUILDUP DURING BURNUP

Figure 4-19 illustrates that the most absorbing isotopes of gadolinium (with natural abundance) burn out at ~276 days after startup. The uranium enrichment and Gd_2O_3 fraction in the fuel will influence the time at which these isotopes burn out, but current results are comparable to (Dalle, et al., 2013). The decreasing trend of the gadolinium isotopes is also visible in the increasing eigenvalue in Figure 4-17 up to ~276 days.

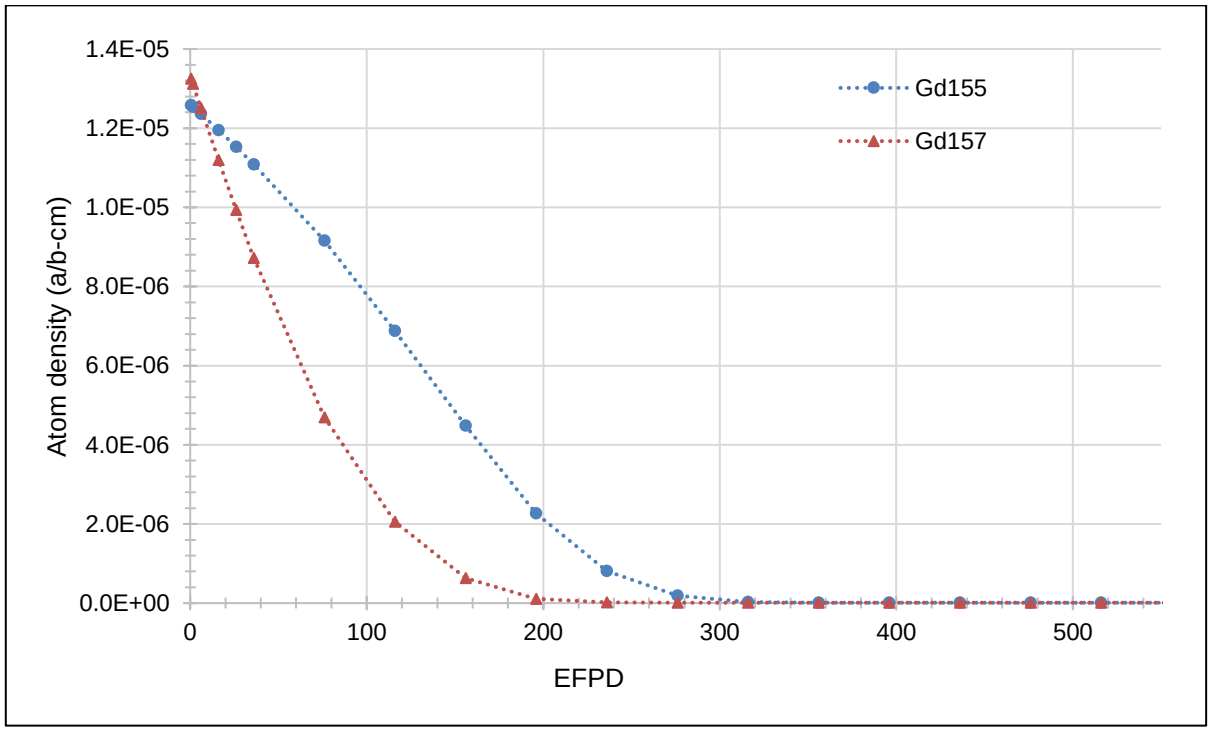

FIGURE 4-19 DEPLETION OF THE MOST ABSORBING ISOTOPES OF GADOLINIUM

The end of the first cycle burnup calculated by MCNP6 is 19.45 GWD/MTU, which is within the specification of 18-22G WD/MTU in the FSAR of the EPR. The end of three cycle accumulated burnup is ~53.96 GWD/MTU, which is smaller than the FSAR value of 55-62 GWD/MTU but still in close proximity. This verifies that the MCNP6 model is in close correlation with the FSAR.

The main fissile isotope ^{235}U, depletes as the first fuel-loading cycle progresses and some of the fission neutrons are absorbed in the ^{238}U to breed ^{239}Pu, which also fissions and contributes to the power of the EPR. However, at the end of the first cycle, the ^{235}U content remains above that of ^{239}Pu being twice as much as the ^{239}Pu. Figure 4-20 shows the depletion and build-up of the main fissile isotopes and evolution of the sum of the fissile isotopes. The sum of the fissile contents declines as the cycle progresses and fuel depletes.

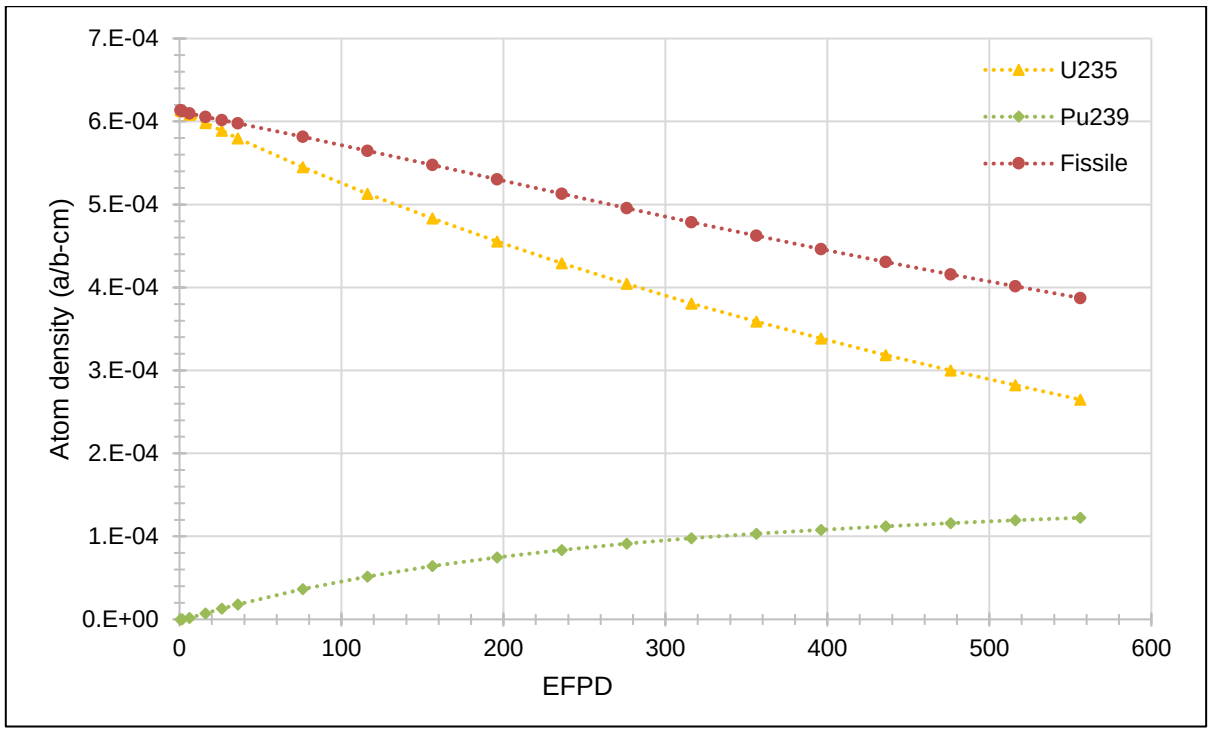

FIGURE 4-20 DEPLETION AND BUILDUP OF MAIN FISSILE ISOTOPES

4.5 CONCLUSION

As set out by the aims of this study, the following was delivered in this chapter:

- Development of a MCNP6 full core model with temperature characteristics of the EPR core,
- Verification of NWURCS in creating such an input,
- Coupling MCNP6 with RELAP5 using NWURCS in line with the goals of the reactor analysis group at the School of Mechanical and Nuclear Engineering at the NWU,
- Further verification of NWURCS in creating burnup models.

Section 4.4 presented the results for the EPR at HFP. ITER01 results included the MCNP6 results with one iteration between MCNP6 and RELAP5. ITERX results presented the coupled solution after multiple iterations between MCNP6 and RELAP5.

The neutronic results for ITER01 in terms of boron worth, axial flux distribution, neutron flux spectrum, power profile, reactivity coefficients and control-rod worth showed similar results compared to the FSAR and are within acceptable limits. The only difference was the delayed neutron fraction and a possible reason might be the different neutron data libraries used for the two cases.

The neutronic results for ITERX are also in good agreement. The power profile shows a steeper gradient. All the results were in good agreement with ITER01 and the FSAR; however, the DC showed a larger value than expected and possible reasons were given. The thermal-hydraulic results for ITERX are in good agreement with the FSAR. Average temperatures due to coupling provided better guess values for temperature fields in ITER01.

The coupling methodology was correctly implemented in NWURCS; however, it is recommended to repeat the process by reducing the relative errors in MCNP6. For the next section of the study coupling will not be included, since temperature fields obtained from the coupling are relatively accurate. The thorium-based fuel design simulations will use the same temperature fields.

In order to design new thorium-uranium fuel for the EPR, a reference burnup model was developed. Results were as expected and this shows that the burnup model for FAB1 was modelled correctly. These results add to the verification of NWURCS in generating the input decks. Verification of the reference EPR model showed no major differences and the model can now be used to adjust for thorium-uranium fuel.

5. TH-EPR

"Great things are done by a series of small things brought together."

~ Vincent Van Gogh ~

Overview

After the verification of the reference uranium EPR model, the baseline model is extended to include thorium-uranium fuel. Chapter 5 provides the design methodology and results. Sections 5.1 and 0 describe the method of modifying the models to develop thorium-based fuel. Section 5.4.1 reports the results of the newly designed Th-EPR FAB1. Section 5.4.2 presents a comparison of the results of the full-core fresh Th-EPR to the EPR, FSAR and other studies. Section 5.4.3 presents the EOL properties for the Th-EPR FAB1 and Section 5.5 provides conclusions on the new thorium-uranium fuel for an EPR.

5.1 DESIGN METHODOLOGY

The principal objective of this work is to design and develop mixed thorium-uranium fuel for the European Pressurised Reactor (EPR), while increasing the burnup and fuel-cycle length. The geometry of the EPR remains fixed, whilst adding thorium and optimising the fissile content of the proposed fuel to reach 24-month fuel-cycles.

Based on the conclusion drawn in Section 3.10, the fuel needs to include:

1. Homogeneously mixed thorium-uranium fuel,
2. Slightly higher enriched (+2.7 wt.%) than conventional uranium fuel to reach extended fuel burnup (24 months),
3. The lowest possible gadolinium content,
4. More ^{232}Th that can replace gadolinium,
5. Enriched soluble boron and natural B_4C control-rods,
6. Maintain properties within design limits (see Section 3.9).

The fuel design should minimise BP requirements as well as initial enrichment requirements, while still achieving a 24-month fuel-cycle. In other words, the goal is to design fuel with the smallest possible reactivity swing. Assembly B1 is the reference design, since it has the closest enrichment compared to the average of the full-core. The thorium-uranium assembly B1 needs to reach three 24-month cycles with the k_∞ eigenvalue larger or equal to that of the reference case at the end of life (0.83590).

After designing the fuel for fuel assembly B1, the next step is changing the rest of the fuel assemblies in the same way and then testing the full-core.

5.2 TH-EPR MODEL

As discussed in Section 1.3 the goal is to keep the geometry of the EPR fixed without compromising safety. Sections 5.2.1 to 5.2.3 describe the only changes made to the reference model. All calculations use the current ENDF/B-VII.1 cross-section libraries. Everything else in the Th-EPR model are similar to the reference EPR model discussed in Section 4.2. Coupling will not be included for this model, since temperature fields obtained from the coupling of Section 4.4.4 are relatively accurate. The thorium-based fuel design simulations will use the same temperature fields.

5.2.1 THERMAL DESIGN

As mentioned in Section 3.2 ThO_2 has a ~9% (from Table 3-1) lower density than UO_2 which will reduce the number of fertile and fissile atoms. Furthermore, Section 3.3.1 notes that ^{233}U has a smaller recoverable fission energy, which is ~1.1% lower than for ^{235}U (from Table 3-3).

If one had to maintain the same power level as specified for the EPR, the thorium-uranium fuel (taking into account above properties) would be burnt more for each time-step. This would mean that more fission products, a higher RIP, cladding and fuel pellet degradation, and pellet cladding interactions would occur for each equivalent time-step of the EPR.

To mitigate these effects caused by the reduction in density and recoverable fission energy the reactor power is reduced by 7.5%. This results in a total thermal power output of 4245.75 MWt instead of 4590 MWt. From initial studies this value produced similar burnup values compared to the uranium only EPR. This value was chosen to be conservative and future studies should determine the optimal power value.

The reduced power will affect the material temperatures when accounting for thermal hydraulic coupling/feedback and therefore requires follow-on studies.

5.2.2 MATERIALS

Thorium-uranium fuel for the EPR is developed by homogeneously mixing in ThO_2 (^{232}Th) with the existing UO_2 (^{235}U & ^{238}U). The model uses a 95% theoretical density for ThO_2 (stated in Table 3-1), which results in a density of 9.5g/cm^3. The proposed fuel is limited to a 19.99 wt.% ^{235}U in enrichment (in uranium) to adhere to the LEU non-proliferation limit (Weaver & Herring, 2002). Note that the overall fissile content remains below 3 wt.% since UO_2 is mixed with ThO_2 to dilute the fissile content. Assembly B1 is the reference design, since it has the closest enrichment compared to the average of the full-core. Once the design of B1 is finalised, the next

step is to alter the remaining six different homogeneous thorium-uranium fresh fuel assemblies similarly.

In order to start designing new thorium-uranium fuel to compare to the EPR B1 fuel assembly, a new definition for enrichment should be used (since an extra fertile isotope ^{232}Th contributes to the fuel mix). Material fractions can be expressed either in wt.% or at.% and at.% was used for a better comparison (since Th has a lower density) and developing the new fuel mixture. Eq. 5-1 shows the new definition for initial fissile content.

$$\text{Initial fissile content} = \frac{\text{at.\% fissile isotopes}}{\text{at.\% fertile isotopes} + \text{at.\% fissile isotopes}} \qquad \text{Eq. 5-1}$$

When applied to UO_2 fuels Eq. 5-1 becomes:

$$\text{Initial fissile content} = \frac{\text{at.\% }^{235}\text{U}}{\text{at.\% }^{238}\text{U} + \text{at.\% }^{235}\text{U}} \qquad \text{Eq. 5-2}$$

This is also the definition of enrichment in uranium fuel in at.%. For (ThO_2/UO_2) fuels Eq. 5-1 becomes:

$$\text{Initial fissile content} = \frac{\text{at.\% }^{235}\text{U}}{\text{at.\% }^{232}\text{Th} + \text{at.\% }^{238}\text{U} + \text{at.\% }^{235}\text{U}} \qquad \text{Eq. 5-3}$$

By setting Eq. 5-2 equal to Eq. 5-3 one can calculate the fraction of uranium required (due to the LEU enrichment limit of 19.99 wt.%). The remaining fraction will be thorium.

As was shown in Table 4-2, four different fuel types are present in fuel assembly B1. Two of the four fuels include Gd_2O_3. Since ternary mixtures of ThO_2, UO_2 and Gd_2O_3 are difficult to achieve (see Section 3.4.4), and the fact that ^{232}Th can act as a burnable absorber, the suggestion is to replace these 12 fuel pins containing Gd and U in the centre with only pure ThO_2. Note that this will reduce the total fissile content, since there is no UO_2 in these fuel types within the assembly.

B_4C rods replace the Cd-Id-Ag rods, because thorium containing cores are expected to have a lower control material worth (Section 3.4.4).

5.2.3 BURNUP

In order to design the thorium-uranium fuel, it needs to be compared to the reference uranium-only FAB1. Section 4.4.6 showed the results for the two different burnup option models. The first option kept the boron concentration constant at 1350 ppm (CBC) and the second option kept the boron concentration constant at 0 ppm. Since the boron worth and CBC of the newly developed thorium-uranium fuel is unknown at this stage, preliminary burnup calculations assumed a boron concentration of 0 ppm. Burnup calculations at 0 ppm boron can now easily be compared with the 0 ppm uranium only FAB1 burnup results. After the final fuel composition selection, the CBC

for the fresh full-core Th-EPR is calculated in Section 5.4.2 as well as the end of life critical boron concentration for Th-EPR FAB1 in Section 5.4.3.

In order for the proposed fuel to reach a 24-month fuel cycle, it should have a higher or the same reactivity as the EPR reference fuel after 18 months. Since the EPR cycle-length is 547.5 EFPD, the Th-EPR should reach 730 EFPDs.

Three cycles of 24-months correspond to an expected EOL burnup of 75 GWd/MTHM. The higher discharge burnup and fuel-cycle length will depend on the clad and fuel performance. The current study does not consider these constraints and further studies should investigate this in more detail.

Burnup time-steps used for thorium-uranium fuel are 45-day time-steps instead of 40-day time-steps. The cycle-length for the thorium-uranium fuel is longer than for the uranium only cycle and extending the time steps will save some computational time. It is common practice to increase the time-steps as the burnup increases (Section 4.3.1.1.5). Table 5-3 shows the time steps for three thorium-uranium cycles. Burnup calculations used fission product “Tier 3” since it is the most detailed.

TABLE 5-1 MCNP6 TIME-STEP DURATION IN EFPD

#	Time-step	Total time	#	Time-step	Total time	#	Time-step	Total time
1	1.5	1.5	**20**	45	630	**39**	45	1485
2	4.5	6	**21**	45	675	**40**	45	1530
3	10	16	**22**	45	720	**41**	45	1575
4	10	26	**23**	45	765	**42**	45	1620
5	10	36	**24**	45	810	**43**	45	1665
6	14	50	**25**	45	855	**44**	45	1710
7	20	70	**26**	45	900	**45**	45	1755
8	20	90	**27**	45	945	**46**	45	1800
9	45	135	**28**	45	990	**47**	45	1845
10	45	180	**29**	45	1035	**48**	45	1890
11	45	225	**30**	45	1080	**49**	45	1935
12	45	270	**31**	45	1125	**50**	45	1980
13	45	315	**32**	45	1170	**51**	45	2025
14	45	360	**33**	45	1215	**52**	45	2070
15	45	405	**34**	45	1260	**53**	45	2115
16	45	450	**35**	45	1305	**54**	45	2160
17	45	495	**36**	45	1350	**55**	45	2205
18	45	540	**37**	45	1395			
19	45	585	**38**	45	1440			

5.3 FUEL DEVELOPMENT

5.3.1 PRELIMINARY FUEL COMPOSITION

After fixing the geometry and defining the fuel material composition in terms of initial fissile content, a model is developed for the new fuel for the first 24-month fuel-cycle without any boron as discussed in Section 5.2.3.

It is important to determine the fuel composition in terms of uranium content and thorium content to compare the reactivity of the proposed fuel design with the uranium only EPR fuel assembly B1. Since the enrichment in the UO_2 is fixed at 19.99 wt.%, an increase in the uranium content (and subsequent decrease in ThO_2 content) will result in an increase in the overall initial fissile content.

According to Section 3.6.2 thorium-uranium fuels require about 2.7 wt.% more overall initial fissile content compared to standard uranium PWRs. However, the fuel designers of the EPR optimised the fuel for maximum fuel utilisation and one can expect that the enrichment in the thorium-uranium fuel can be lower in comparison to previous thorium-uranium studies. Therefore, it was decided to start with a composition of 1.3 at.% higher initial fissile content (compared to standard EPR design) as calculated by Eq. 5-2 and Eq. 5-3. Table 5-2 tabulates the different compositions used in the model. Some of the fuel designs included Gd and some cases had no Gd. These values were obtained using a trial-and-error method. One 24-month fuel cycle is modelled to compare against the uranium FAB1 reference case.

TABLE 5-2 DIFFERENT COMPOSITIONS FOR THORIUM-URANIUM FUEL DESIGNS

Model	Initial fissile content*	Gadolinium
A	+1.30 at.%	No
B	+1.22 at.%	Yes
C	+0.32 at.%	No
D	-0.07 at.%	No

** Difference compared to EPR design*

Figure 5-1 shows that the first attempt (option A in Table 5-2) results in a too high BOL reactivity (even though some Gd was included), which is well above the value for the reference EPR FAB1. This means that the initial fissile content can be reduced. The second attempt, option B where the initial fissile content was decreased to imitate the k_∞ vs. time graph of EPR FAB1, still had a high value for k_∞.

Options C and D showed promise. Option C starts with the same reactivity but has a higher value for k_∞ at EOC compared to EPR FAB1. This means that the initial fissile content can be reduced even further to save on enrichment costs. Option D starts with a lower BOL reactivity but still has a higher value for k_∞ at EOC compared to EPR FAB1.

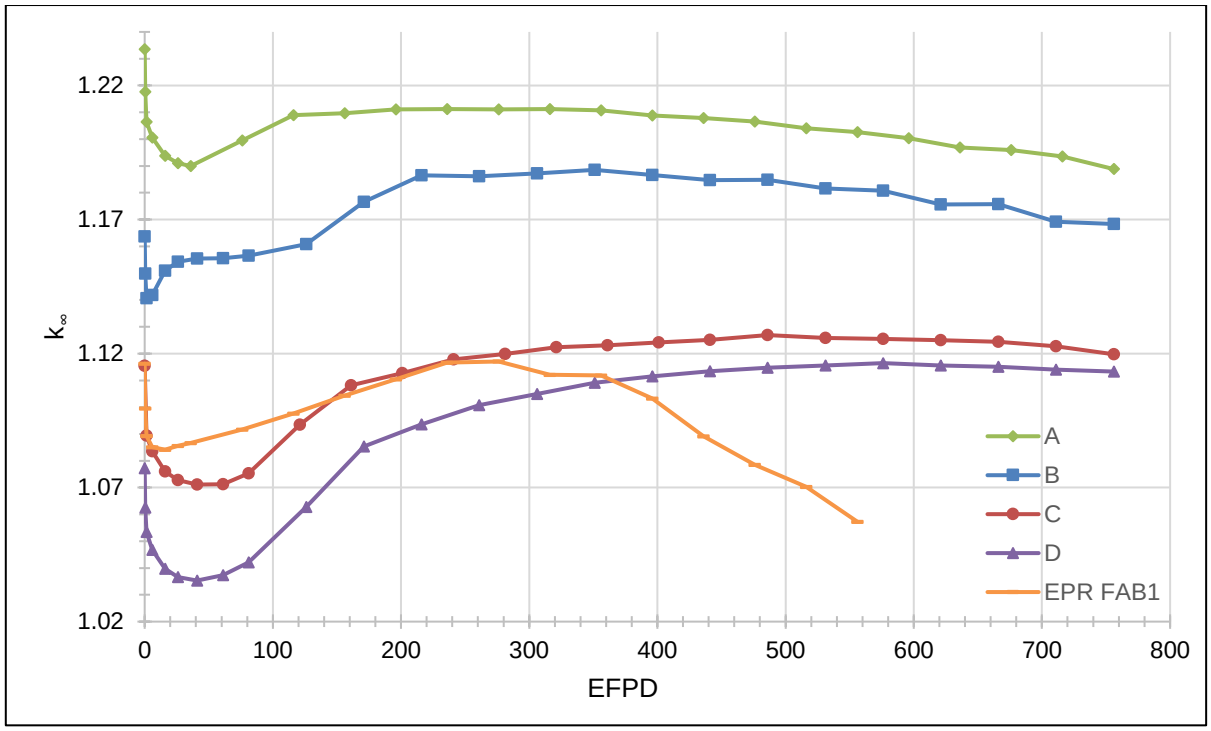

FIGURE 5-1 BURNUP FOR DIFFERENT THORIUM-URANIUM FUEL DESIGNS

Further analyses uses Option D and will be discussed in Section 5.3.2.

5.3.2 FINAL FUEL COMPOSITION

Table 5-3 describes the final design, composition and location of different fuels in terms of thorium-uranium fuel for FAB1. Note that the total FA initial fissile content in at.% will be slightly less compared to the EPR since pure ThO_2 replaces central axial uranium and gadolinium containing sections in 12 pins. This results in the overall fissile content of the average of the fuel assembly of 2.58 at.%.

TABLE 5-3 THORIUM-URANIUM FUEL ASSEMBLY B1 DETAILS

Axial Length (cm)	Zone	Composition		
		Pin type 1	Pin type 2	Pin type 3
Number of pins		253	8	4
20.32	Blanket	89.79% ThO_2 10.21% UO_2 = 2.03 at.% ^{235}U		
15.24	Cut-back	86.19% ThO_2 13.81% UO_2 = 2.73 at.% ^{235}U		
354.95	Central	86.19% ThO_2 13.81% UO_2	Pure ThO_2	Pure ThO_2
15.24	Cut-back	86.19% ThO_2 13.81% UO_2 = 2.73 at.% ^{235}U		
15.24	Blanket	89.79% ThO_2 10.21% UO_2 = 2.03 at.% ^{235}U		

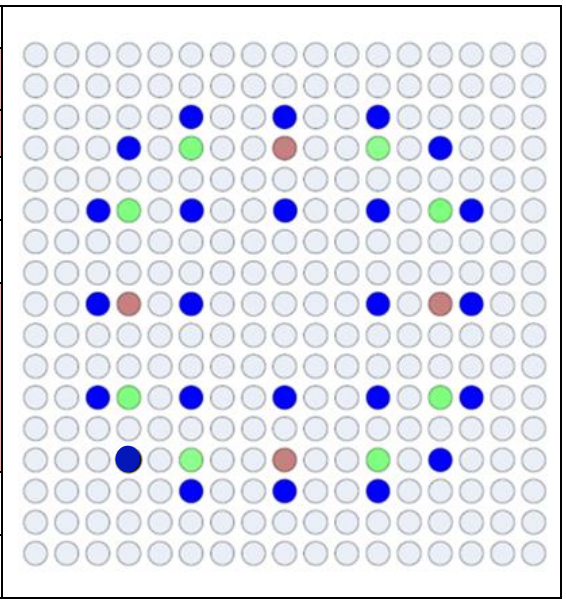

**Composition in wt.% with 19.99 wt.% enrichment in UO_2*

5.3.3 CYCLE ONE

MCNP6 burned the thorium-uranium fuel assembly B1 with equivalent initial fissile content for 730 EFPD without boron. Important factors considered are:

- The infinite multiplication factor of the fuel should not fall below 1.03 (since a leakage factor of 0.03 was assumed as a guide for FAB1 (Weaver, et al., 2000))
- The excess reactivity in the BOL should not be too high, since the limit on max boron is 1780 ppm (Section 3.9).
- The k_∞ value should not drop below the value of the reference uranium EPR FAB1.

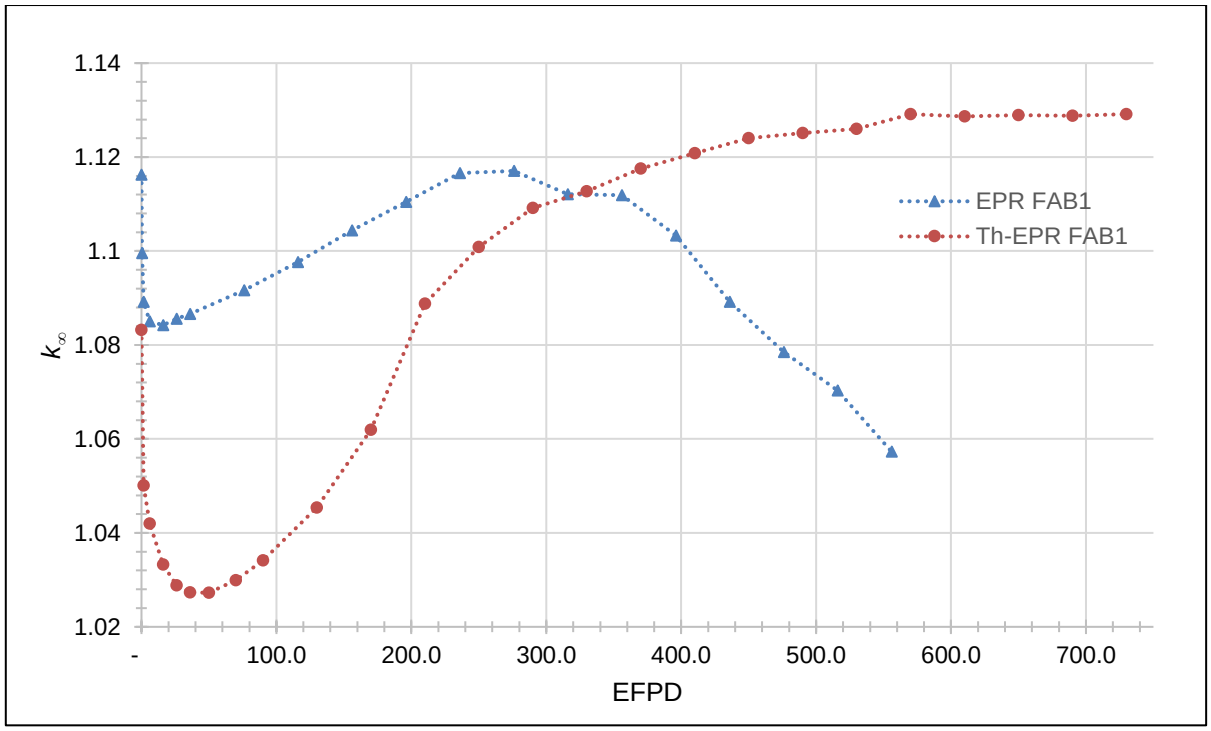

FIGURE 5-2 REACTIVITY FOR EQUIVALENT THORIUM-URANIUM FUEL FOR ONE CYCLE

The thorium-uranium FAB1 showed good behaviour compared to the uranium FAB1 since the k_∞ has a higher value compared to the uranium FAB1 after one cycle. The initial reactivity is however lower than that of the reference EPR, but this is not a problem since it is still above unity and it only results in fewer boron requirements. Between 36 days and 50 days, the infinite multiplication reaches a minimum of ~1.027, which is lower than the requirement of 1.03. This value is close to 1.03 and will not be a problem since a full-core will have different FAs at different stages of burnup. Testing of this composition is subsequently carried out for all three cycles.

Note that it will be shown later in Section 5.4.1 that the boron let-down behaviour will not be the same as that of the EPR or conventional PWRs. This is because of the compensation effects of ^{232}Th acting as a poison at BOC.

The equivalent enrichment case showed great potential for further analysis and there is no need to increase the enrichment in the thorium fuel design. Possible reasons for lower enrichment requirements is because of the optimisation of the EPR fuel composition in the radial and axial directions compared to older PWR designs. In addition, the later production of ^{233}U from ^{233}Pa and better neutron absorbing properties of ^{232}Th compared to ^{238}U. Section 5.4 will discuss the final fuel composition in more detail.

5.3.4 CYCLES TWO AND THREE

When the same fuel burns for three cycles, oscillations arise from day 765, which is in the second cycle. Figure 5-3 shows that k_∞ showed oscillations with time, which needed further investigations.

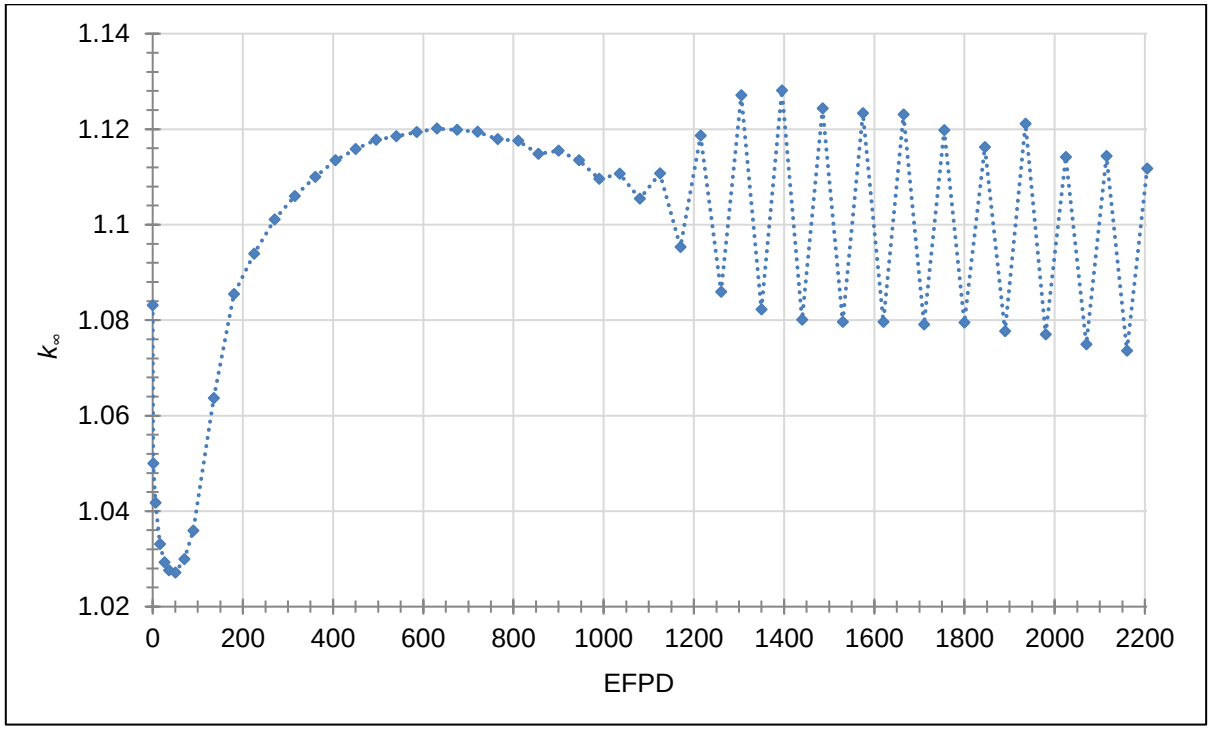

FIGURE 5-3 REACTIVITY FOR EQUIVALENT THORIUM-URANIUM FUEL FOR THREE CYCLES

Section 5.3.4.1 reports on studies that also encountered oscillations and Section 5.3.4.2 investigates the possible causes for these oscillations.

5.3.4.1 LITERATURE ON OSCILLATIONS

Studies showed that present Monte Carlo burnup codes display instabilities. Some commonly used burnup calculation algorithms proved to be unstable, especially in long symme5.3.4.1trical pin cell models (Isotalo, et al., 2013) or spatially large models (Kępisty & Cetnar, 2015). However, these oscillations are dependent on the specific problem and do not appear in all cases (Kotlyar & Shwageraus, 2014).

5.3.4.1.1 POSSIBLE CAUSES

According to Isotalo, these oscillations are caused by xenon. He noted that these xenon oscillations are different from physical xenon oscillations due to time discretization (>12 hours) in burnup calculations. Burnup calculations use step lengths much longer than the timescales associated with physical xenon oscillations. Due to various estimates in burnup algorithms, oscillations in numerical calculations can be much worse than they would in real reactors (Isotalo, et al., 2013). The oscillations occur in the same stage for different asymmetrical cases

showing that the oscillations are initiated by the asymmetry and not statistical variation. The time at which these oscillations start depends on the geometry, material compositions and power density (Isotalo, et al., 2013).

Dufek and Gudowski reported that the instability is caused by spatial oscillation of the burnup distribution as well as a spatial oscillation of xenon when large geometries need to be simulated. In Monte Carlo codes (which are computationally intensive), one has to specify a fairly small number of time-steps, which results in longer time-step lengths. This inadequate time discretisation results in a spatial neutron flux/power oscillation, which negatively affects the burnup process (Dufek & Gudowski, 2005).

Kotlyar and Shwageraus reported that oscillations might appear when the errors due to the depletion algorithm assumptions become similar to the asymmetry in the flux distribution (Kotlyar & Shwageraus, 2014).

5.3.4.1.2 POSSIBLE SOLUTIONS:

Some solutions to these oscillations are:

1. Forcing equilibrium between the neutron flux and saturated xenon distribution (Isotalo, et al., 2013),
2. Explicitly modelling the control system (Kępisty & Cetnar, 2015),
3. Burning the fuel according to a power distribution that does not provoke the oscillation of the fuel burnup distribution (Dufek & Gudowski, 2005).

The reduction of time-step lengths or increases in accuracy of Monte Carlo model will not solve the problem of oscillations as reported by Isotalo and Kępisty and Cetnar respectively (Isotalo, et al., 2013; Kępisty & Cetnar, 2015).

5.3.4.2 INVESTIGATION INTO THE CAUSE OF THE OSCILLATIONS

These oscillations can be categorised as either real-life physical phenomena or oscillations resulting from numerical modelling techniques.

Some possibilities associated with real-life physical phenomena are:

- Physics models in MCNP6,
- The spatial effects of build-up of fission products such as Xe and Sm,
- The spatial effect due to asymmetry in the axial fuel composition profile,
- The number of axial nodes that introduce spatial differences, which is exaggerated as the burnup progresses and material definitions change,
- Pure ThO_2 in the central regions of some fuel pins which introduces subcritical and low power regions,

- The build-up of ^{233}Pa, which has a longer half-life (27days) compared to the 2.3 days of ^{239}Np in the uranium only cycle (therefore 45-day time-steps might be optimal).

Some possibilities related to numerical modelling techniques are:

- The MCNP6 calculation did not converge in terms of source distribution, power distribution or (n,fission) reactions.
- The choice of which tier of fission products to follow.
- Inadequate burnup time-step discretisation.

5.3.4.3 TEST RESULTS AND DISCUSSION

Given all the various possibilities for removing the oscillations, it was decided to test first the power convergence and profile. The power distribution showed an expected sinusoidal (cosine) type curve, which confirms that the cause is not an uneven power distribution. Secondly, the axial nodalisation was tested to eliminate the axial spatial effects. The nodalisation was changed from six axial nodes to one axial node with the burn-up time-steps set to 45 days. For this case, the oscillations did not appear and this was a satisfactory result.

A third set of calculations were performed using six axial nodes, in which the number of source points were increased from 90000 to 180000. The results for these two curves are shown in Figure 5-4 and results showed that (n, fission) errors were decreased from 2.5% to 0.3%. It can be seen that whereas the first oscillation for the 90000 calculation is seen at 945 days, the 180000 calculation does not show such an oscillation at this time. The oscillations only begin to be noticeable at 1260 days in the second case, which is 315 days later than the first case.

It is noted that the statistical uncertainty in the eigenvalue of the 90000 and 180000 source point models are less than ~30 pcm. This shows that that the oscillation in k_∞ is much larger than that of the statistical variation of the Monte Carlo calculation. If the effect was physical, it would start to occur within the same time period of the first oscillation regardless of the size of the source. This therefore indicates that the cause of the oscillation is most probably numerical, and if the source points are further doubled, the oscillations would occur even later. Given the effect of the source size on the oscillations, it was therefore established that the cause of the oscillations was most likely due to a numerical effect, which could also be specific to MCNP6.

To support the studies in the open literature it can then be assumed that the behaviour of xenon and other fission product are a manifestation of the oscillations rather than the cause.

However, with these requirements on the source size, the computing burden becomes very high. In the above two cases, the 90000 source points calculation took ~5.5 days, and the 180000 source points calculation took ~15 days, with the calculations being carried on the HPC cluster, with three nodes, where each node has 48 processors.

The consequences of using a single axial node instead of six nodes had to be then evaluated. Within the burn-up calculation itself, the axial heterogeneity of the fuel rods was still maintained irrespective of the number of axial nodes. This was due to manner in which the cell volumes are defined in the MCNP6 model using the NWURCS input formalism. Referring to Figure 4-2, this means that each of the five sections shown in this figure were burnt as individual volumes. The consequence of using a single axial node is then that the central region would not be further discretized. It was therefore considered that the axial heterogeneity was still captured at a level significant for this study. Note that the 3D modelling of an FA in MCNP6 with continuous energy could still be more accurate than most deterministic codes used for burnup calculations. Given this, it was therefore decided to continue the study using a single axial node.

Figure 5-4 shows the 90000 source point model and 180000 source point model with six nodes and the final model with a single node. Note that all models have the exact same composition outlined in Section 5.3.2 with different axial discretisation and source points.

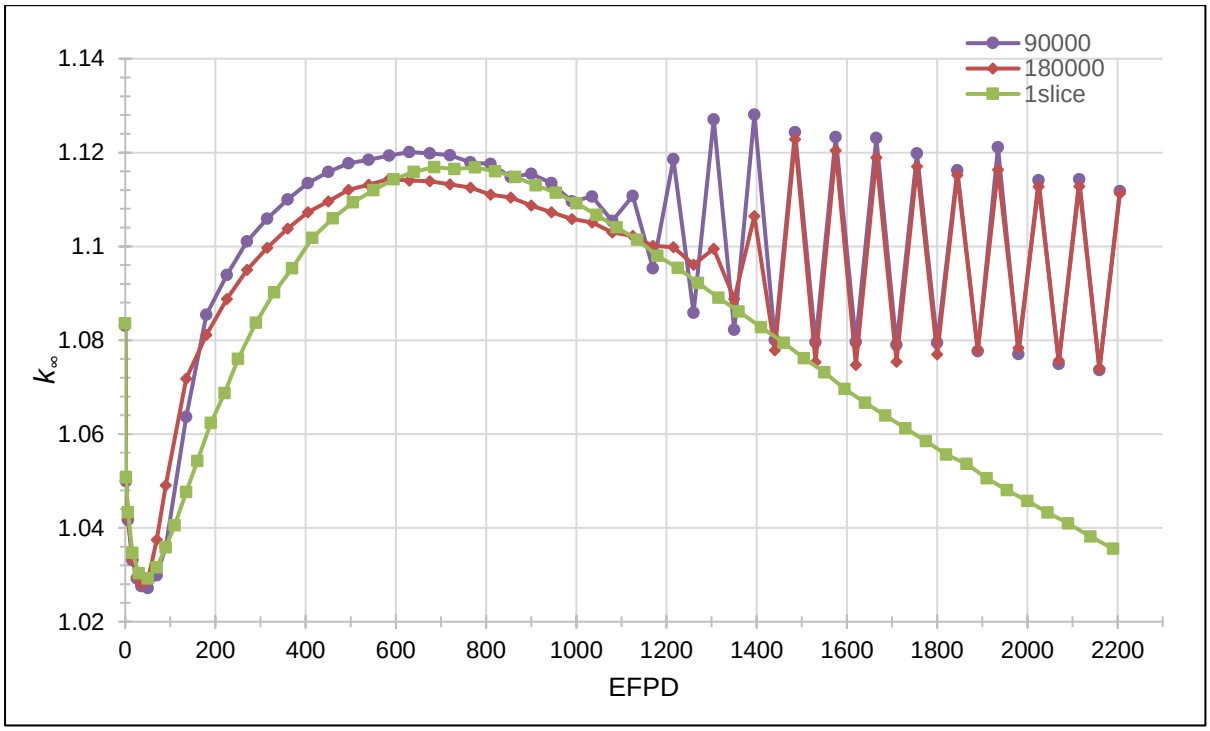

FIGURE 5-4 OSCILLATING AND NON-OSCILLATING REACTIVITY FOR FINAL FUEL DESIGN

The final model used for further analysis is an equivalent (to the EPR) overall initial fissile content, thorium-uranium FAB1 with pure thorium in 12 axial pin sections. Tier 3 fission products were used in the burnup calculations and time-steps used are given in Table 5-4 below.

TABLE 5-4 MCNP6 TIME-STEP DURATION IN EFPD

#	Time-step	Total time	#	Time-step	Total time
1	1.5	1.5	**20**	70	870
2	4.5	6	**21**	70	940
3	10	16	**22**	70	1010
4	14	30	**23**	75	1085
5	20	50	**24**	75	1160
6	25	75	**25**	75	1235
7	30	105	**26**	75	1310
8	35	140	**27**	75	1385
9	40	180	**28**	80	1465
10	45	225	**29**	80	1545
11	50	275	**30**	85	1630
12	55	330	**31**	85	1715
13	60	390	**32**	85	1800
14	65	455	**33**	85	1885
15	65	520	**34**	85	1970
16	70	590	**35**	85	2055
17	70	660	**36**	85	2140
18	70	730	**37**	50	2190
19	70	800			

Section 5.4 presents the results on the newly-designed thorium-uranium fuel.

5.4 RESULTS

Section 5.4.1 presents the results of the burnup of the newly designed Th-EPR FAB1. Sections 5.4.2. and 5.4.3 reports the BOL and EOL properties of Th-EPR FAB1. The new fuel composition is then evaluated on all fuel assemblies in the full-core model at beginning of life in Section 5.4.4.

5.4.1 BURNUP

Figure 5-5 shows the burnup curve for fuel assembly B1 for equivalent overall initial fissile content (except for 12 fuel-pin central regions). The eigenvalue of the Th-EPR FAB1 starts at a lower value of 1.08787 compared to 1.14307, which implies lower boron requirements and fewer neutron captures in Gd compared the EPR FAB1. EOL reactivity is 1.03877 which compared to 0.81509 is much higher and sufficient given the objective of this study. Further reduction on the enrichment for the Th-EPR FAB1 is not possible due to the minimum eigenvalue of 1.02911 at 50 EFPD into the cycle, which is close to unity when assuming 3% leakage.

The total reactivity swing is 6757 pcm compared to 35203 pcm for the uranium only case. The reduction in the reactivity swing can be explained by the better breeding properties of ^{232}Th/^{233}U as expected from Section 3.4 as well as the lower initial excess reactivity due to captures in ^{232}Th. The Th-EPR FAB1 also features no gadolinium in the design, which results in more neutrons available (at BOL) for breeding instead of being captured by Gd.

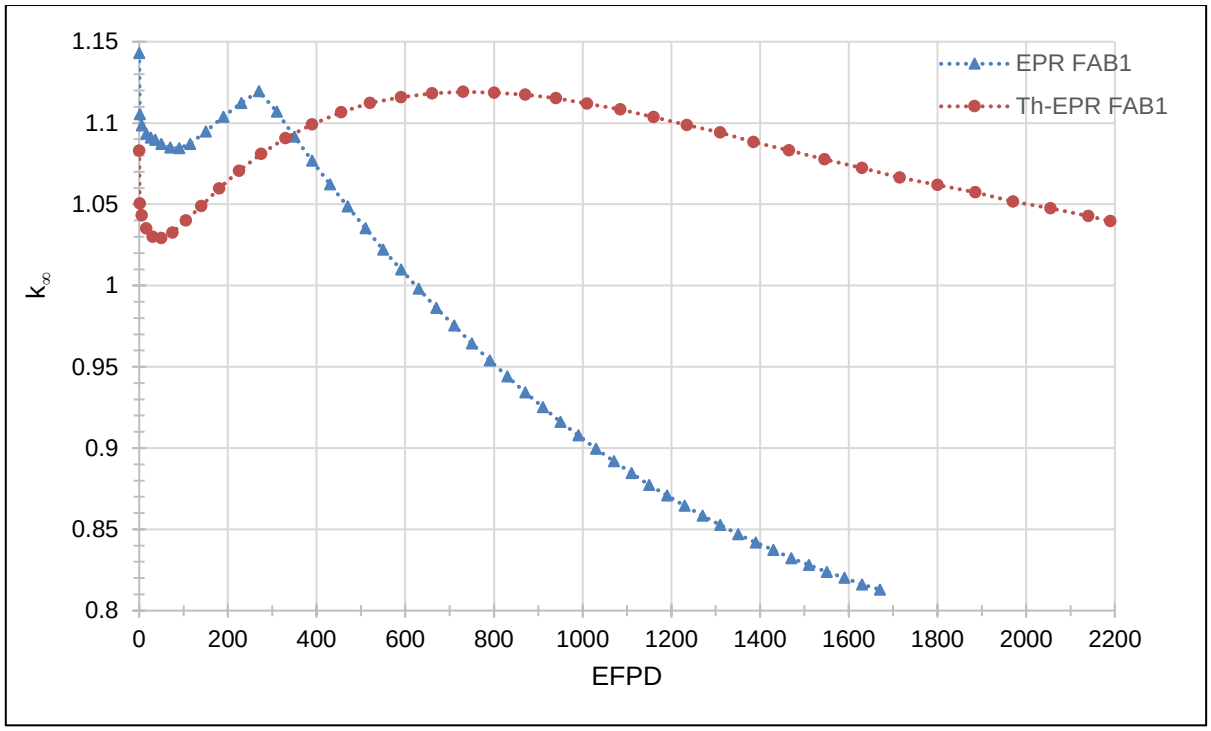

FIGURE 5-5 REACTIVITY FOR THORIUM-URANIUM FUEL FOR THREE CYCLES

The reactivity drops more drastically during days 1-50 than for the EPR FAB1 due to captures in ^{232}Th as well as the build-up of fission products. k_∞ then it starts to increase to a maximum at 730 days due to the absence of Gd and build-up of ^{233}U. This maximum value for k_∞ is above the initial reactivity. This will have implications on the boron let-down curve, which implies diluting boron and then dosing the system with boron again after ~50 days. This is practically plausible only requiring a revisit of operating procedures. Further studies should focus on determining the boron let-down curve.

After 730 days, the reactivity starts to decrease slowly with a flatter gradient compared to the uranium case. This implies that while ^{235}U fissions, production of new ^{233}U also occurs.

Figure 5-6 shows the change in the concentration of main fissile isotopes with time. ^{235}U depletes quickly whilst ^{233}U is bred in the fuel. At day 590 the concentrations of ^{235}U and ^{233}U are almost equal and from day 590 ^{233}U dominates the fissions. The total fissile content shows a decrease with time, which corresponds to the decrease in k_∞.

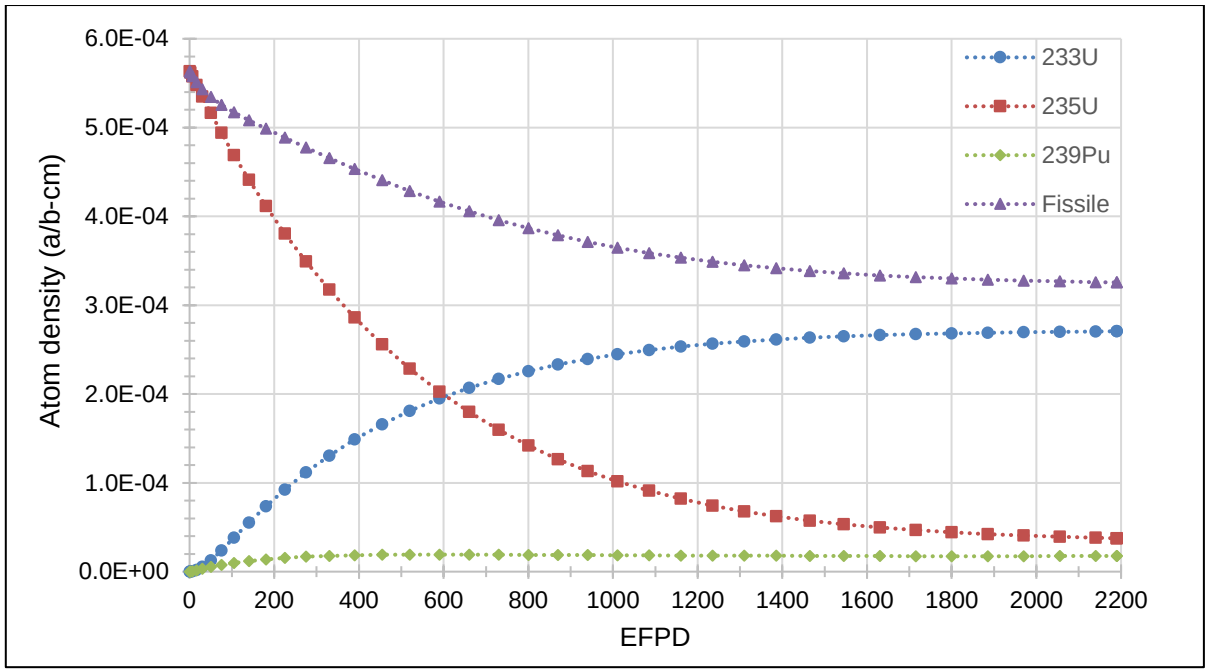

FIGURE 5-6 DEPLETION AND BUILDUP OF MAIN FISSILE ISOTOPES FOR TH-EPR FAB1

Figure 5-7 compares the change in the fissile content with time for the EPR FAB1 with the new Th-EPR FAB1. Note that the initial fissile content for the thorium case is slightly lower at BOL, but at day 225 the fissile content for the Th-EPR case becomes higher than for the uranium EPR case. The decreasing trend of the fissile content exists for both cases; however, the thorium case shows a smaller decrease with time and this implies that longer fuel cycles are possible due to better breeding capabilities.

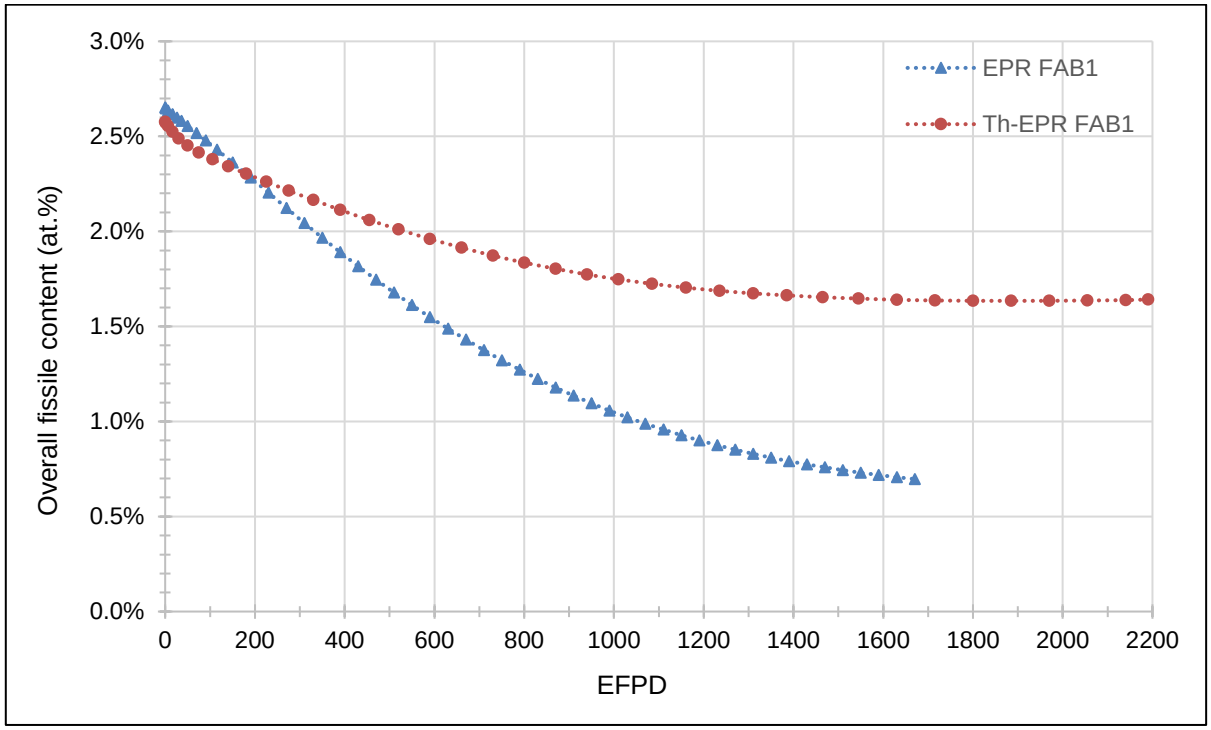

FIGURE 5-7 CHANGE IN FISSILE CONTENT FOR EPR FAB1 AND TH-EPR FAB1

Figure 5-8 and Figure 5-9 show the build-up of the most important fission products. For both Xenon and Samarium, the fission product yields for the thorium containing fuel are lower than for the reference EPR FAB1, which also contributes to a higher value for k_∞ and better breeding.

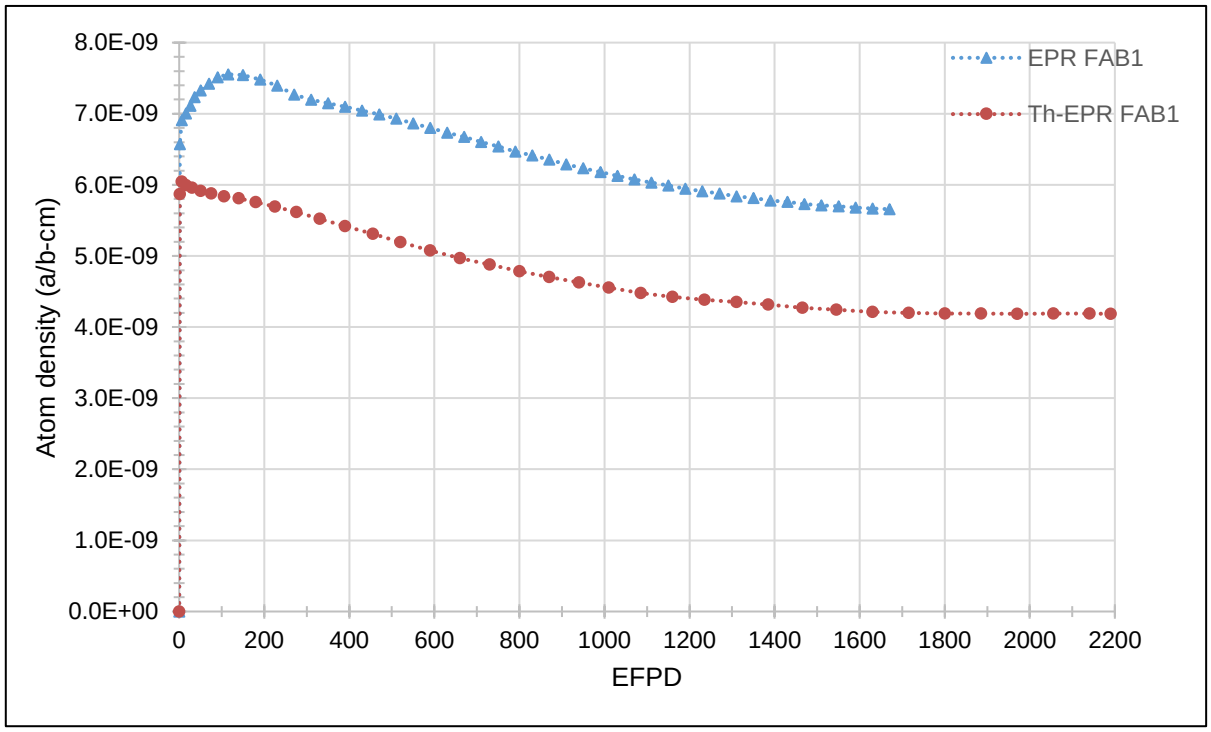

FIGURE 5-8 XENON BUILDUP DURING BURNUP FOR EPR FAB1 AND TH-EPR FAB1

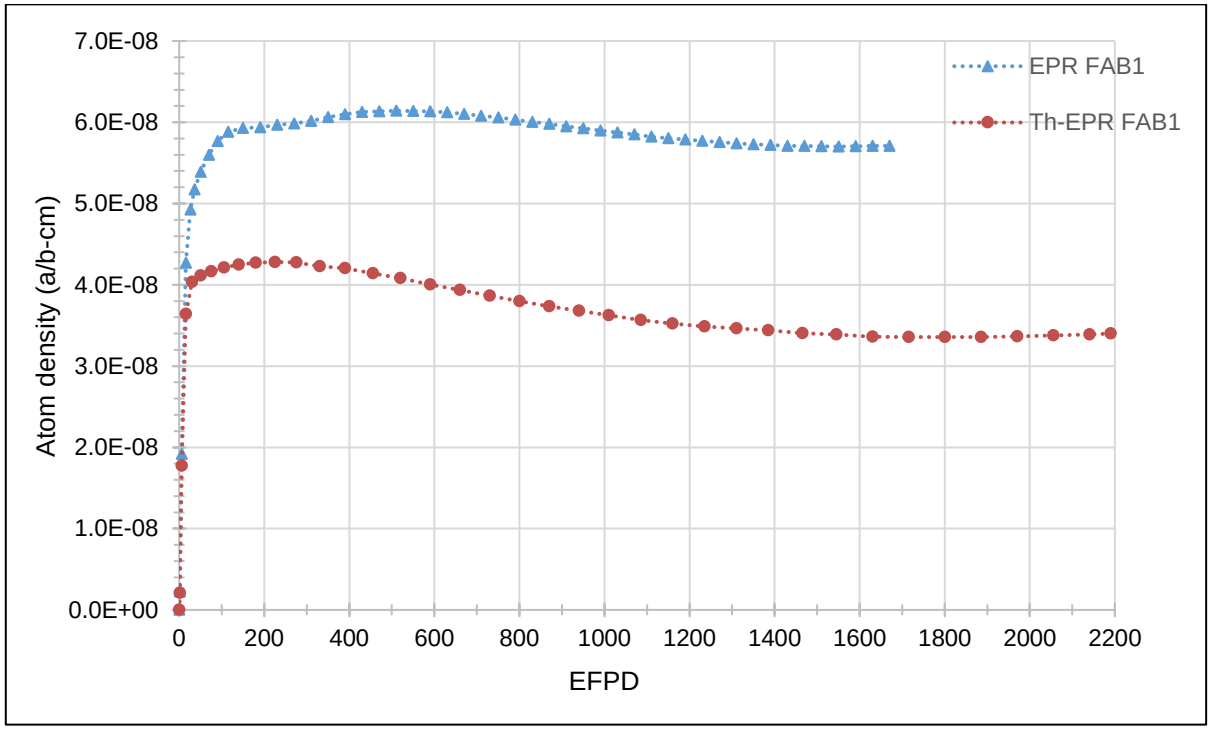

FIGURE 5-9 SAMARIUM BUILDUP DURING BURNUP FOR EPR FAB1 AND TH-EPR FAB1

5.4.2 TH-EPR FAB1 BOL

Section 5.4.1 presented the discussion on burnup of the Th-EPR FAB1 and Section 5.4.2 reports on the fresh core neutronic transport properties of Th-EPR FAB1. Since there were no fuel assembly results available in the FSAR, a comparison will be made to the design limits. A full core comparison of the EPR and the Th-EPR will be made in Section 5.4.4.

5.4.2.1 NEUTRONIC TRANSPORT

The following parameters of the fuel were calculated and are essential for reactor safety and in the licencing of fuel. The MTC, DC, soluble boron worth and delayed neutron fraction.

The neutronic results for a Th-EPR FAB1 with fresh thorium-uranium fuel at CBC and HFP follow. Table 4-7 was used for the assumed temperatures at HFP for the fuel, gap and cladding. The NWU HPC carried out most of the calculations by using one node with 12 processors. The results are in the sections of criticality and reactivity coefficients.

5.4.2.1.1 CRITICALITY

5.4.2.1.1.1 BORON WORTH

The boron worth (BW) for the Th-EPR FAB1 is negative and are within acceptable limits (see Table 5-5 for more details). The critical boron concentration (CBC) is calculated at 667 ppm, which is roughly half of the specification in the FSAR of the EPR. However, this result is in close agreement with Trellue *et al.* who used a lower value of 600 ppm in their design (Trellue, et al., 2011).

5.4.2.1.2 REACTIVITY COEFFICIENTS

Table 5-5 compares the Th-EPR fuel assembly B1 results to the design limits. The Th-EPR FAB1 has negative Doppler Coefficient and is within acceptable limits. The moderator temperature coefficient is also negative and falls within acceptable limits. The delayed neutron fraction, β_{eff} is satisfactory when compared to the limits.

TABLE 5-5 FAB1 COMPARISON OF NEUTRON PARAMETERS

	Limits	Th-EPR FAB1[d]	Units
DC	(-4.90;-2.90[a])	-2.85±0.85	pcm/K
MTC	(-70.0;0.00[a])	-14.84±0.85	pcm/K
$\boldsymbol{\beta_{eff}}$	(0.0043;0.0072[c])	0.0067±0.0002	-
BW	(-10.86;-5.71[a])	-10.23±0.32	pcm/ppm
CBC	(0;1780[b])	667	ppm

a. *(IAEA, 2003)*
b. (Delgado, et al., 1999)
c. (Björk, et al., 2013)
d. *BOL, HFP, k_{eff}=1.00000 RCCAs out, no xenon, CBC, ITER01*
e. *(Lindley & Parks, 2012)*
f. *(Trellue, et al., 2011)*
g. *(Joo, et al., 2003)*
h. *(Wah Lau, et al., 2013)*

5.4.3 TH-EPR FAB1 EOL

The fresh Th-EPR FAB1 results were all within acceptable limits. However, thorium-uranium fuels need to be evaluated at EOL as well. Section 5.4.3 compares the BOL properties of fuel assembly B1 to the EOL. These results will also be compared with literature.

5.4.3.1 REACTIVITY COEFFICIENTS

Table 5-6 compares the Th-EPR fuel assembly B1 results at BOL and EOL to the design limits and other literature. The Th-EPR FAB1 has a more negative Doppler Coefficient at end of life compared to beginning of life, as expected from literature (Section 3.4.3) but it is still within acceptable limits and close to the reported values from literature.

The moderator temperature coefficient at EOL is more negative than BOL, which is also expected from literature in Section 3.4.3. The MTC for EOL falls within the acceptable limits and is in close agreement with results from previous thorium-uranium studies. The lower CBC at EOL also caused the MTC to be more negative.

The delayed neutron fraction, β_{eff} calculated for the Th-EPR FAB1 at EOL is significantly smaller than at BOL. This is due to the β_{eff} of ^{233}U, which dominates fissions at EOL. Table 3-3 reported the delayed neutron values for ^{233}U at ~0.0030 compared to 0.0065 of ^{235}U. The delayed neutron fraction is lower as expected, similar to MOX cores and very close to acceptable limits.

The boron worth at EOL is stronger (more negative) than at BOL. A value of -12 pcm/ppm falls outside the limits and standard deviations. Nonetheless, the BW remains negative. The stronger boron worth at the EOL can be explained by a slightly higher thermal neutron spectrum (B^{10} has a higher absorption cross-section in thermal energy ranges). Due to a high value for k_∞ at EOL (Figure 5-5) for Th-EPR FAB1, a critical boron concentration of 186 ppm is still required.

TABLE 5-6 COMPARISON OF NEUTRON PARAMETERS

	Limits	Th-EPR FAB1[i]	Th-EPR FAB1[j]	References	Units
DC	(-4.90;-2.90[a])	-2.85±0.85	-4.44±1.20	-3.14[h],-3.75[e],-4.5[g]	pcm/K
MTC	(-70.0;0.00[a])	-14.84±0.85	-34.14±1.59	-35[g]	pcm/K
β_{eff}	(0.0043;0.0072[c])	0.0067±0.0002	0.0040±0.0002	0.00504[f]	-
BW	(-10.86;-5.71[a])	-10.32±0.32	-12.1±0.02	-6.80[h],-6.85[g],-8.8[f]	pcm/ppm
CBC	(0;1780[b])	667	186	600[f]	ppm

a. (IAEA, 2003)
b. (Delgado, et al., 1999)
c. (Björk, et al., 2013)
d. Full-core, BOL, HFP, k_{eff}=1.00000 RCCAs out, no xenon, CBC
e. (Lindley & Parks, 2012)
f. (Trellue, et al., 2011)
g. (Joo, et al., 2003)
h. (Wah Lau, et al., 2013)
i. Fuel assembly, BOL, HFP, k_{eff}=1.00000 RCCAs out, no xenon, CBC
j. Fuel assembly, EOL, HFP, k_{eff}=1.00000 RCCAs out, equilibrium xenon, CBC

5.4.3.2 NEUTRON SPECTRUM

Figure 5-10 compares the neutron energy spectrum tallied in the fuel for the Th-EPR FAB1 at EOL and BOL. The end of life spectrum has a higher thermal neutron spectrum peak and lower intermediate and fast spectrum peak.

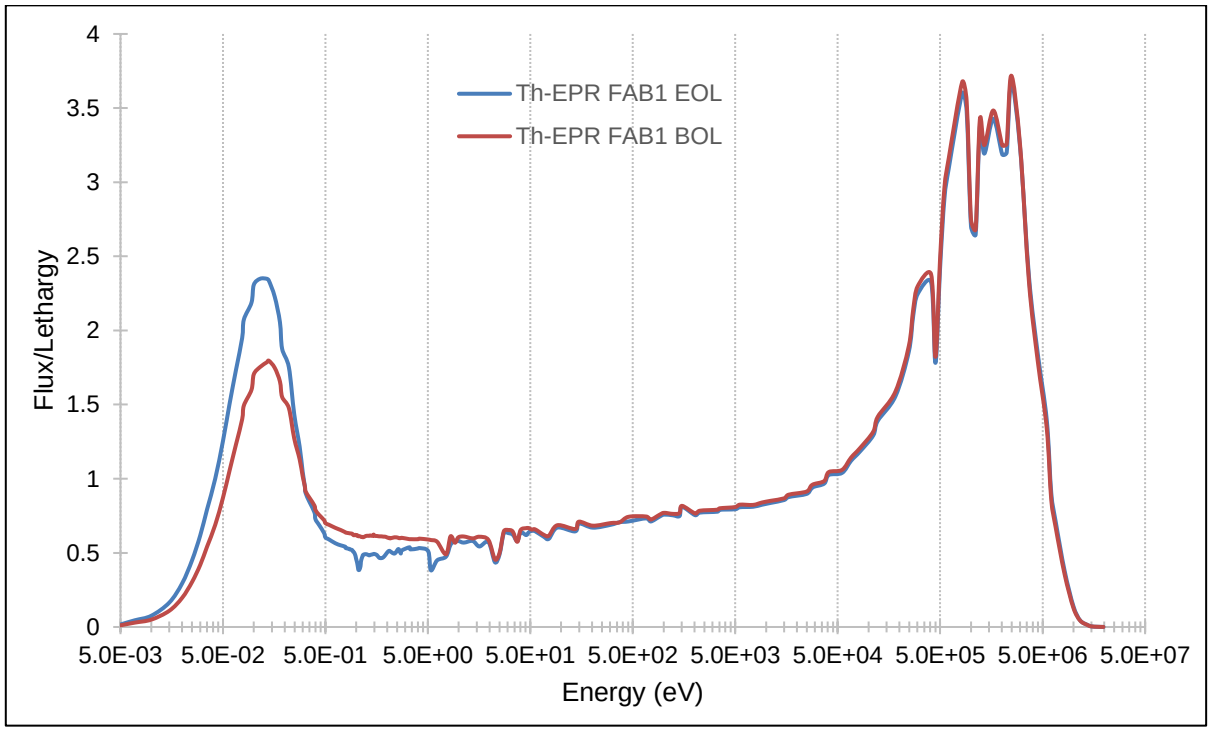

FIGURE 5-10 NEUTRON ENERGY SPECTRUM IN FUEL FOR TH-EPR FAB1 AT BOL AND EOL

The difference is due to the lower fissile content at EOL, because of fuel depletion. A lower fissile content can result in fewer thermal fission absorptions and fewer fast neutrons generated through to fission. Fewer fast neutrons due to less fissions results in fewer neutron thermalisation and therefore less resonance absorptions, which increases the thermal neutron population compared to cases with more resonance abortions. The effects, however, are not isolated and are most probably 2nd or 3rd order effects. Another reason might be that thorium has depleted at EOL making resonance captures in thorium less probable, which will result in more thermal neutrons.

5.4.4 TH-EPR FULL CORE BOL

Section 5.4.1 presented the discussion on burnup of the Th-EPR. From the discussions, one can note that the modification of the fresh fuel at BOL as applied to a FAB1 can now be applied to the rest of the FAs in the core. The rest of the fuel assemblies in the EPR core is modelled by using the equivalent (to the EPR) overall initial fissile content in at.% except for fuel pin sections, where pure ThO_2 will replace the U-Gd compositions. See Appendix B for details on each fuel assembly composition of the new thorium-uranium fuel. For comparison to the original EPR design, compare Appendix A to B.

Calculations were then performed on the full-core. The full-core results for the new fuel design are called Th-EPR and will be discussed in the next section.

Note that full core comparison of flux and burnup distributions between BOL and EOL is not possible since the burnup of only one type of fuel assembly was modelled.

5.4.4.1 NEUTRONIC TRANSPORT

The following parameters of the fuel were calculated and compared to those of the reference uranium EPR, design limits and the BOL Th-FAB1. These neutronic factors are essential for reactor safety and in the licencing of fuel: MTC, DC, control-rod worth, soluble boron worth and delayed neutron fraction. The radial and axial profiles are also evaluated.

The neutronic results for a full-core EPR with fresh thorium-uranium fuel at CBC and HFP follow. Table 4-7 was used for the assumed temperatures at HFP for the fuel, gap and cladding. The NWU HPC carried out most of the calculations by using one node with 12 processors. The results are in the sections of criticality, flux, power, reactivity coefficients, and control-rod worth.

5.4.4.1.1 CRITICALITY

5.4.4.1.1.1 BORON WORTH

The boron worth (BW) for the EPR, Th-EPR FAB1 and Th-EPR are all negative and are in close agreement with the result for Th-EPR at -10.3 pcm/ppm. This value is still acceptable and within the specified limits (see Table 5-7 for more details).

The stronger boron worth for the present case compared to the EPR result in Section 4.4.3.1.1.1 can be explained by a neutron spectrum that shifted to a more thermal spectrum compared to the EPR (^{10}B has a higher absorption cross-section in thermal ranges) as will be shown in Section 5.4.4.1.2.2.

The critical boron concentration (CBC) required resulting in a k_{eff}=1.00000 is calculated at 615 ppm, which is roughly half of the value for the EPR. The CBC is much lower than the EPR due to the presence of large amounts of ^{232}Th, which reduces the excess reactivity at BOL. Trellue *et al.* also used a lower value of 600 ppm in their design (Trellue, et al., 2011).

5.4.4.1.2 FLUX

5.4.4.1.2.1 AXIAL FLUX DISTRIBUTION

Figure 5-11 shows the flux distribution in the EPR core in a 19x19 core and the effects of the axial enrichment on the flux. The flux increases from the bottom to middle sections and decreases from middle to top again. This is a typical sinusoidal (cosine) type flux distribution in the axial direction as expected for a homogeneous cylinder (Stacey, 2007, p. 60) where the maximum of the curve is near the axial midpoint. The middle axial section shows a “smooth”

radial flux distribution due to the distribution of lower enriched assemblies between higher enriched assemblies. Fuel assemblies in the corners of the core show higher fluxes than the inner core. This is due to the presence of FA C3, which has the highest enrichment of all the assemblies without any Gd.

This axial flux distribution is different from the results in Section 4.4.3.1.2.1, which shows a much flatter axial and radial distribution. The main difference between the two cores is the presence of gadolinium distributed axially and radially in the EPR, which flattens the flux profiles. For the Th-EPR, ^{232}Th replaces Gd but does not have the same potent effect; however, the neutrons absorbed by thorium will not go to waste as with Gd.

1000 000 Source points	
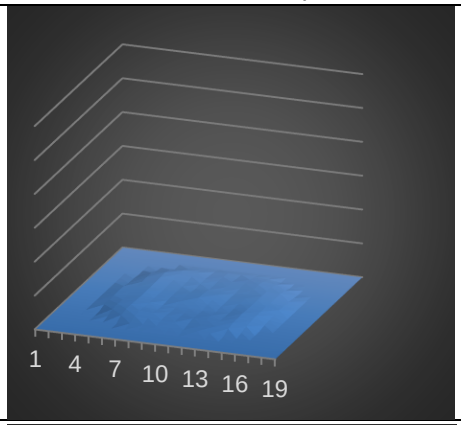	Top [420 cm-399 cm]
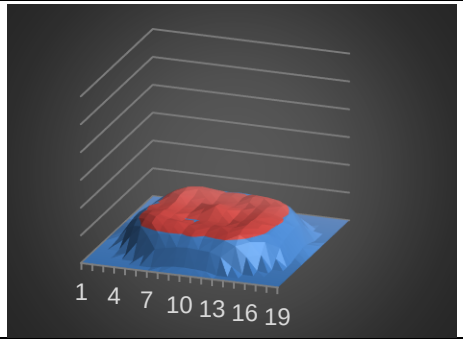	Top middle [378 cm-399 cm]
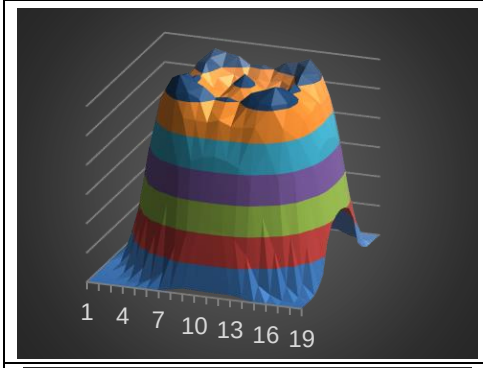	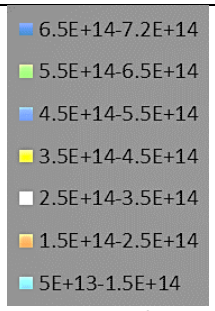 (n/s.cm^2) Middle [189 cm-231 cm]
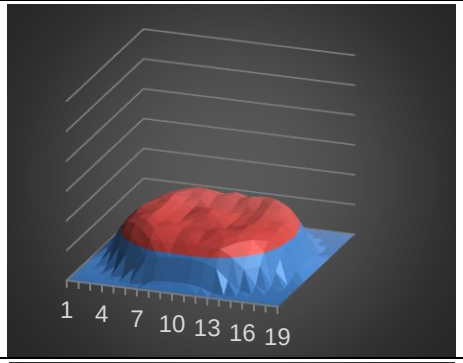	Bottom middle [21 cm-42 cm]
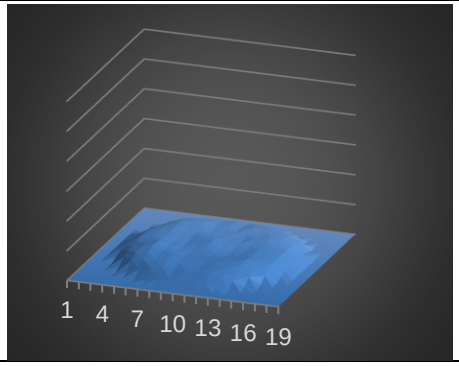	Bottom [0 cm-21 cm]

FIGURE 5-11 AVERAGE FLUX OF DIFFERENT AXIAL SECTIONS OF THE CORE (N/S.CM^2)

5.4.4.1.2.2 NEUTRON FLUX SPECTRUM

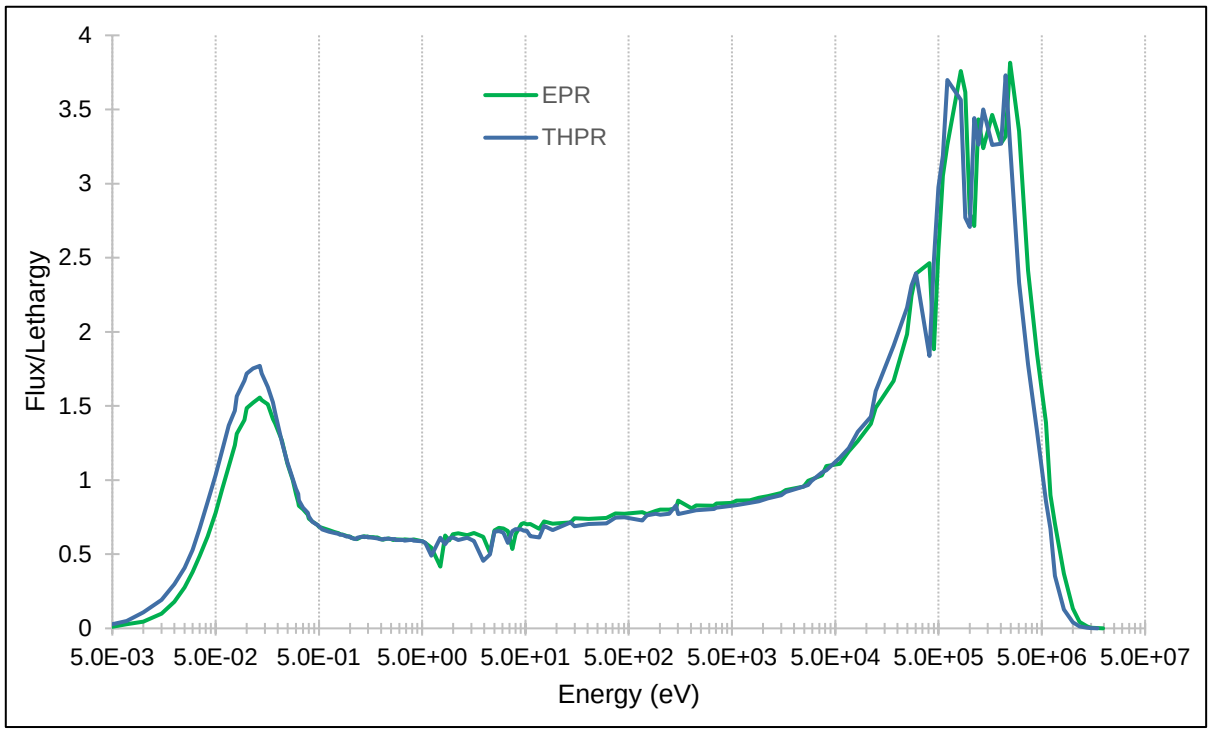

FIGURE 5-12 NEUTRON ENERGY SPECTRUM IN FUEL FOR TH-EPR AT BOL

Figure 5-12Figure 5-13 compares the neutron energy spectrum tallied in the fuel for the Th-EPR to the reference EPR. The Th-EPR has a higher thermal neutron spectrum peak and lower fast spectrum peak, but the difference is small.

The slight difference is due to the slightly lower enrichment due to pure thorium in the centre of 12 fuel pins (that contain Gd and U in the EPR case). A lower fissile content can result in fewer thermal fission absorptions and fewer fast neutrons due to fission. Fewer fast neutrons due to fewer fissions results in fewer neutron thermalisation and therefore fewer resonance absorptions, which increases the thermal neutron population compared to cases with more resonance absorptions. Gd is a strong thermal absorber and the absence of Gd in the Th-EPR tends to increase the thermal spectrum. Another reason is the smaller number of fast fissions in ^{232}Th compared to ^{238}U. Although there is still some ^{238}U present in the Th-EPR, most of the fertile material is thorium. The effects, however, are not isolated and are most probably second or third order effects.

5.4.4.1.3 POWER PROFILE

Figure 5-13 shows the difference in the axial power shapes of the beginning of life (BOL) with fresh fuel for the EPR and the Th-EPR. The axial sinusoidal (cosine) power shape for the Th-EPR is noticeable. The cause of the axial power profile is due to the absence of strong neutron absorbing gadolinium in the centre of the proposed fuel. The difference between these two power

profiles may seem large; however, conventional PWRs have similar sinusoidal (cosine) power profiles.

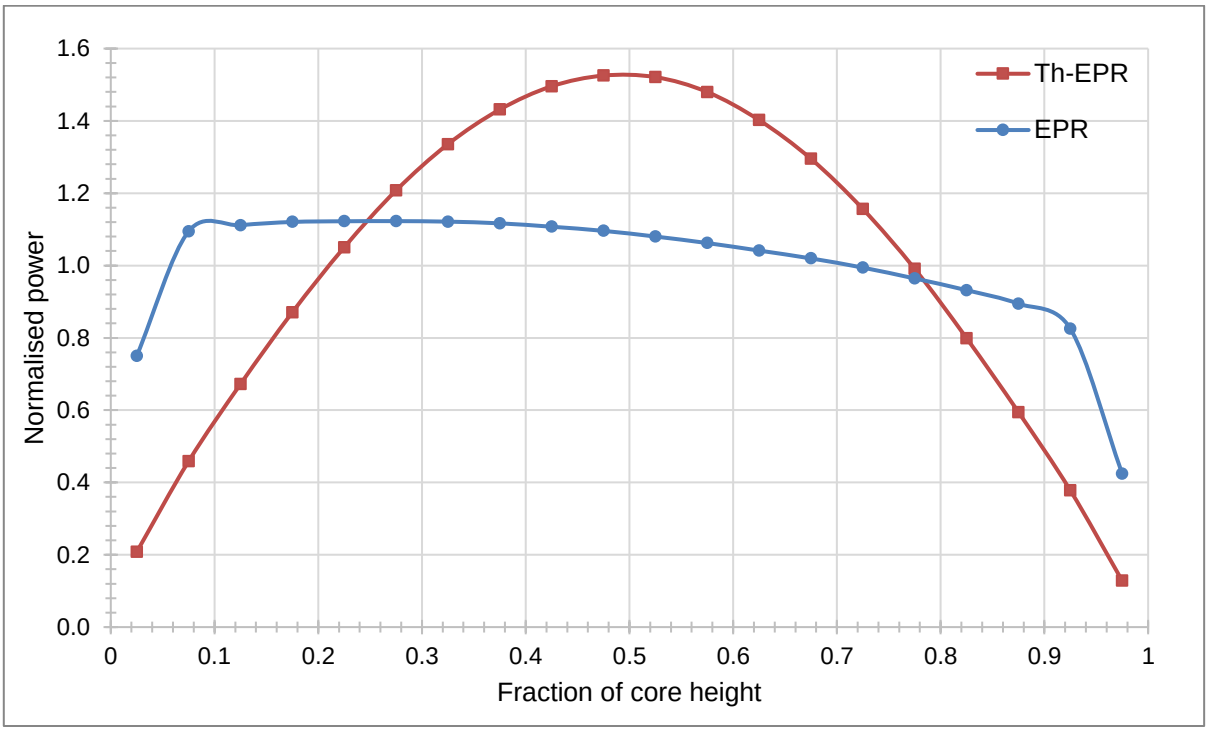

FIGURE 5-13 AXIAL POWER SHAPE FOR TH-EPR AT BOL

5.4.4.1.4 REACTIVITY COEFFICIENTS

Table 5-5 compares the Th-EPR results to the, Th-EPR FAB1, limits and EPR. The Th-EPR has a more negative Doppler Coefficient compared to the EPR, as expected from literature (Section 3.4.3) but it is still within acceptable limits.

The moderator temperature coefficient is slightly more negative compared to the EPR and Th-FAB1; this is due to the lower critical boron concentration for the Th-EPR. The MTC is in close agreement with the EPR as well as the limits and is sufficient.

The delayed neutron fraction, β_{eff} calculated for the Th-EPR is (4.2%) smaller than the result for the EPR and can be considered to be in good agreement. The delayed neutron fraction is expected to be smaller for thorium-fuelled cores and will decrease as the fuel cycle progresses.

TABLE 5-7 FULL-CORE COMPARISON OF NEUTRON PARAMETERS

	Limits	EPR[d]	Th-EPR FAB1[d]	Th-EPR[d]	Units
DC	(-4.90;-2.90[a])	-2.00±0.57	-2.85±0.85	-3.70±0.43	pcm/K
MTC	(-70.0;0.00[a])	-17.45±0.57	-14.84±0.85	-23.46±0.46	pcm/K
β_{eff}	(0.0043;0.0072[c])	0.0069±0.0001	0.0067±0.0002	0.0066±0.0001	-
BW	(-10.86;-5.71[a])	-9.01±1.13	-10.23±0.32	-10.29±0.10	pcm/ppm
CBC	(0;1780[b])	1349.5	667.5	615	ppm

a. *(IAEA, 2003)*
b. (Delgado, et al., 1999)
c. (Björk, et al., 2013)
d. *BOL, HFP, k_{eff}=1.00000 RCCAs out, no xenon, CBC, ITER01*
e. *(Lindley & Parks, 2012)*
f. *(Trellue, et al., 2011)*
g. *(Joo, et al., 2003)*
h. *(Wah Lau, et al., 2013)*

5.4.4.1.5 CRW

The total CRW from all banks was determined to be 15218±10 pcm compared to 10942 pcm from the FSAR. The Th-EPR has a much higher control-rod worth because the control material is B_4C. The expectation is that the control-rod worth will reduce later on in the fuel cycle and sufficient control-rod worth should be built into the system.

Figure 5-14 compare the integral rod worth (IRW) curve for bank B of the Th-EPR to the ITER01 result reported in Section 4.4.3.1.6. Results for the Th-EPR shows higher worth at the middle of the core compared to the EPR result. This can be due to higher fluxes at the centre of the Th-EPR compared to the EPR. The IRW curve resembles the typical S-curve, as outlined in (Lamarsh & Baratta, 2001).

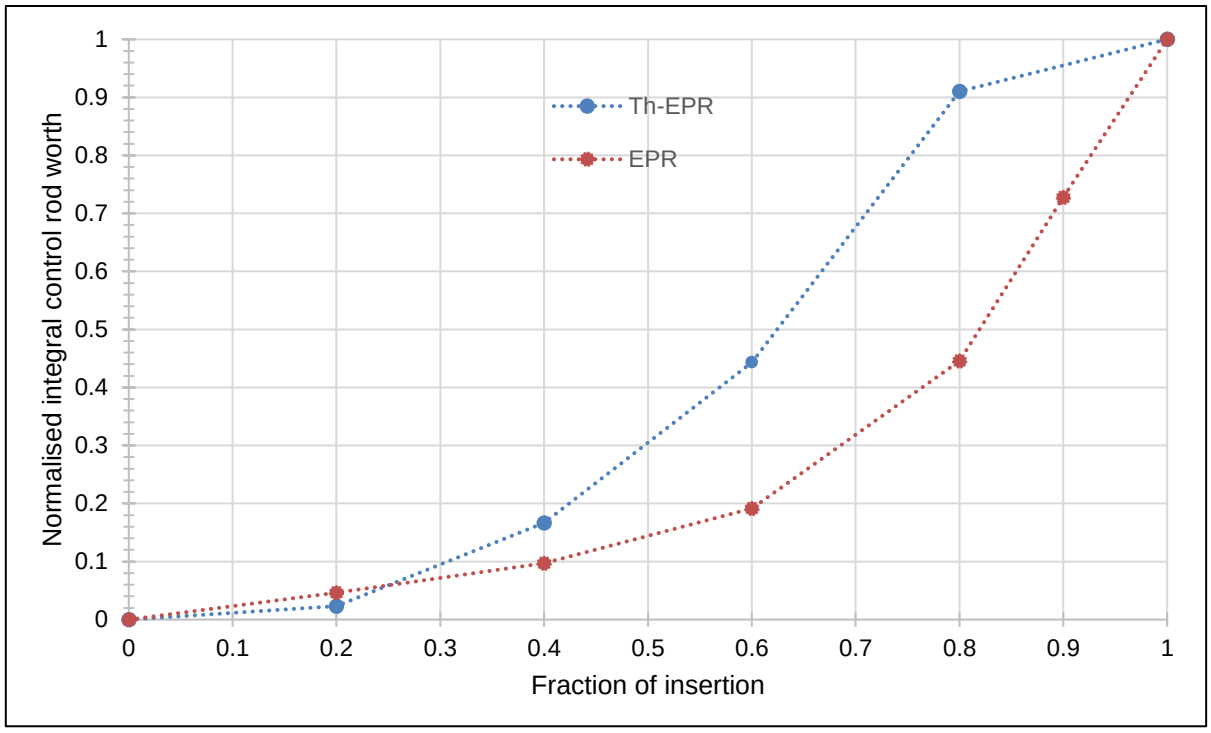

FIGURE 5-14 INTEGRAL CONTROL-ROD WORTH FOR TH-EPR AT BOL

5.4.4.1.6 CONCLUSION

Section 5.4.2.1 presented the neutronic transport results for a full-core Th-EPR with fresh fuel and CBC at HFP. Comparison of the Th-EPR results to those of the reference uranium EPR and the Th-EPR FAB1 brought out valuable information. The power profile of the Th-EPR showed a sinusoidal (cosine) shape for the axial power profile and the thermal neutron spectrum is higher than for EPR. All the results (MTC, DC, control-rod worth, soluble boron worth and delayed neutron fraction) were within acceptable limits and the fuel design choice did not exceed design limits at BOL.

In a fresh core Th-EPR, the main fissile isotope is the same as for an EPR, and changes in the design will only be noticed after ^{235}U has been depleted and ^{233}U dominates fission reactions. Therefore, it is necessary to evaluate the properties at EOL. Since only one fuel assembly was burned, EOL full-core calculations could not be attained.

5.5 CONCLUSION

As set out by the aims of this study, thorium was successfully introduced into the EPR geometry as a means to realise extended burnup (24-month fuel cycles). The newly designed thorium-uranium fuel was evaluated in Chapter 5 and the final fuel design had an equivalent overall at.% initial fissile content as the EPR. This was with the exception for fuel-pin sections where pure ThO_2 replaced the $(U\text{-}Gd)O_2$ sections in the original EPR design.

This design followed the developed methodology in Section 5.1 by reducing and ultimately removing the burnable poison (Gadolinium) requirements, reducing the overall initial fissile content, while still achieving a 24-month fuel-cycle. It was shown that there was no need to increase the enrichment as predicted by (Herring, et al., 2001; Saglam, et al., 2003; Galperin, et al., 2001; Joo, et al., 2003). Due to the optimized fuel design of the EPR (five axial zones), it was possible to save on fuel enrichment while achieving longer fuel cycles than the EPR design. Not only does one save on fuel costs by keeping the overall initial fissile content similar, but this also results in reactor properties that are similar to those of the EPR and no serious changes needs to be made. There was no need to increase the soluble boron enrichment and the reactivity coefficients and design limits for a fresh full-core Th-EPR are all within acceptable limits.

The burnt EOL Th-EPR FAB1 properties are also satisfactory. Some minor differences are the axial power profile and expected boron let-down curve. The boron addition and dilution can be accounted for in operations. The newly-designed thorium-uranium fuel for the EPR is therefore feasible and moderation control can now be applied to further enhance breeding.

6. TH-EPR WITH MODERATION CONTROL

"Learning gives creativity, Creativity leads to thinking, Thinking provides knowledge, knowledge makes you great."

~ Abdul Kalam ~

Overview

Chapter 5 showed the feasibly of the newly-designed thorium-uranium fuel for the EPR, and moderation control studies is presented here to further enhance breeding. Section 6.2 describes the method of controlling the moderation in current EPR designs. Section 6.3 provides details on the modelling of moderation control and Section 6.4 evaluates the different moderation control options in order to choose the best design.

6.1 INTRODUCTION

Section 3.5 discussed using reduced moderation or increased moderation to enhance certain properties in the fuel cycle. Previous studies have either used reduced moderation or increased moderation, but if a system can employ both these methods at different times, the system could enhance breeding. Ultimately, one would favour reduced moderation in the BOL to breed ^{233}U in thorium-uranium fuel. Then increase moderation (making the spectrum more thermal) in a later stage of the cycle, after enough ^{233}U is present in the system to enhance ^{233}U fission.

6.2 METHODOLOGY

The use of the existing pitch and 24 available positions in the available fuel assemblies can alter the neutron spectrum to some extent. We insert moderation rods filled with helium (of the same diameter as the control-rods) at BOC. This is the equivalent of reduced moderation by displacing the water with helium. The moderation rods are then later pulled out to be automatically replaced by water, which increases the thermal spectrum again. These moderation rods, therefore, need to be isolated/closed, so that the water does not flood the helium rods.

Rachamin *et al.* proposed something similar by modifying the CANDU design, with on-power moderator addition. They varied the moderator, which shifted the neutron spectrum to enhance (15%) fuel utilisation. The H/HM ratio was changed between 2.18 and 4.19 (Rachamin, et al., 2013; Rachamin, et al., 2015).

In the EPR, moderation control is limited to the number of usable control-rod positions as moderation rod positions as well as the size of the control-rods. In other words, the spectrum can only be altered by the volume of water being displaced. 189 of the 214 fuel assemblies are available for these purposes.

Another consideration is that the helium-rods cannot be pulled out at any time during the cycle since it can result in power transients and reactivity excursions. Therefore, it is suggested to pull out the rods (change the moderation) during a refuelling outage when the reactor is shut down, before the second or third cycle. The optimal point to change moderation will be determined by running different scenarios and choosing the one with the smallest reactivity swing.

Equilibrium cycles are not considered in this study and need to be investigated in future studies.

6.3 MODEL

The novel idea of changing the spectrum during the cycle is tested for the Th-EPR fuel assembly B1 model as discussed in Section 3.5. The volume of 24 moderation rods inside a fuel assembly makes up ~3.2% of the total FA volume or ~4.9% of the total FA water volume. The H/HM Ratio for standard PWRs is 3.4. By using Eq. 3-1, the H/HM ratio is calculated for the Th-EPR FAB1 as 4.09 with the moderation rods out and 3.84 with the MR inserted. Note that even with the helium rods inserted the EPR has a higher H/HM ratio compared to standard PWRs.

Table 6-1 presents moderation control tests for four different cases as shown in. The first case is for a standard design without adding any moderation (helium-filled) rods as a reference for comparison. The second case starts with the moderation rods inserted and then pulled out during refuelling before the start of the 2nd cycle. The third case also starts with moderation rods inserted, but pulled out before the start of the 3rd cycle. The final case is where the moderation rods stays inserted during all three cycles.

TABLE 6-1 MODERATION RODS POSITION FOR DIFFERENT OPTIONS

	Cycle 1	Cycle 2	Cycle 3
1	OUT	OUT	OUT
2	IN	OUT	OUT
3	IN	IN	OUT
4	IN	IN	IN

NWURCS extracts the data of the materials composition and density from the MCNP6 output at the end of each cycle and creates a new MCNP6 input, depending on whether the moderation rods are inserted or withdrawn. The refuelling outage time is not taken into account, in other words the build-up of ^{233}Pa and ^{135}Xe was not taken into account. This ensures that only the effect of the moderation control will be present in the results.

6.4 RESULTS

The H/HM for the Th-EPR FAB1 is already higher than for a standard PWR, meaning that the resulting neutron spectrum will be more thermal compared to standard PWRs, which was also confirmed in Section 4.4.3.1.2.2. One would expect that by adjusting the H/HM ratio would only decrease the neutron spectrum peak and not significantly alter the neutron spectrum as literature predicted for standard PWRs.

Figure 6-1 shows that by inserting the moderation rods at BOL decreases the thermal neutron spectrum and a slight increase in the fast spectrum can also be noticed. The diameter of the current control-rods should be increased or more than 24 rods should be tested to obtain more insight into the spectral effect.

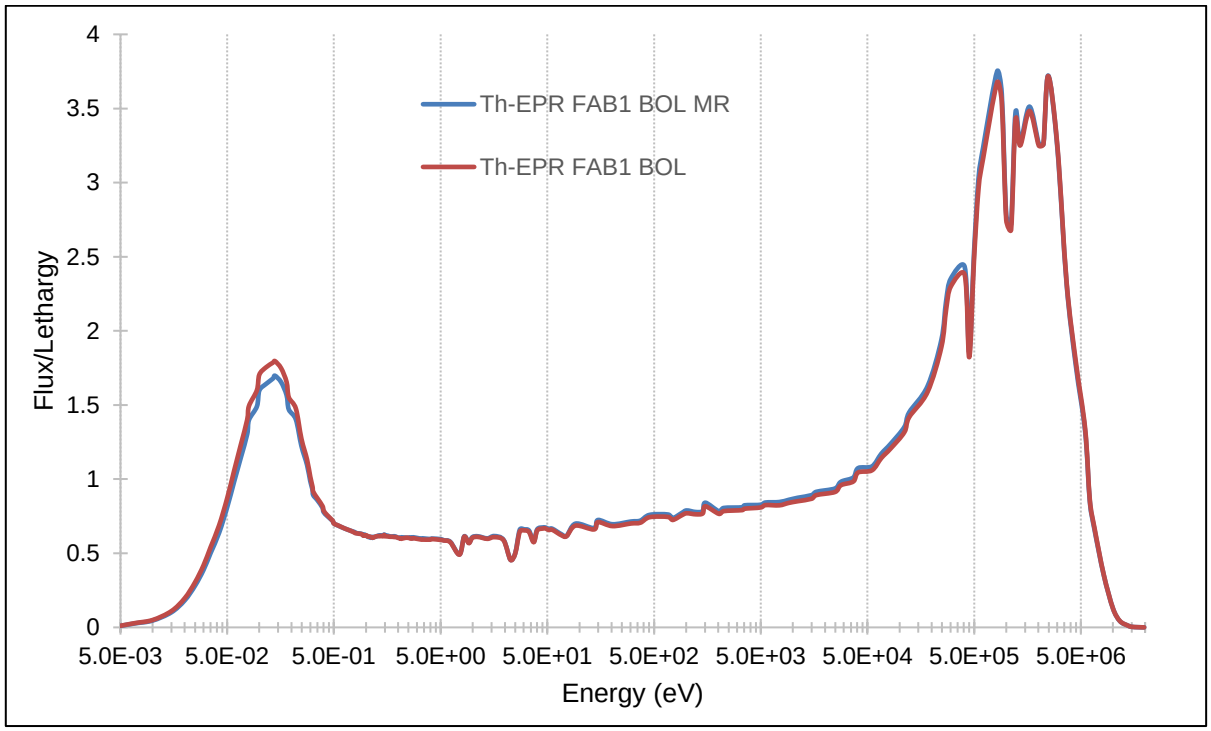

FIGURE 6-1 NEUTRON SPECTRUM WITH AND WITHOUT MODERATION RODS

Figure 6-2 shows the reactivity for the different moderation options listed in Table 6-1 during three 24-month cycles. It is clear that Option 1 (without any moderation rods inserted) has the highest reactivity at EOL. Options 2 and 3 showed an immediate increase in k_∞ when water replaced the moderation rod vacancies. This is due to the increase in thermal neutrons, which increases the reactivity. However, Options 2-4 had almost identical EOL reactivity. One expected that Options 2 and 3 to produce more fuel, due to reduced moderation (which enhanced breeding) at the early stages of the cycle, but the fuel burns quickly as soon as the moderation is increases again. These changes in k_∞ are small and the EOL difference between Option 1 (highest) and 3 (lowest) is 560 pcm.

The effect of power production with the increase in reactivity must be investigated in future studies. One should note that the boron concentration in the water should be increased to keep the core critical.

It should be noted from previous calculations that the output/input conversion from MCNP6 with NWURCS decreases the k_∞ by ~400 pcm when the k_∞ at the end of the cycle is compared with the k_∞ of the start of the next cycle. This reduction in k_∞ can be attributed to rounding off values in the output of MCNP6. When the deficit of 400 pcm is accounted for in the reactivity, Option 4 becomes more attractive, but is still below the value for Option 1.

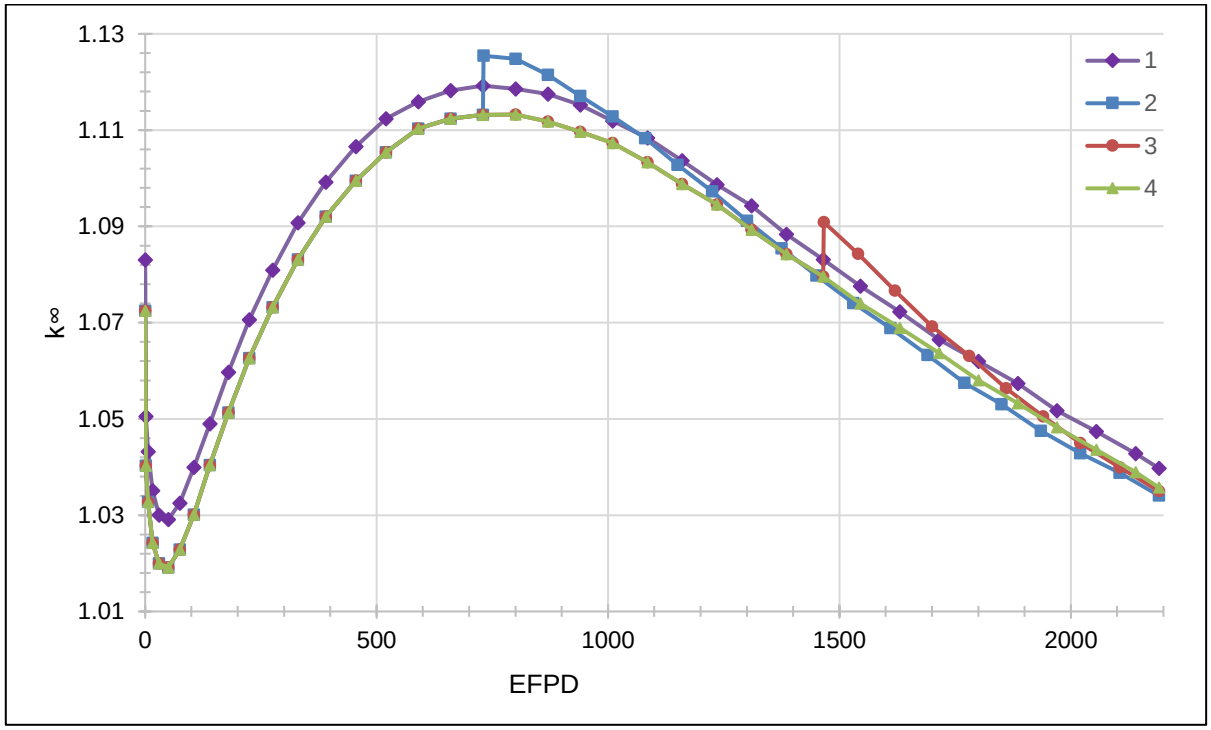

FIGURE 6-2 REACTIVITY FOR DIFFERENT MODERATION CONTROL OPTIONS

Figure 6-3 shows the depletion of fissile content with time as the fuel cycle progresses. Figure 6-3 proves that Option 4 had better breeding due to reduced moderation and has the highest amount of fissile content at EOL. Option 4 has 3% more fissile material relative to Option 1. Although Option 4 has the highest fissile content, it had a lower k_∞ compared to Option 1 in Figure 6-2.

A lower value for k_∞ with higher fissile content could arise due to a higher amount of absorbing fission products like Xe and Sm when a larger concentration of ^{239}Pu is present. This is now investigated further. The Xe and Sm yields for ^{233}U and ^{239}Pu are different (IAEA, 2006). An increased production of ^{239}Pu can also increase the concentration of the fission products. Since these fission products are strong absorbers, the behaviour of k_∞ will also be affected, as discussed above.

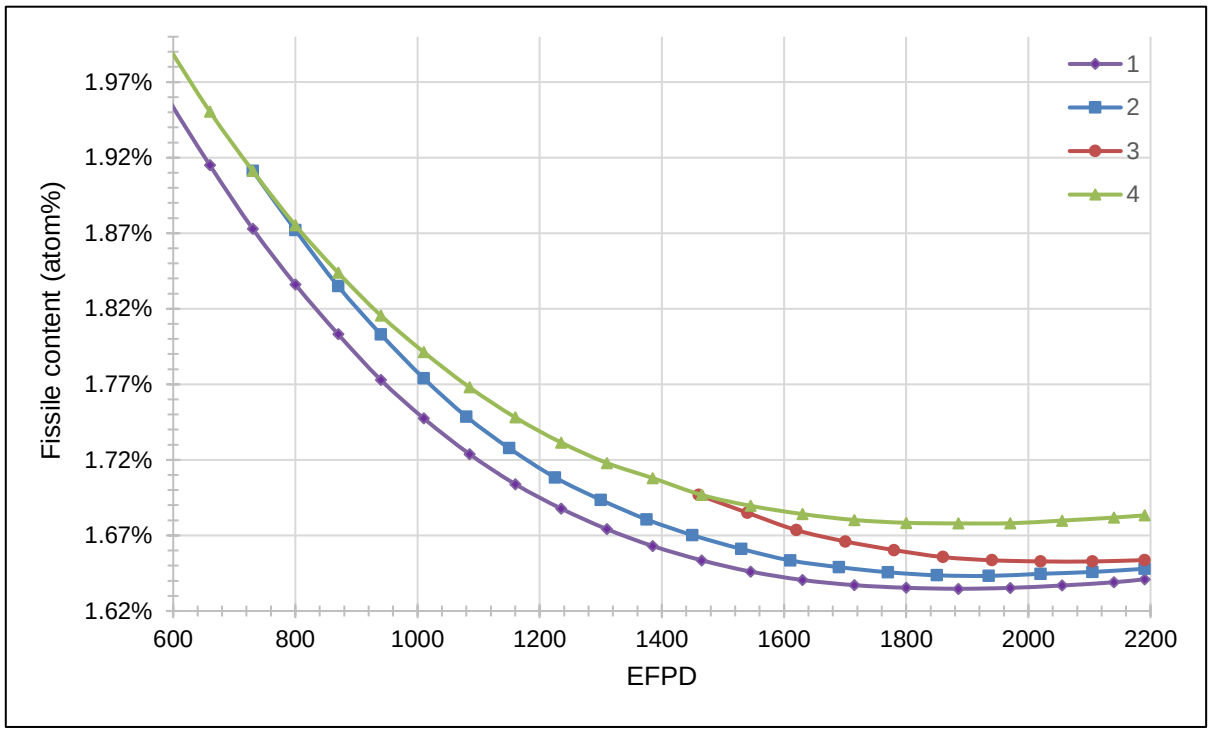

FIGURE 6-3 CHANGE IN FISSILE CONTENT FOR DIFFERENT MODERATION CONTROL OPTIONS

Figure 6-4 and Figure 6-5 compare the build-up of xenon and samarium respectively. Option 4 had the highest amount of both Xe and Sm throughout the cycle. Option 1 had the lowest amount of Xe and Sm. The ratio of Xe and Sm for Option 4 to Option 1 is 5% higher, which indicates that 5% more absorbing fission products are produced in Option 4. Options 2 and 3 had concentrations larger than Option 1 but smaller than Option 4.

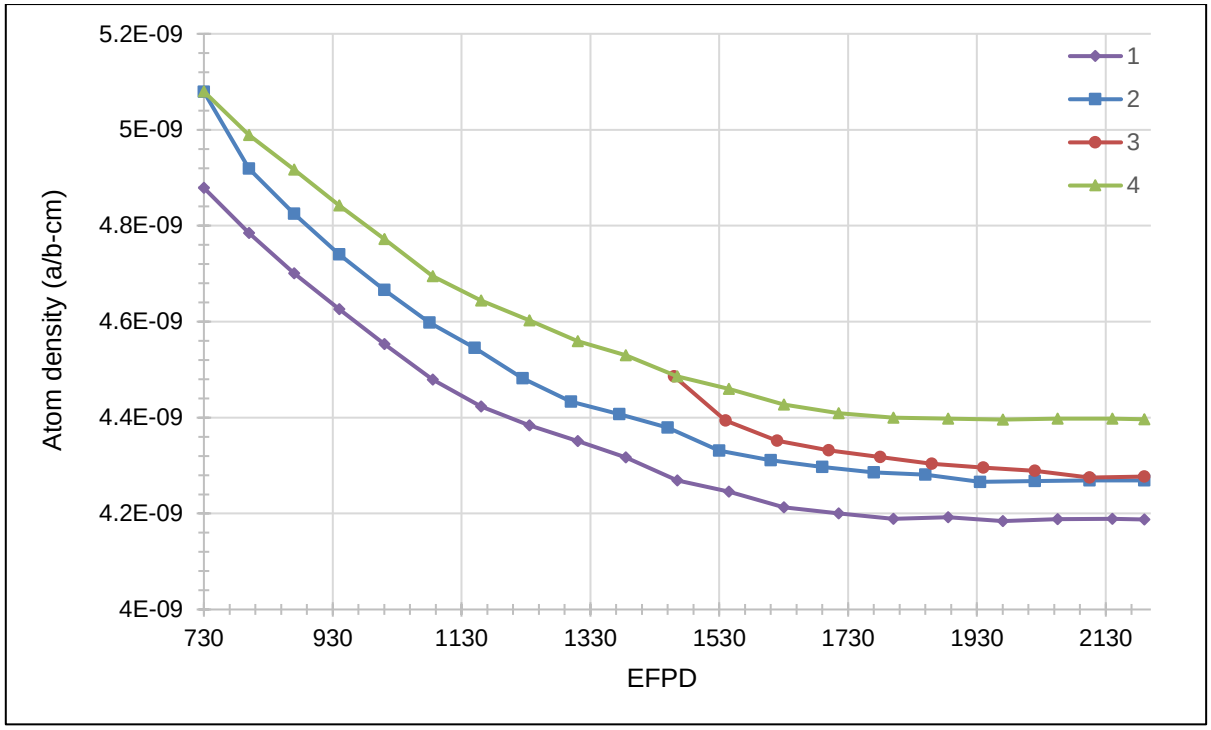

FIGURE 6-4 CHANGE IN XE FOR DIFFERENT MODERATION CONTROL OPTIONS

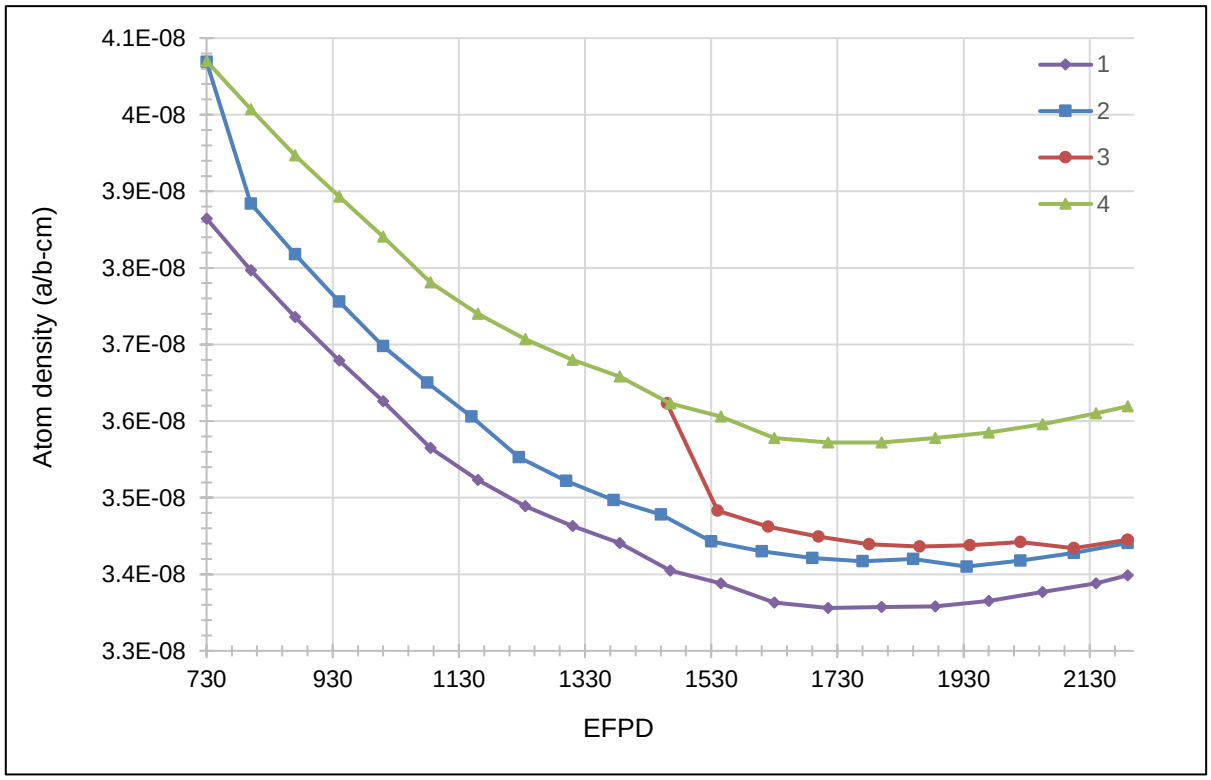

FIGURE 6-5 CHANGE IN SM FOR DIFFERENT MODERATION CONTROL OPTIONS

Even though Option 4 had better breeding capabilities (+3%), the fission products were also increased (+5%) which offset the reactivity. The increased production of Xe and Sm in Option 4 may be the result of increased breeding and subsequent fission of ^{239}Pu as will be shown in

Figure 6-6 as discussed earlier. The cumulative yield of the most important fission products (Xe and Sm) for ^{239}Pu is ~38% more than for ^{233}U (IAEA, 2006). This therefore resulted in a higher concentration of ^{135}Xe and ^{149}Sm.

The overall fissile content increased but more ^{239}Pu could have been bred in addition to the desired ^{233}U. This is highly likely since the resonance integral for ^{238}U is larger than for ^{232}Th as shown in Section 3.3.1.1. By changing the spectrum to more epithermal energies, the resonance captures increased. Figure 6-6 shows that the depletion in ^{239}Pu for Option 4 is less than for Option 1, which implies more captures in ^{238}U and Figure 6-7 confirms that more ^{233}U is bred in Option 4.

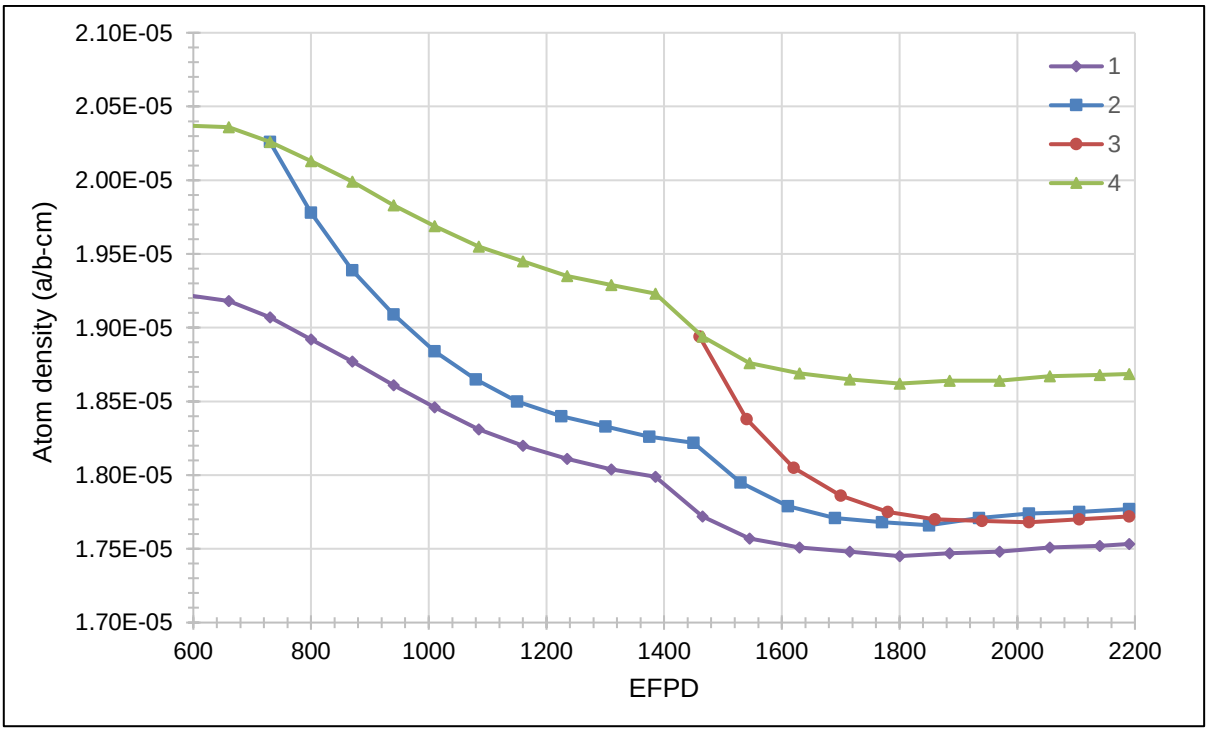

FIGURE 6-6 DEPLETION OF ^{239}PU FOR DIFFERENT MODERATION CONTROL OPTIONS

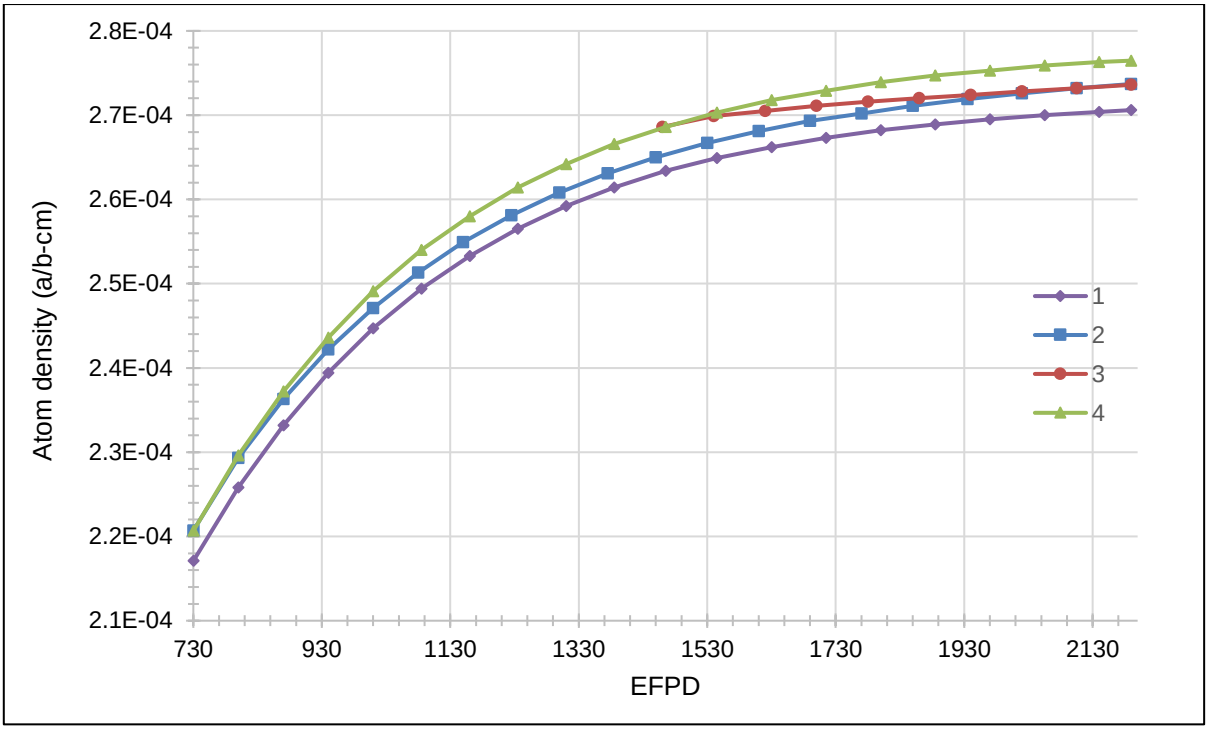

FIGURE 6-7 BREEDING OF ^{233}U FOR DIFFERENT MODERATION CONTROL OPTIONS

Another possible reason for an increased concentration of Xe and Sm may be due to the spectral shift in the neutron spectrum, which changed the fission product yield for each isotope. The IAEA showed an increase in the ^{135}Xe yield from thermal to fast spectrum fissions for ^{233}U. For ^{239}Pu, both the xenon and samarium yields increased with fast fissions (IAEA, 2006).

By comparing the reactivity, fissile content and fission product concentrations, it is clear that Option 1 is the best choice for current fuel design.

6.5 CONCLUSION

Chapter 6 focusses on the plausibility of moderation control in the Th-EPR using helium-filled control rods in accordance with the primary objectives set out in this study.

By comparing the reactivity, fissile content and fission product concentrations, Option 1 represents the preferred choice for current fuel design. However, an increase in the breeding of fissile content resulted in the Th-EPR FAB1 when the moderation rods were inserted during the fuel lifetime. Unfortunately, an increase in xenon and samarium production was also observed which reduced reactivity to below values compared to the case without helium filled moderation rods. These changes in k_∞ and fission product concentrations are small to negligible at the EOL. A more drastic change in moderation is required before decisive conclusions may be drawn.

Possible ways of achieving this are changing the thickness of moderation rods or including more than 24 moderation rods. Another alternative is to increase the diameter of the Th-EPR fuel to effectively decrease the H/HM ratio. However, such changes could result in geometry modifications to the design, which is in breach of the objective at outset to allow only changes to the fuel composition.

An alternate is to test for the plausibility of the moderation control on systems with lower values for H/HM, or systems with neutron spectrums with less thermal neutrons. For instance, the uranium only EPR FAB1, which had a slightly lower thermal neutron peaks.

7. CONCLUSION AND RECOMMENDATIONS

"Success is simply the wisdom born out of so called failures"

~ Rasheed Ogunlaru ~

Overview

This chapter concludes the research of the current study and makes recommendations for further research and development.

7.1 INTRODUCTION

Nuclear power technology has received increased attention in South Africa, especially after the publication of the IRP2010. The nuclear industry should be prepared to take on the responsibility of generating electric power for years to come, should governments decide to move forward with nuclear power. However, enough resources are required to succeed in this endeavour.

The IAEA & NEA reported that the available uranium resources are enough to provide nuclear energy for about 100 more years at the current rate of use (NEA & IAEA, 2012). This will, however, not be the case should nuclear power demand increases worldwide, thereby necessitating utilization of other resources to supply the growing global energy market. Uranium alone cannot carry this load and produces dangerous plutonium. Therefore, a need for an alternative nuclear fuel source exists. The current pressure on governments has forced researchers to investigate alternative fuel technologies that can burn more efficiently in order to increase fuel lifetime and therefore fuel-cycle length and minimise plutonium production.

The majority of thorium fuel research on PWRs is limited to reactor physics investigations and therefore require further R&D in core design and fuel-cycle optimisation in order to achieve practical and commercial implementation (IAEA, 2012). This thesis focuses on contributing research in terms of core design and fuel-cycle optimisation to help close the gap of reaching commercial readiness for thorium-uranium fuel.

7.2 RESULTS

This study focussed on developing a full-core reference 3D model of the EPR for neutron transport simulations using MCNP6. The reference model was compared with the Final Safety

Analysis Report of the EPR. Coupling was introduced between MCNP6 and RELAP5 to take into account the feedback from the thermal hydraulic network in support of the research activities of the reactor analysis group at the School of Mechanical and Nuclear Engineering at the North West University. The coupling methodology was correctly implemented in NWURCS (as set out by the goals of this study); however, it is recommended to repeat the process by reducing the relative errors in MCNP6. These results gave confidence in the verification of NWURCS in generating the input decks. The FSAR was considered as the standard for comparison in terms of verification and validation. The reference EPR model was evaluated and no major differences were reported compared to the FSAR. This model was then used to adjust for thorium-uranium fuel.

The systematic literature review was integral in understanding reactor physics when analysing thorium-based fuel in a standard PWR. The literature provided a solid foundation for the new fuel design, which forms the starting point for thorium-uranium fuel in the EPR. The design goals were that the fuel should be compatible with the EPR core design, while running 24-month fuel cycles and still adhering to the neutronics and thermal-hydraulic requirements and limits.

Next, the new thorium-uranium fuel for the EPR was developed and evaluated. The initial fissile content was changed to produce similar reactivity as compared with the uranium EPR. Different fuel compositions and combinations were tested. The preliminary fuel composition looked promising, but oscillations occurred in MCNP6 during the third fuel cycle. Investigation of these oscillations identified possible causes and solutions. The oscillations disappeared when a single node was used and when more source points were considered. The result of using more source point led to the conclusion that the oscillations were more probably caused by a numerical effect.

The final fuel composition has an equivalent (to the EPR) at.% overall initial fissile content except for fuel-pin sections in the assemblies where pure ThO_2 replaces the U-Gd sections in the original EPR design. In this way there was no need to increase the enrichment as predicted by (Herring, et al., 2001; Saglam, et al., 2003; Galperin, et al., 2001; Joo, et al., 2003) due to the effective fuel design of the EPR. This design followed the developed methodology in Section 5.1 by reducing the burnable poison (Gadolinium) requirements, optimising the initial fissile content and still achieving a 24-month fuel-cycle. There was no need to increase the soluble boron enrichment, since lower equivalent overall fissile content can be used.

Due to the fact that the overall initial fissile content was not increased, the reactivity coefficients and design limits for a fresh full-core Th-EPR are all within acceptable limits. The burnt EOL Th-EPR FAB1 properties were shown to be satisfactory. Some minor differences are the axial power profile and expected boron letdown curve. The boron adjustment can be accommodated for in operations. The newly designed thorium-uranium fuel for the EPR is therefore feasible and moderation control was applied to further enhance breeding.

The novel idea of utilising moderation control using existing control-rod positions in available fuel assemblies was tested on the Th-EPR FAB1. Results showed an increase in the breeding of fissile content when helium-filled moderation rods were inserted (to change the neutron spectrum to be slightly more epithermal). The breeding of ^{233}U increased. Also an increase in ^{239}Pu caused the Xe and Sm concentrations to increase, which offset the addition of excess reactivity due to higher fissile content. The initial Th-EPR FAB1 design without the addition of moderation rods proved to be the best choice.

7.3 RECOMMENDATIONS

Due to the scope and time constraints in terms of current study, it is suggested to pursue the following aspects in more detail for further studies:

1. The higher discharge burnup and fuel-cycle length in the newly designed thorium-uranium fuel will depend on the cladding and fuel performance. These constraints are not taken into consideration in the current analysis and are suggested for further studies.
2. Determine the boron let-down curve for suggested thorium-uranium design.
3. Test power peaking in the pure thorium sections for suggested thorium-uranium design.
4. Do burnup calculations for all seven types of fuel assemblies for better representation of the full-core behaviour.
5. Test the current thorium-uranium fuel design by modelling more axial nodes and optimising the time-step length to remove the oscillations.
6. Test the same fuel composition of the proposed thorium-uranium design by additionally changing the geometry to annular fuel.
7. Enhance the coupling by decreasing the maximum tally error to 0.5% instead of 2.5% by increasing the KCODE parameters in the MCNP6 models.

7.4 SUMMARY

The project succeeded in designing thorium-uranium fuel for a new Gen 3+ PWR that exceeded 24-month fuel cycles without altering the geometry and disregarding any design limits.

As was shown in Section 3.4, thorium has been investigated as a fuel in Gen 2 PWRs. These reactors had a homogeneous fuel composition in the axial direction. The EPR is a 3+ Gen PWR with five different axial fuel zones, which are optimized for leakage and fuel utilization. The current study contributes to current thorium research by further exploring the potential of thorium in Gen 3+ PWR with a more complex fuel description in three dimensions.

CONCLUSION AND RECOMMENDATIONS

Due to the optimized fuel design of the EPR (five axial zones), it was possible to save on fuel enrichments while achieving longer fuel cycles than what the EPR is designed for without increasing the enrichment. Not only does one save on fuel costs by keeping the overall initial fissile content the same, but this also results in reactor properties that are similar to those of the EPR and no serious changes needs to be made. However, the current design did not produce a more favourable result.

Moderation control has received increased attention lately (see Section 3.5). However, it is shown that one can either increase or decrease the moderation for PWRs and then it is fixed throughout the life of the reactor. The ideal would be to change the moderation between cycles to enhance breeding. This study contributes to the field of moderation control by suggesting using current geometry (control rod positions in non-control assemblies). Filling these rods with helium will displace water thereby adding or removing water depending on whether the rods are pulled out or not.

A complex 3D full core model of the EPR was developed successfully for MCNP6, which is a high fidelity code. During this process, NWURCS was verified in terms of input generation for criticality calculations and burnup calculations. Coupling of MCNP6 and RELAP5 using NWURCS was also demonstrated.

Although a comprehensive analysis has been presented, the work shows that a number of important questions still needs investigation, the completion of which was beyond the allotted time for the project. Therefore, the proposed fuel design can be investigated further as suggested in recommendations to continue the process of fuel commercialisation.

REFERENCES

Aghaie, M., Zolfaghari, A. & Minuchehr, A., 2012. Coupled neutronic thermal–hydraulic transient analysis of accidents in PWRs. *Annals of Nuclear Energy,* Volume 50, p. 158–166.

Agung, A., Bánáti, J., Stålek, M. & Demazière, C., 2013. Validation of PARCS/RELAP5 coupled codes against a load rejection transient at the Ringhals-3 NPP. *Nuclear Engineering and Design,* Volume 257, p. 31– 44.

Anders, D. et al., 2012. *RELAP-7 Level 2 Milestone Report: Demonstration of a Steady State Single Phase PWR Simulation with RELAP-7,* Idaho: Idaho National Laboratory.

Anglart, H., 2005. *Control Rods and Sub-critical Systems,* Stockholm: KTM, Nuclear Reactor Technology Division.

Anglart, H., 2005. *Reactivity and Reactivity Coefficients,* Stockholm,: KTH, Nuclear Reactor Technology Division.

AREVA NP Inc., 2006. *Codes and Methods Applicability Report for,* Lynchburg: AREVA NP Inc.

AREVA, 2011. *IAEA.* [Online]
Available at: https://www.iaea.org/NuclearPower/Downloadable/Meetings/2011/2011-07-04-07-08-WS-NPTD/5_FRANCE_EPR_AREVA_Frontigny.pdf
[Accessed 22 02 2016].

AREVA, N., 2013. *U.S. EPR Final Safety Analysis Report.* Revision 5 ed. s.l.:United States Nuclear Regalatory Commission.

Ashley, S. F. et al., 2014. Fuel cycle modelling of open cycle thorium-fuelled nuclear energy. *Annals of Nuclear Energy,* Volume 69, pp. 314-330.

Babuska, I. & Oden, J., 2004. Verification and validation in computational engineering and science: basic concepts. *Computer methods in applied mechanics and engineering,* Volume 193, pp. 4057-4066.

Bakkari, B. E. et al., 2009. Development of an MCNP-tally based burnup code and validation through PWR benchmark exercises. *Annals of Nuclear Energy,* Volume 36, p. 626–633.

Bennett, A., 2015. *Development and Testing of a Coupled MCNP6/CTF Code,* Pennsylvania: The Pennsylvania State University.

Björk, K. I., 2012. *Thorium-plutonium for long operating cycles in PWR's- Preliminary calculations.* Cape Town, Thorium and Rare Earths Conference.

Björk, K. I., Wah Lau, C., Nylén, H. & Sandberg, U., 2013. Study of Thorium-Plutonium Fuel for Possible Operating Cycle Extension in PWRs. *Science and Technology of Nuclear Installations,* 2013(Article ID 867561), pp. 1-8.

Bomboni, E. et al., 2010. Comparison among MCNP-based depletion codes applied to burnup calculations of pebble-bed HTR lattices. *Nuclear Engineering and Design,* Volume 240, p. 918–924.

Caner, M. & Dugan, E. T., 2000. ThO2-UO2 annular pins for high burnup fuels. *Annals of Nuclear Energy,* Volume 27, pp. 759-770.

Chen, N. C. J., Ibn-Klmyat, M., March-Leuba, J. A. & Wende, M. W., 1993. *Validation and verification of RELAP5 for advanced neutron surce accident analysis: Part 1, comparisons to ANSDM and PRSDYN codes,* Tennessee: OAK RIDGE NATIONAL LABORATORY.

Chiang, M., Wang, J., Sheu, R. & Liu, Y., 2014. Evaluation of the HTTR criticality and burnup calculations with continuous-energy and multigroup cross sections. *Nuclear Engineering and Design,* Volume 271, p. 327–331.

Dalle, H. M., 2009. *Monte Carlo Burnup Simulation of the Takahama-3 Benchmark Experiment.* Rio de Janeiro, ISBN: 978-85-99141-03-8.

Dalle, H. M., Mattos, J. R. L. d. & Dias, M. S., 2013. Enriched Gadolinium Burnable Poison for PWR Fuel –Monte Carlo Burnup Simulations of Reactivity, Current Research in Nuclear Reactor Technology in Brazil and Worldwide. *InTech,* pp. 73-89.

Delgado, L. G., Driscoll, M. J. & Meyer, J. E., 1999. An economically optimum PWR reload core for a 36-month cycle. *Annals of Nuclear Energy,* Volume 26, pp. 659-677.

Du Toit, M. H., 2013. *Introducing advanced thorium-based fuel cycles in SA: an evolutionary approach,* Potchefstroom: NWU, North West University.

Dufek, J. & Gudowski, W., 2005. *Managing Xenon Oscillations in Monte-Carlo Burnup Simulations of Thermal Reactors.* Halden, s.n., pp. 1-8.

Dziadosz, D., Ake, T. N. & Saglam, M., 2004. Weapons-Grade Plutonium-Thorium PWR Assembly Design And Core Safety Analysis. *Nuclear Technology,* Volume 147, pp. 69-83.

ESKOM, 2011. *Nuclear energy: Koeberg Power Station,* Durban: ESKOM.

Espel, F. P., 2010. *High accuracy modeling for advanced nuclear reactor core designs using Monte Carlo based coupled calculations.* Pennsylvania: Pennsylvania State University.

Espe, W., 1968. *Materials of High Vacuum Technology.* Volume 2 ed. Berlin: Peragon Press.

European Nuclear Society, 2015. *Nuclear power plants, world-wide, reactor types.* [Online] Available at: https://www.euronuclear.org/info/encyclopedia/n/npp-reactor-types.htm [Accessed 09 03 2016].

Faghihi, F., Khalafi, H. & Mirvakili, S. M., 2011. A literature survey of neutronics and thermal hydraulic codes for investigating reactor core parameters artificial neural networks as the vver 1000 core predictor. *Nuclear Power - System Simulations and Operation,* Issue ISBN: 978-953-307-506-8, pp. 103-122.

Faghihi, F. & Mirvakili, M., 2011. Shut-down margin study for the next generation VVER-1000 reactor including 13 x13 hexagonal annular assemblies. *Annals of Nuclear Energy,* Volume 23, p. 2533–2540.

Fetterman, R., 2009. AP1000 core design with 50% MOX loading. *Annals of Nuclear Energy,* Volume 36, p. 324–330.

Francois, L., del Campo, C. M. & Hernandez, J., 2002. Design of an overmoderated fuel and a full MOX core for plutonium consumption in boiling water reactors. *Annals of Nuclear Energy,* Volume 29, p. 1953–1965.

Fridman, E. & Kleim, S., 2011. Pu recycling in a full Th-MOX PWR core. Part I: Steady state analysis. *Nuclear engineering and design,* Volume 241, pp. 193-202.

Galperin, A., Shwageraus, E. & Todosow, M., 2001. Assessment of Homogeneous Thorium Uranium fuel for Pressurized Water Reactors. *Nuclear Technology,* Volume 138, pp. 111-122.

García, C. et al., 2013. Evaluation of uranium thorium and plutonium thorium fuel cycles in a very high temperature hybrid system. *Progress in Nuclear Energy,* Volume 66, pp. 61-72.

Ghrayeb, S. Z., 2008. *Investigations of Thorium Based Fuel to Improve Actinide Burning Rate in S-Prism Reactor,* Pennsylvania: The Pennsylvania State University.

Greifenkamp, T., Clarno, K. & Gehin, J., 2008. *Effect of Fuel Temperature Profile on Eigenvalue Calculations.* Cincinnati, University of Cincinnati, Department of Mechanical, Industrial, and Nuclear Engineering.

Greneche, D., 2010. *Thorium cycle- An overview,* s.l.: PowerPoint presentation.

Greneche, D., Szyncsak, W. J. & Buchheit, J. M., 2007. *Rethinking the Thorium Fuel Cycle An Industrial Point of View.* Nice, s.n.

Hania, P. R. & Klaassen, F. C., 2012. Thorium Oxide Fuel. *Nuclear Research and Consultancy Group,* pp. 88-108.

Harvard University, 2007. *A Summary of Error Propagation.* [Online]
Available at: http://ipl.physics.harvard.edu/wp-uploads/2013/03/PS3_Error_Propagation_sp13.pdf
[Accessed 13 10 2016].

Herring, J. S., Macdonald, P. E., Weaver, K. D. & Kullberg, C., 2001. Low cost, proliferation resistant, uranium-thorium dioxide fuels for light water reactors. *Nuclear engineering and design,* Volume 203, pp. 65-85.

Holschuh, T. V., Parma, E. J. & Lewis, T. G., 2013. *Burnup Concept for a Long Life Fast Reactor Core using MCNPX,* Albuquerque: Sandia National Laboratories.

IAEA, 2003. *Safety margins of operating reactors,* Vienna: International Atomic Energy Agency.

IAEA, 2006. *Nuclear Data Services.* [Online]
Available at: https://www-nds.iaea.org/sgnucdat/c3.htm
[Accessed 14 11 2016].

IAEA, 2012. *Role of Thorium to Supplement Fuel Cycles of Future Nuclear Energy Systems,* Vienna: Nuclear Energy Series No NF-T-2.4.

IAEA, 2013. *Nuclear Data For Safeguards.* [Online]
Available at: http://www-nds.iaea.org/sgnucdat/a5.htm
[Accessed 2 August 2013].

Isotalo, A., Leppänen, J. & J., D., 2013. Preventing xenon oscillations in Monte Carlo burnup calculations by enforcing equilibrium xenon distribution. *Annals of Nuclear Energy,* Volume 60, p. 78–85.

Ivanov, A., Sanchez, V., Stieglitz, R. & Ivanov, K., 2013. High fidelity simulation of conventional and innovative LWR with the coupled Monte-Carlo thermal-hydraulic system MCNP-SUBCHANFLOW. *Nuclear Engineering and Design,* Volume 262, p. 264– 275.

Joo, H., Noh, J., Yoo, J. & Cho, J., 2003. Alternative Application OF Homogeneous Thoria-Urania Fuel In Light Water Reactors To Enhance The Economic Of The Thorium Fuel Cycle. *Nuclear Technology,* Volume 147, pp. 37-53.

Kahler, A. C. I. et al., 2012. *LANL Evaluation and Data Testing Support for ENDF/B-VII.1,* New Mexico: Los Alamos National Laboratory.

Kang-Mok, B. & Myung-Hyung, K., 2005. Core design for heterogeneous thorium fuel assemblies for PWR(I)-nuclear design and fuel cycle economy. *Nuclear Engineering and Technology,* 37(1), pp. 91-100.

Kazimi, M. S. et al., 1999. *On the use of thorium in LWRs,* Cambridge: Massachusetts Institute of Technology. MIT-NFC-TR-016..

Kępisty, G. & Cetnar, J., 2015. Assesment of advanced step models for steady state Monte Carlo burnup calculations in application to prismatic HTGR. *Nukleonika,* 60(3), pp. 523-529.

Key to Metals AG, 2014. *Key to metals.* [Online]
Available at: http://www.keytometals.com/page.aspx?ID=Home&LN=EN
[Accessed 20 05 2014].

Kim, T. K. & Downar, T. J., 2001. *Thorium Fuel Performance in a Tight Pitch LWR Lattice,* West Lafayette: Purdue University.

Kok, K. D., 2009. *Nuclear Engineering Handbook.* 1 ed. Boca Raton: CRC Press.

Kotlyar, D., Shaposhnik, Y., Fridman, E. & Shwageraus, E., 2011. Coupled neutronic thermo-hydraulic analysis of full PWR core with Monte-Carlo based BGCore system. *Nuclear Engineering and Design,* Volume 241, p. 3777– 3786.

Kotlyar, D. & Shwageraus, E., 2014. Monitoring and preventing numerical oscillations in 3D simulations with coupled Monte Carlo codes. *Annals of Nuclear Energy,* Volume 71, p. 198–205.

Lahoda, E., Mazzoccoli, J. & Beccerle, J., 2007. High-Power-Density Annular Fuel for Pressurized Water Reactors Manufacturing costs and Economic Benefits. *Nuclear Technology,* Volume 160, pp. 112-134.

Lamarsh, J. R. & Baratta, A. J., 2001. *Introduction to Nuclear Engineering.* Third Edition ed. New Jersey: Prentice Hall.

LANL, 2013. *MCNP6 user's manual Version 1.0.* LA-CP-13-00634, Rev. 0 ed. Los Alamos: Los Alamos National Laboratory.

Lindley, B. A. et al., 2014. Steady-state and transient core feasibility analysis for a thorium-fuelled reduced-moderation PWR performing full transuranic recycle. *Annals of Nuclear Energy,* Volume 72, p. 320–337.

Lindley, B. A., Franceschini, F. & Parks, G. T., 2014. The closed thorium–transuranic fuel cycle in reduced-moderation PWRs and BWRs. *Annals of Nuclear Energy,* Volume 63, p. 241–254.

Lindley, B. A. & Parks, G. T., 2012. Near-complete transuranic waste incineration in a thorium fuelled pressurised. *Annals of Nuclear Energy,* Volume 40, p. 106–115.

Lindley, B. A. & Parks, G. T., 2012. The performance of closed reactor grade plutonium–thorium fuel cycles in reduced-moderation pressurised water reactors. *Annals of Nuclear Energy,* Volume 47, p. 192–203.

Little, R. C., 2012. *V&V of MCNP and Data Libraries at Los Alamos (U),* New Mexico: Los Alamos National Laboratory.

Lorenzo, D. E. M., Pérez, D. M. & García, L. P. R., 2013. Study of Thorium Fuel Cycles for Light Water Reactor VBER-150. *International Journal of Nuclear Energy,* Issue Article ID 491898, pp. 1-9.

Lung, M. & Gremm, O., 1998. Perspectives of the thorium fuel cycle. *Nuclear engineering and design,* Volume 180, pp. 133-146.

McDeavitt, S. M. et al., 2005. *Cermet Fuel Development for Advanced Nuclear Systems (Th,U)O2 in a Metal Matrix,* West Lafayette: Final Report from U.S. Department of Energy Nuclear Energy Research Initiative.

MIT, 2010. *Engineering of Nuclear Systems.* Massachusetts: MIT.

Montwedi, E. O., 2014. *Neutronic simulation of a European Pressurized Reactor,* Potchefstroom: North-West University, Master of Engineering.

Mosteller, R. D., 2002. *Validation Suites for MCNP,* New Mexico: Los Alamos National Laboratory.

Mozafari, M. A. & Faghihi, F., 2013. Design of annular fuels for a typical VVER-1000 core Neutronic investigation, pitch optimization and MDNBR calculation. *Annals of Nuclear Energy,* Volume 60, p. 226–234.

Naicker, V. V., Du Toit, M. H. & Nyalunga, G. P., 2015. *NWURCS user guide,* Potchefstroom: North-West University.

NEA, O. & IAEA, 2012. *Uranium 2011: Resources, Production and Demand,* Paris: OECD.

NRC, U.S., n.d. *Reactivity Balance Calculations & Shutdown Margin.* [Online] Available at: http://pbadupws.nrc.gov/docs/ML1121/ML11216A193.pdf [Accessed 23 10 2015].

Nuttin, A. et al., 2013. *Facing Challenges for Monte Carlo Analysis of Full PWR Cores : Towards Optimal Detail Level for Coupled Neutronics and Proper Diffusion Data for Nodal Kinetics.* Paris, Joint International Conference on Supercomputing in Nuclear Applications and Monte Carlo.

Nuttin, A. et al., 2012. Comparative analysis of high conversion achievable in thorium-fueled slightly modified CANDU and PWR reactors. *Annals of Nuclear Energy,* Volume 40, p. 171–189.

Nuttin, A. et al., 2006. *Study of CANDU thorium-based fuel cycles by deterministic and Monte Carlo methods.* Vancouver, American Nuclear Society, pp. 1-10.

Nyalunga, P. G., 2015. *Developing a fresh core neutronic model at 300K for a VVER-1000 reactor type using MCNP6,* Potchefstroom: North West University, Masters in Engineering.

Odoi, H. C. et al., 2014. Study of Criticality Safety and Neutronic Performance for a 348-Fuel-Pin Ghana Research Reactor-1 LEU Core Using MCNP Code. *World Journal of Nuclear Science and Technology,* Volume 4, pp. 46-52.

Olander, D. & Motta, A., 2011. *Light Water Reactor Materials.* 1 ed. California: University of California, Berkeley, CA.

Pal, P. & Jagannathan, V., 2008. Physics design of initial and approach to equilibrium cores of a reactor concept for thorium utilization. *Annals of Nuclear Energy,* Volume 35, p. 1232–1245.

Permana, S., Takaki, N. & Sekimoto, H., 2008. Power density effect on feasibility of water cooled thorium breeder reactor. *Progress in Nuclear Energy,* Volume 50, pp. 308-313.

Permana, S., Takaki, N. & Sekimoto, H., 2008. Preliminary study on feasibility of large and small water cooled thorium breeder reactor in equilibrium states. *Progress in Nuclear Energy,* Volume 50, pp. 320-324.

Ponomarev, A., Travleev, A., Pfrang, W. & Sanchez, V., 2015. *Coupled MCNP – SAS-SFR Calculations for Sodium Fast Reactor Core at Steady-State.* Nice, s.n., pp. 1964-1977 .

Puill, A., 2002. *Thorium utilization in PWRs, neutronics studies. Thorium fuel utilization: Options and trends,* Gif-sur-Yvette: IAEA Tecdoc 1319.

Rachamin, R., Fridman, E. & Galperin, A., 2013. Design and analysis of an innovative pressure tube light water reactor with variable moderator control. *Annals of Nuclear Energy,* Volume 60, p. 248–255.

Rachamin, R., Fridman, E. & Galperin, A., 2015. Feasibility assessment of the once-through thorium fuel cycle for the PTVM LWR concept. *Annals of Nuclear Energy,* Volume 85, p. 1119–1130.

RELAP, 2001. *RELAP5/MOD3.3 code manual,Volume II: User's guide and input requirements.* s.l.:Nuclear Safety Analysis Division.

Rubbia, C., 1999. *An energy amplifier for "clean" nuclear energy production driven by a particle beam accelerator.* Switzerland, Patent No. EP0725967 B1.

SA, 2011. *Integrated Resource Plan for Electricity 2010-2030,* s.l.: Department of Energy.

Saglam, M., Saptyta, J. J. & Spetz, S. W., 2003. Core Designs and Economic Analyses of Homogeneous Thoria-Urania Fuel in Light Water Reactors. *Nuclear Technology,* Volume 147, pp. 8-19.

Saidinezhad, M. & Hamieh, S. D., 2012. A 13x13 annular fuel assembly 1000 MWe PWR response to a reactivity excursion. *Annals of Nuclear Energy,* Volume 47, p. 155–159.

Sartor, R. F., Greenfield, B. A. & Brown, F., 2015. *MCNP6 Criticality Calculations Verification and Validation Report,* New Mexico: Los Alamos National Laboratory.

Shieh, A. S., Ransom, V. H. & Krishnamurthy, R., 1994. *RELAP5/MOD3 code manual Volume 6: Validation of numerical techniques in RELAP5/MOD3.0,* Maryland: Nuclear Safety Analysis Division Information Systems Laboratories, Inc.

Shultis, J. K. & Faw, R. E., 2002. *Elements of Nuclear Science and Engineering.* New York: Marcel Dekker.

Si, S., 2009. *Roadmap Design for Thorium-Uranium Breeding Recycle in PWR,* Shanghai: IAEA-CN-164-5S09.

Stacey, W. M., 2007. *Nuclear Reactor Physics.* Second edition ed. Atlanta: Wiley.

Stacey, W. M., 2007. *Nuclear Reactor Physics.* 2nd ed. Atlanta: Wiley.

Stankovskiy, A. & Van den Eynde, G., 2012. Advanced Method for Calculations of Core Burn-Up, Activation of Structural Materials, and Spallation Products Accumulation in Accelerator-Driven Systems. *Hindawi Publishing Corporation Science and Technology of Nuclear Installations,* Volume 2012, pp. 1-12.

STEELGS, 2014. *Stainless Steel Heat Resistant Steel and Special Alloy Steel..* [Online] Available at: http://www.steelgs.com/Materials/Stainless-Steel-Heat-Resistant-Steel-and-Special-Alloy-Steel/31/670/SA-240_Type_304LN.html#Chemical_composition. [Accessed 20 05 2014].

Todosow, M. & Kazimi, M., 2004. *Optimization for Heterogeneous Utilization of Thorium in PWRs to Enhance Proliferation Resistance and Reduce Waste,* New York: Brookhaven National Laboratory.

Trellue, H. R., Bathke, C. G. & Sadasivan, P., 2011. Neutronics and material attractiveness for PWR thorium systems using Monte Carlo techniques. *Progress in Nuclear Energy,* Volume 53, pp. 698-707.

Tsige-Tamirat, H., 2011. Neutronics assessment of the use of thorium fuels in current pressurized water reactors. *Progress in Nuclear Energy,* Volume 53, pp. 717-721.

Tucker, L. P., Alajo, A. & Usman, S., 2015. Thorium-based mixed oxide fuel in a pressurized water reactor: A beginning of life feasibility analysis with MCNP. *Annals of Nuclear Energy,* Volume 76, p. 323–334.

U.S. NRC, 2016. *U.S. NRC.* [Online]
Available at: http://www.nrc.gov/about-nrc.html
[Accessed 17 05 2016].

Uto, N., 1999. *Evaluation of Temperature Dependence of Doppler Coefficient,* Ibaraki: JAEA.

Vazquez, M., Tsige-Tamirat, H., Ammirabile, L. & Fuertes, F., 2012. Coupled neutronics thermal-hydraulics analysis using Monte Carlo and sub-channel codes. *Nuclear Engineering and Design,* Volume 250, p. 403– 411.

Wah Lau, C., Demazière, C., Nylén, H. & Sandberg, U., 2012. Improvement of LWR thermal margins by introducing thorium. *Progress in Nuclear Energy,* Volume 61, pp. 48-56.

Wah Lau, C., Nylen, H., Demaziere C. & Sandberg, U., 2014. Reducing axial offset and improving stability in PWRs by using uranium-thorium fuel. *Progress in Nuclear Energy,* Volume 76, pp. 137-147.

Wah Lau, C., Nylén, H., Demazière, C. & Sandberg, U., 2013. *Investigation of the Equilibrium Core Characteristics for the Ringhals-3 PWR with Improved Thermal Margins Using Uranium-thorium Fuel.* Jeju Island, Korea, ICAPP.

Waris, A. et al., 2009. *Study on Equilibrium Characteristics of Thorium-Plutonium-Minor Actinides Mixed Oxides Fuel in PWR.* Bandung, America Institute of Physics, pp. 85-90.

Weaver, K. D. & Herring, J. S., 2002. *The Effect Of The Hydrogen To Heavy Metal Ratio (H:HM) On Reactivity And Discharge Isotopics Of Homogeneous Thoria-Urania Fuel.* Arlington, 10th International Conference On Nuclear Engineering (ICONE-10).

Weaver, K. D., Zhao, X., Pilat, E. & Hejzlar, P., 2000. *A PWR Thorium Pin Cell Burnup Benchmark,* Idaho: INEEL.

WNA, 2011. *Thorium.* [Online]
Available at: http://www.world-nuclear.org/info/inf62.html
[Accessed 30 October 2011].

Xu, Z., 2003. *Design Strategies for Optimizing High Burnup Fuel in Pressurized Water Reactors,* Massachusetts: MIT. (Thesis – PhD).

Yang, J., Kang, K., Song, K. & Lee, C., 2004. Fabrication and Thermal Conductivity of (Th,U)O2 Pellets. *Nuclear Technology,* Volume 147, pp. 113-119.

Zare, N. et al., 2010. Introducing and validating a new method for coupling neutronic and thermal-hydraulic calculations. *Nuclear Engineering and Design,* Volume 240, p. 3727–3739.

APPENDIX A

Tables A-1 to A-6 provide the details on the composition and arrangement of the EPR fuel assemblies A1, A2, B2, C1, C2 and C3.

TABLE A-1 FUEL ASSEMBLY A1 DETAILS (AREVA, 2013)

Axial Length (cm)	Zone	Composition
		Pin type 1
Number of pins		265
20.32	Blanket	2% ^{235}U
15.24	Cut-back	
354.95	Central	2.25% ^{235}U
15.24	Cut-back	2% ^{235}U
15.24	Blanket	

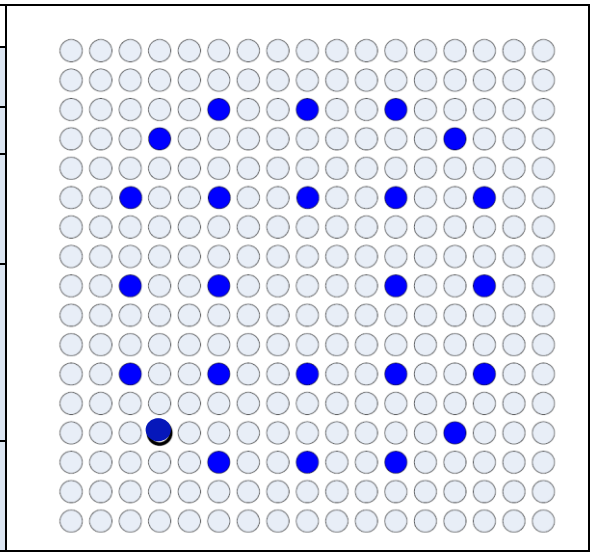

*Composition in wt.%

TABLE A-2 FUEL ASSEMBLY A2 DETAILS (AREVA, 2013)

Axial Length (cm)	Zone	Composition	
		Pin type 1	Pin type 2
Number of pins		261	4
20.32	Blanket	2% ^{235}U	2% ^{235}U
15.24	Cut-back	2.25% ^{235}U	2.25% ^{235}U
354.95	Central		2.13% ^{235}U 4% Gd_2O_3
15.24	Cut-back		2.25% ^{235}U
15.24	Blanket	2% ^{235}U	2% ^{235}U

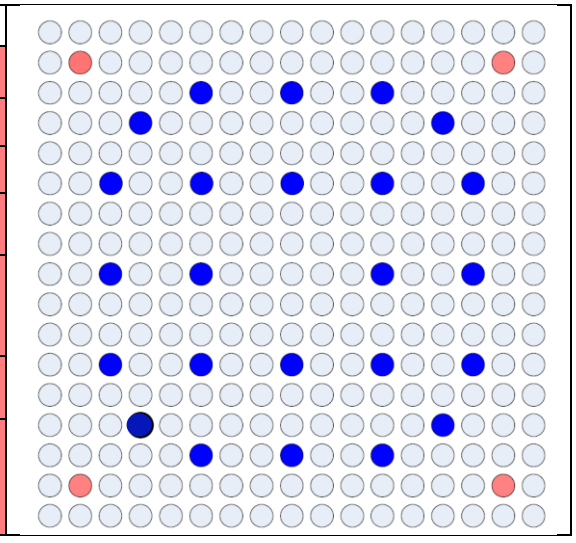

*Composition in wt.%

TABLE A-3 FUEL ASSEMBLY B2 DETAILS (AREVA, 2013)

Axial Length (cm)	Zone	Composition		
		Pin type 1	Pin type 2	Pin type 3
Number of pins		249	12	4
20.32	Blanket	2% ^{235}U	2% ^{235}U	2% ^{235}U
15.24	Cut-back	2.7% ^{235}U	2.7% ^{235}U	2.7% ^{235}U
354.95	Central	2.7% ^{235}U	1.89% ^{235}U 8% Gd_2O_3	2.56% ^{235}U 2% Gd_2O_3
15.24	Cut-back	2.7% ^{235}U	2.7% ^{235}U	2.7% ^{235}U
15.24	Blanket	2% ^{235}U	2% ^{235}U	2% ^{235}U

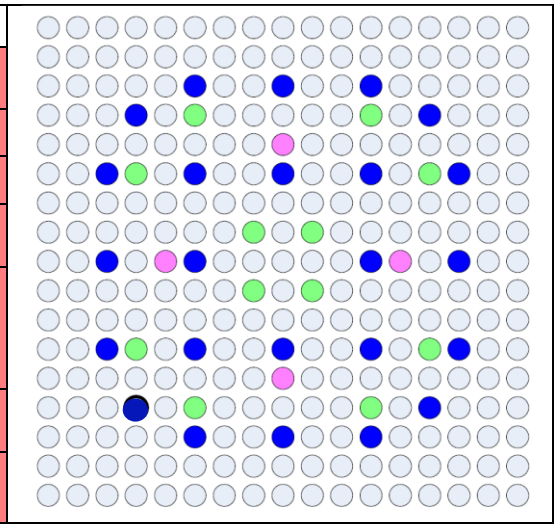

*Composition in wt.%

TABLE A-4 FUEL ASSEMBLY C1 DETAILS (AREVA, 2013)

Axial Length (cm)	Zone	Composition		
		Pin type 1	Pin type 2	Pin type 3
Number of pins		257	4	4
20.32	Blanket	2% ^{235}U	2% ^{235}U	2% ^{235}U
15.24	Cut-back	3.25% ^{235}U	3.25.7% ^{235}U	3.25% ^{235}U
354.95	Central		2.76% ^{235}U 6% Gd_2O_3	3.08% ^{235}U 2% Gd_2O_3
15.24	Cut-back		3.25% ^{235}U	3.25% ^{235}U
15.24	Blanket	2% ^{235}U	2% ^{235}U	2% ^{235}U

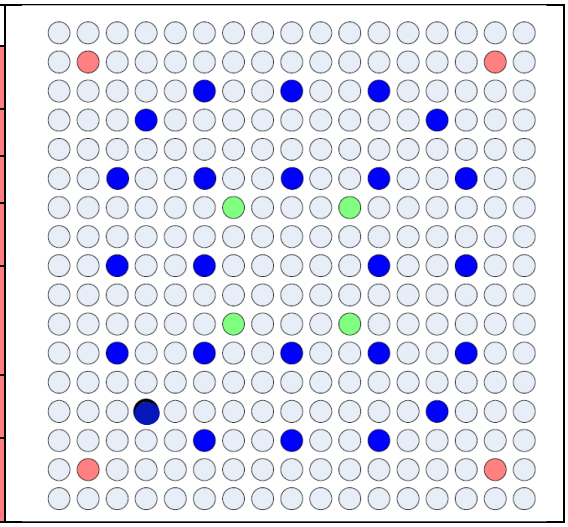

*Composition in wt.%

TABLE A-5 FUEL ASSEMBLY C2 DETAILS (AREVA, 2013)

Axial Length (cm)	Zone	Composition		
		Pin type 1	Pin type 2	Pin type 3
Number of pins		253	8	4
20.32	Blanket	2% ^{235}U	2% ^{235}U	2% ^{235}U
15.24	Cut-back	3.25% ^{235}U	3.25% ^{235}U	3.25% ^{235}U
354.95	Central		2.67% ^{235}U 6% Gd_2O_3	3.08% ^{235}U 2% Gd_2O_3
15.24	Cut-back		3.25% ^{235}U	3.25% ^{235}U
15.24	Blanket	2% ^{235}U	2% ^{235}U	2% ^{235}U

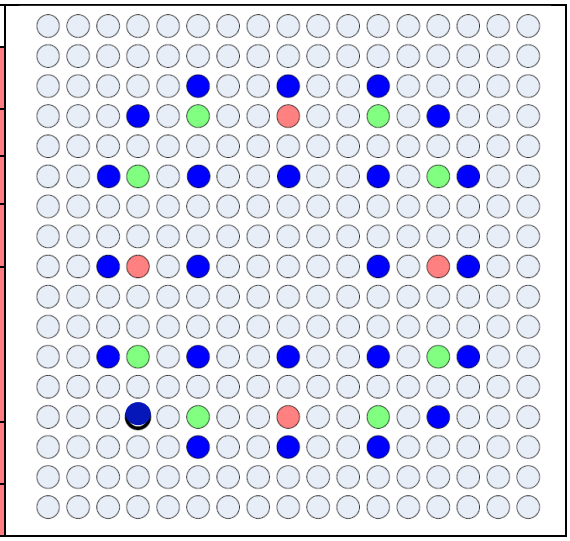

Composition in wt.%

TABLE A-6 FUEL ASSEMBLY C3 DETAILS (AREVA, 2013)

Axial Length (cm)	Zone	Composition		
		Pin type 1	Pin type 2	Pin type 3
Number of pins		249	12	4
20.32	Blanket	2% ^{235}U	2% ^{235}U	2% ^{235}U
15.24	Cut-back	3.25% ^{235}U	3.25% ^{235}U	3.25% ^{235}U
354.95	Central		2.27% ^{235}U 8% Gd_2O_3	3.08% ^{235}U 2% Gd_2O_3
15.24	Cut-back		3.25% ^{235}U	3.25% ^{235}U
15.24	Blanket	2% ^{235}U	2% ^{235}U	2% ^{235}U

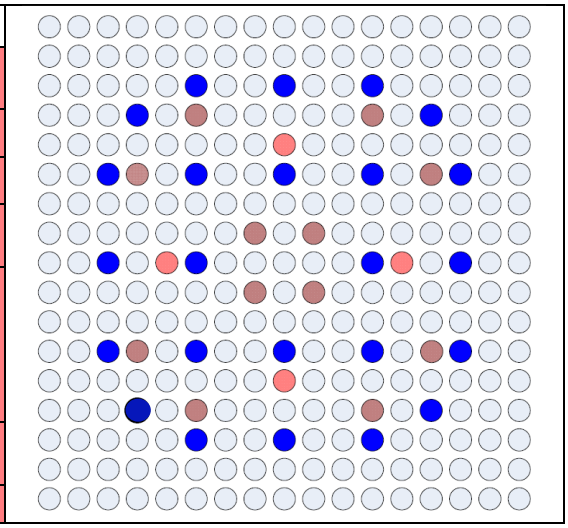

Composition in wt.%

APPENDIX B

Tables B-1 to B-6 provide the details on the composition and arrangement of newly designed thorium-uranium fuel assemblies A1, A2, B2, C1, C2 and C3.

TABLE B-7 THORIUM-URANIUM FUEL ASSEMBLY A1 DETAILS

Axial Length (cm)	Zone	Composition
		Pin type 1
Number of pins		265
20.32	Blanket	89.79% ThO_2 10.21% UO_2 = 2.03 at.% ^{235}U
15.24	Cut-back	88.49% ThO_2 11.51% UO_2 = 2.28 at.% ^{235}U
354.95	Central	
15.24	Cut-back	
15.24	Blanket	89.79% ThO_2 10.21% UO_2 = 2.03 at.% ^{235}U

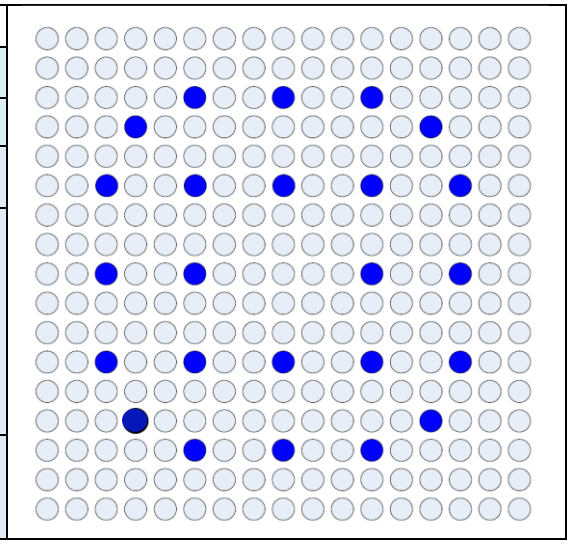

*Composition in wt.% with 19.99 wt.% enrichment in UO_2

TABLE B-8 THORIUM-URANIUM FUEL ASSEMBLY A2 DETAILS

Axial Length (cm)	Zone	Composition	
		Pin type 1	Pin type 2
Number of pins		261	4
20.32	Blanket	89.79% ThO_2 10.21% UO_2 = 2.03 at.% ^{235}U	
15.24	Cut-back	88.49% ThO_2 11.51% UO_2 = 2.28 at.% ^{235}U	
354.95	Central	88.49% ThO_2 11.51% UO_2= 2.28 at.% ^{235}U	Pure ThO_2
15.24	Cut-back	88.49% ThO_2 11.51% UO_2 = 2.28 at.% ^{235}U	
15.24	Blanket	89.79% ThO_2 10.21% UO_2 = 2.03 at.% ^{235}U	

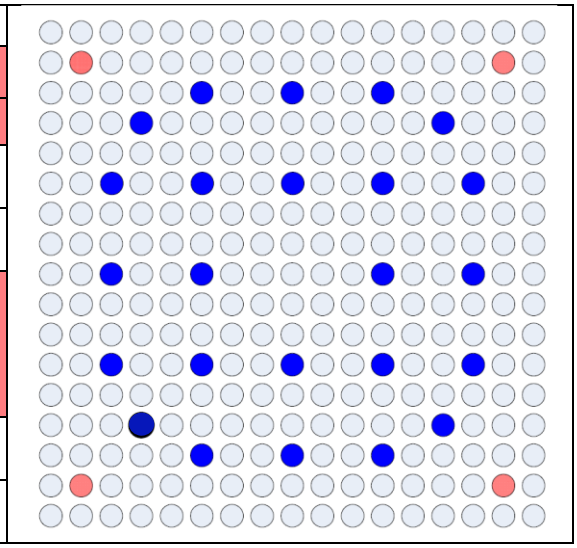

*Composition in wt.% with 19.99 wt.% enrichment in UO_2

TABLE B-9 THORIUM-URANIUM FUEL ASSEMBLY B2 DETAILS

Axial Length (cm)	Zone	Composition		
		Pin type 1	Pin type 2	Pin type 3
Number of pins		249	12	4
20.32	Blanket	89.79% ThO_2 10.21% UO_2 = 2.03 at.% ^{235}U		
15.24	Cut-back	86.19% ThO_2 13.81% UO_2 = 2.73 at.% ^{235}U		
354.95	Central	86.19% ThO_2 13.81% UO_2 = 2.73 at.% ^{235}U	Pure ThO_2	Pure ThO_2
15.24	Cut-back	86.19% ThO_2 13.81% UO_2 = 2.73 at.% ^{235}U		
15.24	Blanket	89.79% ThO_2 10.21% UO_2 = 2.03 at.% ^{235}U		

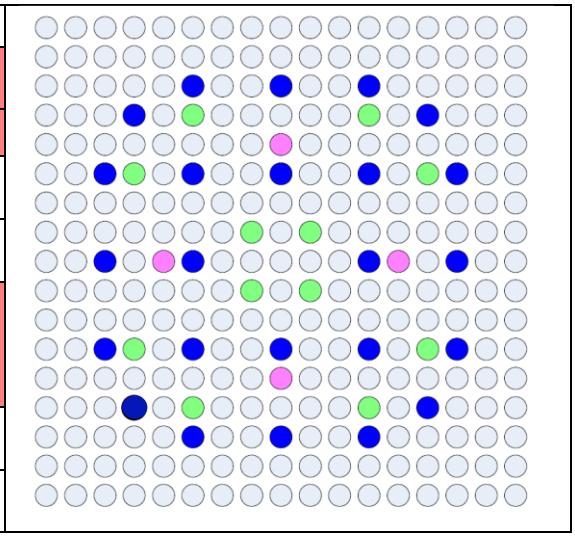

*Composition in wt.% with 19.99 wt.% enrichment in UO_2

TABLE B-10 THORIUM-URANIUM FUEL ASSEMBLY C1 DETAILS

Axial Length (cm)	Zone	Composition		
		Pin type 1	Pin type 2	Pin type 3
Number of pins		257	4	4
20.32	Blanket	89.79% ThO_2 10.21% UO_2 = 2.03 at.% ^{235}U		
15.24	Cut-back	83.39% ThO_2 16.61% UO_2 = 3.29 at.% ^{235}U		
354.95	Central	83.39% ThO_2 16.61% UO_2 = 3.29 at.% ^{235}U	Pure ThO_2	Pure ThO_2
15.24	Cut-back	83.39% ThO_2 16.61% UO_2 = 3.29 at.% ^{235}U		
15.24	Blanket	89.79% ThO_2 10.21% UO_2 = 2.03 at.% ^{235}U		

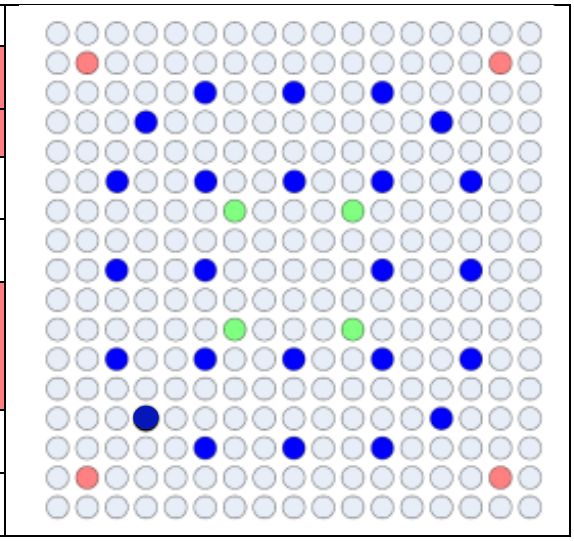

*Composition in wt.% with 19.99 wt.% enrichment in UO_2

TABLE B-11 THORIUM-URANIUM FUEL ASSEMBLY C2 DETAILS

Axial Length (cm)	Zone	Composition		
		Pin type 1	Pin type 2	Pin type 3
Number of pins		253	8	4
20.32	Blanket	89.79% ThO_2 10.21% UO_2 = 2.03 at.% ^{235}U		
15.24	Cut-back	83.39% ThO_2 16.61% UO_2 = 3.29 at.% ^{235}U		
354.95	Central	83.39% ThO_2 16.61% UO_2 = 3.29 at.% ^{235}U	Pure ThO_2	Pure ThO_2
15.24	Cut-back	83.39% ThO_2 16.61% UO_2 = 3.29 at.% ^{235}U		
15.24	Blanket	89.79% ThO_2 10.21% UO_2 = 2.03 at.% ^{235}U		

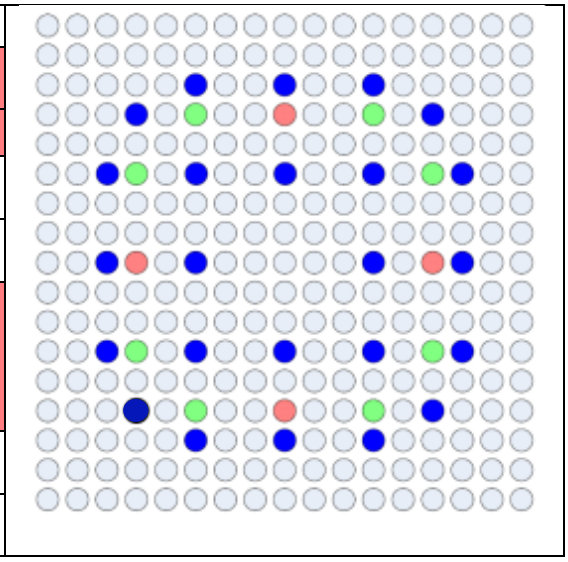

*Composition in wt.% with 19.99 wt.% enrichment in UO_2

TABLE B-12 THORIUM-URANIUM FUEL ASSEMBLY C3 DETAILS

Axial Length (cm)	Zone	Composition		
		Pin type 1	Pin type 2	Pin type 3
Number of pins		249	12	4
20.32	Blanket	89.79% ThO_2 10.21% UO_2 = 2.03 at.% ^{235}U		
15.24	Cut-back	83.39% ThO_2 16.61% UO_2 = 3.29 at.% ^{235}U		
354.95	Central	83.39% ThO_2 16.61% UO_2 = 3.29 at.% ^{235}U	Pure ThO_2	Pure ThO_2
15.24	Cut-back	83.39% ThO_2 16.61% UO_2 = 3.29 at.% ^{235}U		
15.24	Blanket	89.79% ThO_2 10.21% UO_2 = 2.03 at.% ^{235}U		

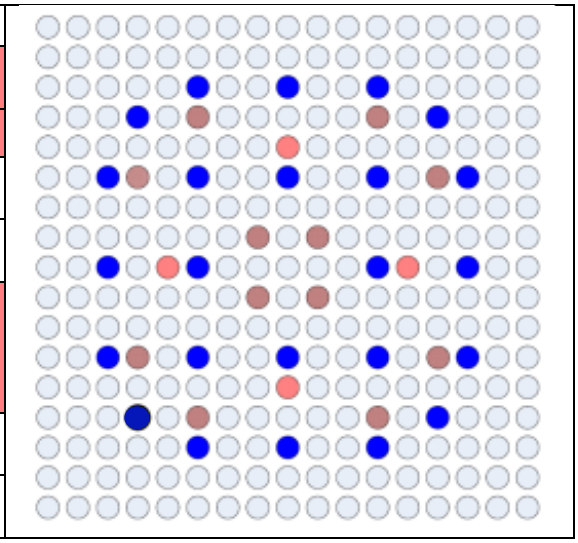

*Composition in wt.% with 19.99 wt.% enrichment in UO_2